11-13-2015

Innovative Modular High Performance Lightweight Decks for Accelerated Bridge Construction

Sahar Ghasemi
Florida International University, sghas006@fiu.edu

DOI: 10.25148/etd.FIDC000152

FLORIDA INTERNATIONAL UNIVERSITY

Miami, Florida

INNOVATIVE MODULAR HIGH PERFORMANCE LIGHTWEIGHT DECKS FOR ACCELERATED BRIDGE CONSTRUCTION

A dissertation submitted in partial fulfillment of

the requirements for the degree of

DOCTOR OF PHILOSOPHY

in

CIVIL ENGINEERING

by

Sahar Ghasemi

2015

To: Interim Dean Ranu Jung
College of Engineering and Computing

This dissertation, written by Sahar Ghasemi, and entitled Innovative Modular High Performance Lightweight Decks for Accelerated Bridge Construction, having been approved in respect to style and intellectual content, is referred to you for judgment.

We have read this dissertation and recommend that it be approved.

_____
Irtishad U. Ahmad

_____
Ton-Lo Wang

_____
Arindam Gan Chowdhury

_____
Amir Mirmiran, Major Professor

Date of Defense: November 13, 2015

The dissertation of Sahar Ghasemi is approved.

_____
Interim Dean Ranu Jung
College of Engineering and Computing

_____
Dean Lakshmi N. Reddi
University Graduate School

Florida International University, 2015

DEDICATION

To my parents Shahla Ghasemi and Ghasem Ghasemi,

For their endless love from long distance; without them this dream would never come true.

ACKNOWLEDGMENTS

First and foremost I would like to express my deepest gratitude to my major advisor, Dr. Amir Mirmiran for his enthusiastic endless scientific support, insightful guidance and patience throughout the course of this research. Working with him has been a constant learning experience for me. Also, I appreciate the sound advice and constructive suggestions I received from my PhD committee members, Dr. Irtishad U. Ahamad, Dr. Ton-Lo Wang, and Dr. Arindam Gan Chowdhury.

I cannot thank enough my good friends and colleagues, Dr. Mohammad Sima, Dr. Arash Tarighi, Mr. Xiong Yang and Mr. Mohammadreza Shafiefar. Their kind help was really significant throughout my research. Also, I thank my very close friends for their care and encouragement.

I also want to acknowledge the help of Dr. Pedram Zohrevand and Mr. Edgar Polo with all the personnel and graduate students at the Titan America Structures and Construction Testing Laboratory of the Florida International University.

The support of Lafarge North America for providing its UHPC (Ductal®), and MMFX Technologies of Irvine, CA, for providing its HSS bars are also acknowledged.

Last but not the least; I would like to thank my parents and my brothers (Bahman and Bijan) for having faith in me and motivating me in pursuing my goal.

ABSTRACT OF THE DISSERTATION

INOVATIVE MODULAR HIGH PERFORMANCE LIGHTWEIGHT DECKS FOR ACCELERATED BRIDGE CONSTRUCTION

by

Sahar Ghasemi

Florida International University, 2015

Miami, Florida

Professor Amir Mirmiran, Major Professor

At an average age of 42 years, 10% of the nation's over 607,000 bridges are posted for load restrictions, with an additional 15% considered structurally deficient or functionally obsolete. While there are major concerns with decks in 75% of structurally deficient bridges, often weight and geometry of the deck further limit the load rating and functionality of the bridge. Traditional deck systems and construction methods usually lead to prolonged periods of traffic delays, limiting options for transportation agencies to replace or widen a bridge, especially in urban areas.

The purpose of this study was to develop a new generation of ultra-lightweight super shallow solid deck systems to replace open grid steel decks on movable bridges and as well serve as a viable alternative in bridge deck replacements across the country. The study has led to a lightweight low-profile asymmetric waffle deck made with advanced materials. The asymmetry comes from the arrangement of primary and secondary ribs, respectively perpendicular and parallel to the direction of traffic. The waffle deck is made with ultrahigh performance concrete (UHPC) reinforced with either high-strength steel (HSS) or carbon fiber reinforced polymer (CFRP) reinforcement. With this combination,

the deck weight was limited to below 21 psf and its overall depth to only 4 inch, while still meeting the strength and ductility demands for 4 ft. typical stringer spacing. It was further envisioned that the ultra-high strength of UHPC is best matched with the high strength of HSS or CFRP reinforcement for an efficient system and the ductile behavior of UHPC can help mask the linear elastic response of CFRP reinforcement and result in an overall ductile system. The issues of consideration from the design and constructability perspectives have included strength and stiffness, bond and development length for the reinforcement, punching shear and panel action. A series of experiments were conducted to help address these issues. Additionally full-size panels were made for testing under heavy vehicle simulator (HVS) at the accelerated pavement testing (APT) facility in Gainesville. Detailed finite element analyses were also carried out to help guide the design of this new generation of bridge decks. The research has confirmed the superior performance of the new deck system and its feasibility.

TABLE OF CONTENTS

LIST OF TABLES

TABLE PAGE

LIST OF FIGURES

FIGURE PAGE

1. INTRODUCTION

1.1. Problem Statement

At an average age of 42 years, 10% of the nation's 607,380 bridges are posted for load restrictions, with an additional 15% considered structurally deficient or functionally obsolete (ASCE 2013). While there are major concerns with decks in 75% of structurally deficient bridges, often weight and geometry of the deck further limit the load rating and functionality of the bridge. Currently, most of the movable bridges use open grid steel decks (Figure 1.1). There are major concerns with these types of decks, such as poor rideability, susceptibility to fatigue, and high noise levels and maintenance cost.

Besides, traditional deck systems and construction methods usually lead to prolonged periods of traffic delays, limiting options for transportation agencies to replace or widen a bridge, especially in urban areas. A new generation of lightweight decks with solid riding surface are sought to address these issues, while staying within the weight limit of 21 lb/ft^2 for a movable bridge with a stringer spacing of 4 ft., which is the prevailing configuration of the movable bridges with steel open grid decks.

Accordingly, three alternative deck systems were developed and studied in the first phase of this research project (Mirmiran et al. 2009). The three deck systems included ultra-high performance concrete (UHPC)-high-strength steel (HSS) deck, and UHPC-fiber-reinforced polymer (FRP) deck, and FRP sandwich panel deck.

Although detailed experimental and analytical evaluation of the UHPC-HSS deck system indicated its viability to serve as an alternative to conventional open steel grid decks, deck weight exceeded the weight limitation of 21 lb/ft^2. On the other hand, more

studies were deemed necessary to improve the design of UHPC-FRP waffle deck and FRP sandwich panel deck.

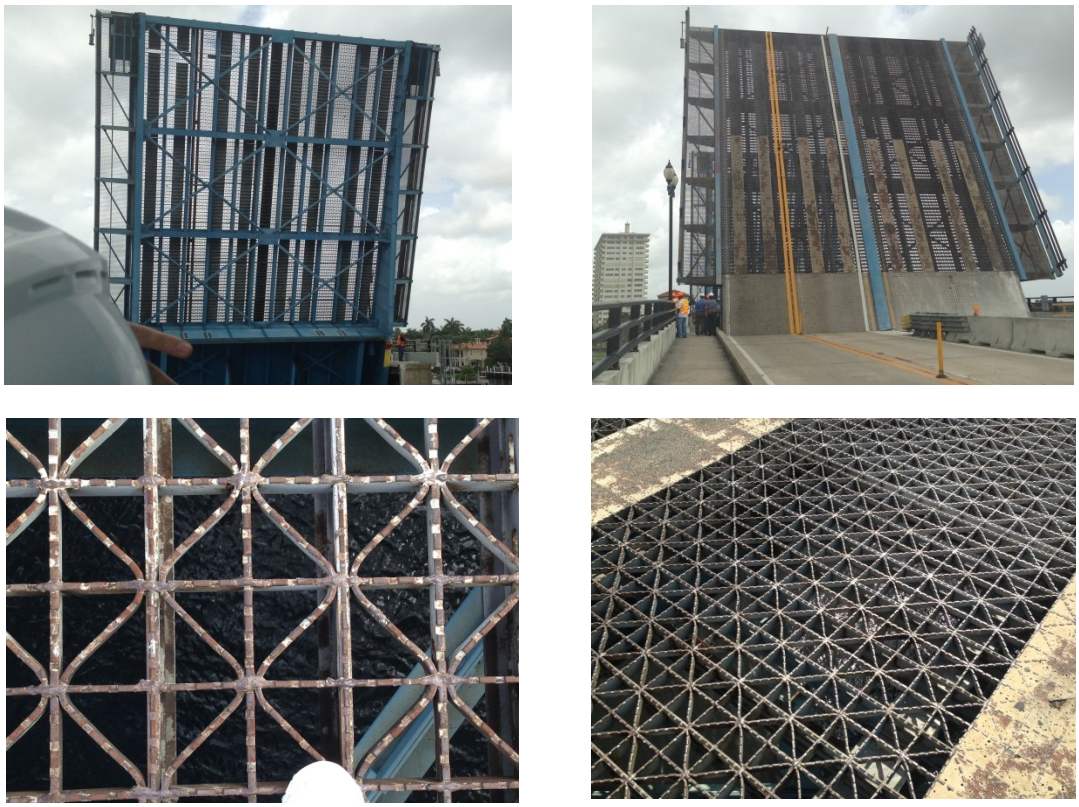

Figure 1.1 Open Steel Grid Deck (Las Olas Bridge, Fort Lauderdale, FL)

1.2. Research Objectives

The primary objective of this project was to develop lightweight deck system alternatives for movable bridges. Four different deck systems were developed and studied as:

1- UHPC-HSS Deck System:

The development of ultra-high performance concrete (UHPC) has had a revolutionary impact on concrete technology over the last two decades. The microstructure of this

advanced material is optimized to significantly enhance its compressive strength, tensile strength, elastic modulus, and ductility. Also, the lower permeability and porosity of UHPC, while having an excellent damage tolerance, lead to its excellent durability. Such exceptional properties make UHPC a promising material for new bridge construction, deck replacement and bridge widening in existing bridges.

Accordingly, the goal for this part of the research was to optimize the design of proposed UHPC-HSS deck system, which was studied in the first phase of the project (Mirmiran et al., 2009), to meet the weight limits for existing movable bridges. The size and reinforcement of the proposed deck were modified in two phases, and a number of specimens with single or multiple ribs were tested in simple or two-span configurations.

2- UHPC-FRP Deck System:

Fiber reinforced polymer (FRP) is another advanced material with high strength-to-weight ratio and excellent corrosion resistance. A novel deck system was developed as an ultra-lightweight low profile waffle slab of UHPC reinforced with carbon fiber reinforced polymer (CFRP) bars. A number of specimens at two different overall depths, with single or multiple ribs, and in simple or two-span configuration were tested in two consecutive phases in this study.

1.3. Research Methodology

Three deck systems were considered in this study:

1. Ultra-high Performance Concrete (UHPC) Deck with High Strength Steel (HSS) reinforcement
2. Ultra-high Performance Concrete (UHPC) Deck with Fiber Reinforce Polymer (FRP) reinforcement
3. FRP Sandwich Panel Deck System

This research includes comprehensive experimental and analytical studies on the three deck systems as well as some ancillary tests on the connections and anchorage systems.

1.4. Organization of the Dissertation:

This report is comprised of nine chapters. This first chapter serves as an introduction, mainly describing the problem statement, research objectives, and research approach. Chapter 2 covers the experimental work related to UHPC-HSS deck, including component-level and system-level tests along with finite element modeling. Chapter 3 focuses on the experimental work related to UHPC-CFRP deck as well as ancillary tests for developing and enhancing anchorage system as well as finite element modeling. Chapter 4 describes the accelerated pavement testing of the UHPC waffle decks with two types of reinforcement (i.e., HSS and CFRP). The accelerated pavement testing of the FRP hybrid deck made by Structural Composites Inc. is provided in Chapter 5, followed by summary and conclusions for the project, as well as recommendations for future research in chapter 6.

2. A SUPER LIGHTWEIGHT UHPC-HSS DECK PANEL FOR MOVABLE BRIDGES

2.1. Introduction

Movable bridges often include open grid steel deck for its light weight and ease of installation. However, inherent problems with these decks include poor rideability, susceptibility to fatigue, and high noise levels and maintenance cost (Mirmiran et al., 2009, 2012). A new generation of lightweight decks with solid riding surface are sought to address these issues, while staying within the weight limit of 21 psf for a movable bridge with a stringer spacing of 4 ft. (Saleem, 2011). With applications well beyond movable bridges, such lightweight decks are expected to include advanced construction materials, e.g., ultra-high performance concrete (UHPC) and high-strength steel (HSS).

UHPC, first developed in France in the 1990's (Keierleber, 2007), consists of high-strength cementitious materials, steel fibers, ground quartz, and super plasticizer (Habel, 2006, Graybeal, 2007). UHPC has less permeability, creep and shrinkage as compared to conventional concrete (Graybeal, 2006), while it also features compressive strengths above 21 ksi, elastic moduli over 66720 ksi, usable tensile strengths in excess of 0.7 ksi, and high durability and damage tolerance (Graybeal, 2006, Ahlborn, 2008). UHPC is also shown as a suitable pavement overlay (Graybeal, 2003), and has recently been applied in several bridges in the U.S., Canada, Europe and Asia (Blais et al., 1999, Hajar et al., 2003, and Graybeal, 2011).

HSS rebars offer another advanced option in bridge construction (El-Hacha et al., 2006), with almost 25% higher yield strength, six times more corrosion resistance and two times slower corrosion rate than conventional steel. These exceptional properties can lead to less reinforcement, longer service life and lower life-cycle costs (Kahl, 2007).

Saleem et al. (Saleem, 2011 and 2012) developed a novel bridge deck system, utilizing UHPC in the form of a low-profile solid waffle slab reinforced with HSS rebars, and an asymmetric arrangement of primary and secondary ribs, respectively perpendicular and parallel to traffic. The feasibility of the proposed system was shown through a number of experiments with single and multiple ribs, and in simple or two-span configurations. Although the weight of each panel was reasonably low as 32.37 psf, the total weight of the deck system including haunches and accessories turned out to exceed the weight limits for existing movable bridges. Therefore, the main objective of this study was to improve the proposed UHPC-HSS deck system by reducing its weight below 21 psf, while still meeting the strength and ductility demands.

2.2. Experimental Work

2.2.1. Test Matrix

Table 2.1 presents the test matrix for two groups of UHPC-HSS deck specimens tested in two consecutive phases. The specimen names in the table include number of primary ribs (1 or 4), number of spans (1 or 2), overall depth (5, 4½, or 4 in.), and the duplicate number in the case of identical specimens. In Phase 1, both section geometry and reinforcement were modified from those tested by Saleem (2011), which are also shown as Phase 0 for comparison. The overall section depth, slab thickness, and the

width of the primary rib were each reduced by ½ in., while the spacing of the primary ribs was increased by 3 in. The reinforcement was also reduced from No.4 to No.3 in the slab and from No.7 to No.5 in the rib. Two identical 4½ in. deep single-rib simple-span specimens were tested in this phase (Figure 2.1).

The specimens in Phase 1 weighed 0.15 psf or 33% less than those of Saleem (2011). The weight was calculated using a unit weight of 150 lb/ft^3 for UHPC, and includes a 4½ in. wide solid block to support the deck on each stringer. Test results, as will be presented later, still showed excess capacity over demand. Hence, the section was further optimized in Phase 2, reducing its depth by another 12 mm (Figure 2.1) and lowering its weight to only 20.26 psf. In this phase, one single-rib simple-span specimen was tested, along with a single-rib two-span specimen and a multi-rib simple-span specimen (Figures 2.1 and 2.2). The two-span and multi-rib specimens were utilized to investigate the continuity behavior of the deck, its punching shear behavior, and load distribution among the ribs.

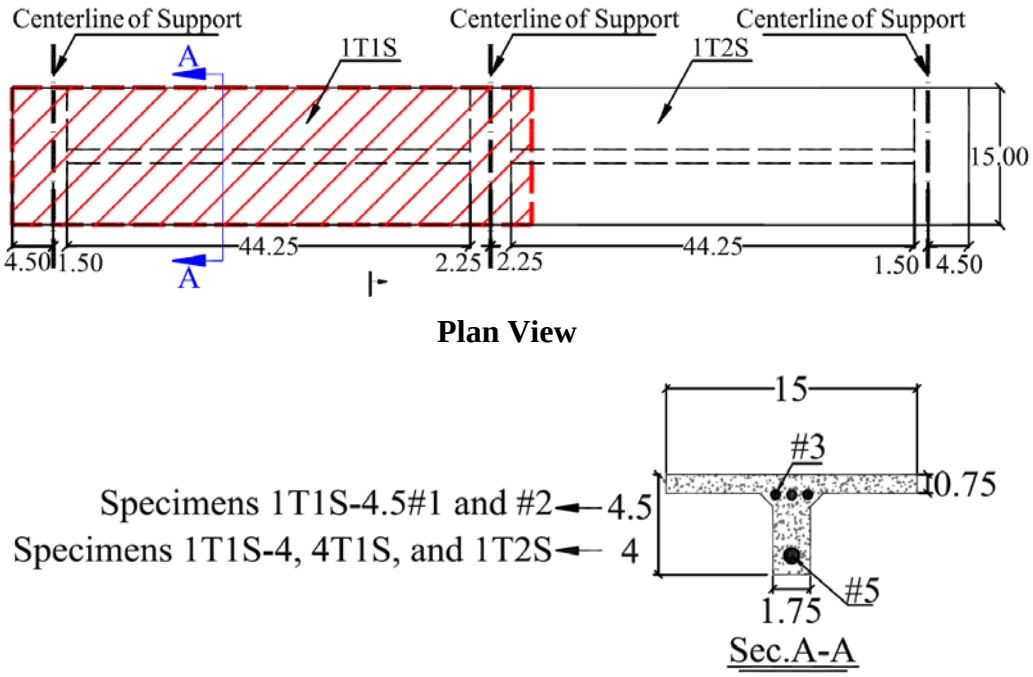

Figure 2.1 Schematics of Single-Rib, Simple-Span, or Two-Span Specimens

Table 2.1 Test Matrix

Phase	Specimen Name	Overall Depth (in.)	Rib Spacing (in.)	Slab Thickness (in.)	Unit Weight (psf)	28-Day UHPC Compressive Strength (ksi)	Flexural Reinforcement	
							Slab	Primary Rib
0*	1T1S-5#1	5	12	1¼	32.37	18	No. 4	No. 7
	1T1S-5#2					27		
	4T1S-5					26		
	1T2S-5					22		
1	1T1S-4½#1	4½	15	¾	21.72	24	No. 3	No. 5
	1T1S-4½#2					24		
2	1T1S-4	4	15	¾	20.26	27		
	4T1S					27		
	1T2S					25		

* Taken from Saleem (2011).

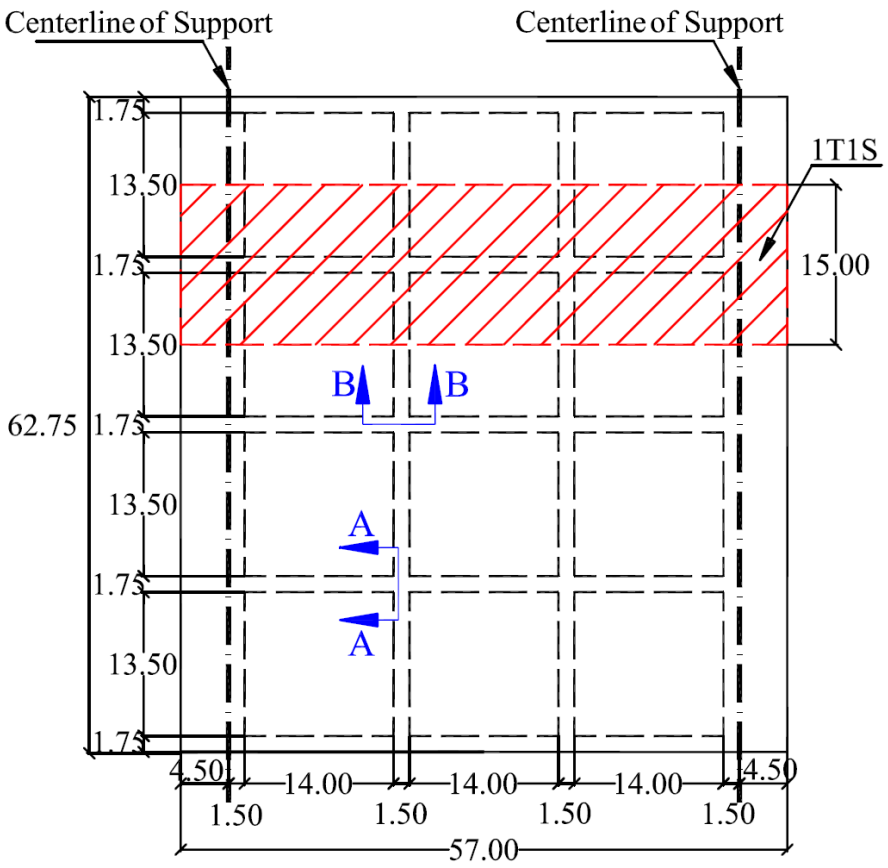

Plan View

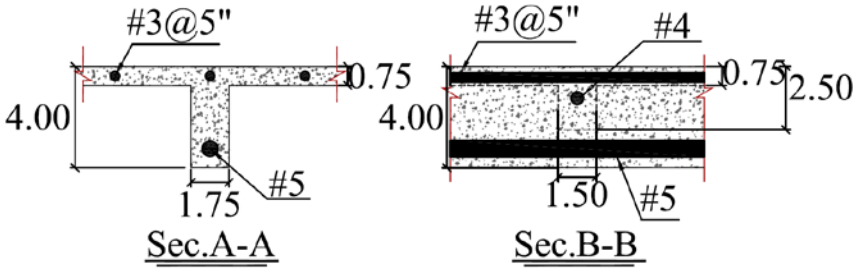

*All measurements are in inch.

Figure 2.2 Schematics of Multi-Rib Simple-Span Specimen

2.2.2. Specimen Preparation and Material Properties

Formwork was made using Styrofoam and timber (Figure 2.3). HSS rebars made by HSS Technologies of Irvine, CA, were used as primary reinforcement with yield strength of 100 ksi, as reported by the manufacturer. Rebars in primary ribs were all anchored using 180^{o} hook at both ends. Transverse ribs included a No. 4 rebar. Only the multi-rib specimen featured transverse ribs to help with load distribution among its ribs, and to assess the punching shear behavior of the deck. A clear cover of ½ in. was maintained for all rebars.

(a)

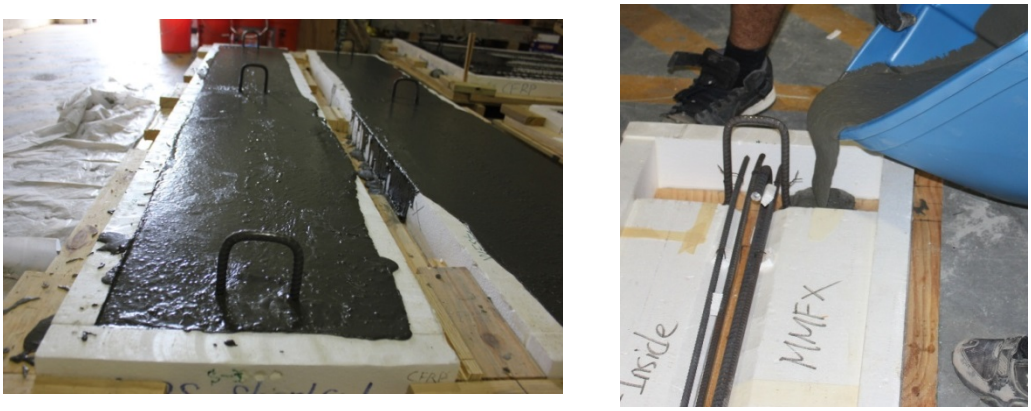

(b)

Figure 2.3 Specimen Preparation: (a) Formwork, and (b) Casting

Ductal®, a commercially available UHPC product, made by Lafarge North America, was used in this study. It is composed of premix powder (cement, silica fume, ground quartz and sand), water, superplasticizer, and 2% metallic fibers by volume. The fibers were ½ in. long with a tensile strength of 406 ksi. Six different batches of UHPC were mixed for casting the specimens (Figure 2.3). All specimens were air cured in the laboratory for a period of 28 days. Two companion 4 in. × 8 in. cylinders were used to measure the average 28-day compressive strength of each batch, as reported in Table 2.1.

2.2.3. Test Setup and Instrumentation

A 10 in. × 20 in. steel plate was used to simulate the prescribed dual tire wheel load of an HS20 truck. The simple-span specimens were subjected to a single load at mid-span (Figures 2.4a and 2.6a), whereas the two-span specimen was under two equal loads applied simultaneously in the middle of both spans (Figure 2.9a). At the conclusion of its flexure test, the multi-rib specimen was further tested using the same load patch to determine the punching shear capacity of its thin slab (Figure 2.8a). Several strain gauges were used to monitor responses of HSS rebars and UHPC at critical points. String pots were used to measure deflections at strategic locations. Loading was applied using a 230-kip capacity hydraulic actuator, at an average rate of 0.03 in./min. The data were recorded at a frequency of 1 Hz, and tests were stopped at 30% load drop, unless preceded by a clear sign of failure due to significant deflection, which may make the specimens unbalanced.

2.2.4. Test Results and Discussion

Table 2.2 presents a summary of test results. Also shown in the table are the required live load demands calculated using the equivalent strip method and the deck slab design table for each group of specimens based on the specimen width, load factors, multiple presence factors, dynamic load allowance, and the loading configuration. The table shows the over-capacity for each specimen as well as over-capacity per unit weight of the deck panel. The optimized specimens have comparable over-capacity per unit weight as those of Saleem (2011), demonstrating the effectiveness of the new design. The table also shows measured deflections for each specimen at the levels of service and ultimate loads. The ratio of these two deflection levels indirectly suggests a reasonable ductility for each deck specimen.

Figure 2.4 shows the test setup, failure mode, and load-deflection responses of single-rib simple-span specimens. Failure was initiated by minor web shear cracks near supports. Minor flexural cracks were also present near mid-span, but did not seem to have an impact on the failure. As the load increased, shear cracks propagated towards the slab near the loading plate. These cracks gradually widened, leading to eventual failure and a significant load drop, much the same as those observed by Saleem (2011). Figure 2.4c shows the load-deflection responses of the three specimens tested in this study, as well as the two deeper specimens tested by Saleem (2011). Deflections are averages of three recorded values (D1-D3) at mid-span, as shown in the figure inset. The ultimate and service demand loads are also shown, as described earlier. Given its smaller section and

reduced reinforcement, while the capacity of Specimen 1T1S-4 is about half of those tested by Saleem (2011), it is still twice its expected demand.

Table 2.2 Summary of the Test

Phase	Specimen Name	Service Load Deflection (in.)	Ultimate Deflection (in.)	Ultimate Load (kip)	Demand Load (kip)	Capacity/ Demand	Capacity/ Demand per Unit Weight
0*	1T1S-5#1	0.06	0.98	40.02	8.21	4.9	0.15
	1T1S-5#2	0.1	0.98	46.99		5.7	0.18
	4T1S-5	0.19	0.79	84.98	34.17	2.5	0.08
	1T2S-5	0.9	1.26	55.08	12.52	4.4	0.14
1	1T1S-4½#1	0.1	0.83	27.65	10.25	2.7	0.12
	1T1S-4½#2	0.14	0.87	24.73		2.4	0.11
2	1T1S-4	0.15	0.91	22.71		2.2	0.11
	4T1S	0.18	0.87	51.48	42.04	1.2	0.06
	1T2S	0.07	0.87	44.96	15.65	2.9	0.14

* Taken from Saleem (2011)

(a)

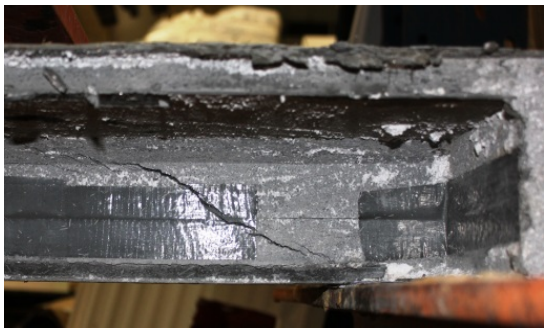

(b)

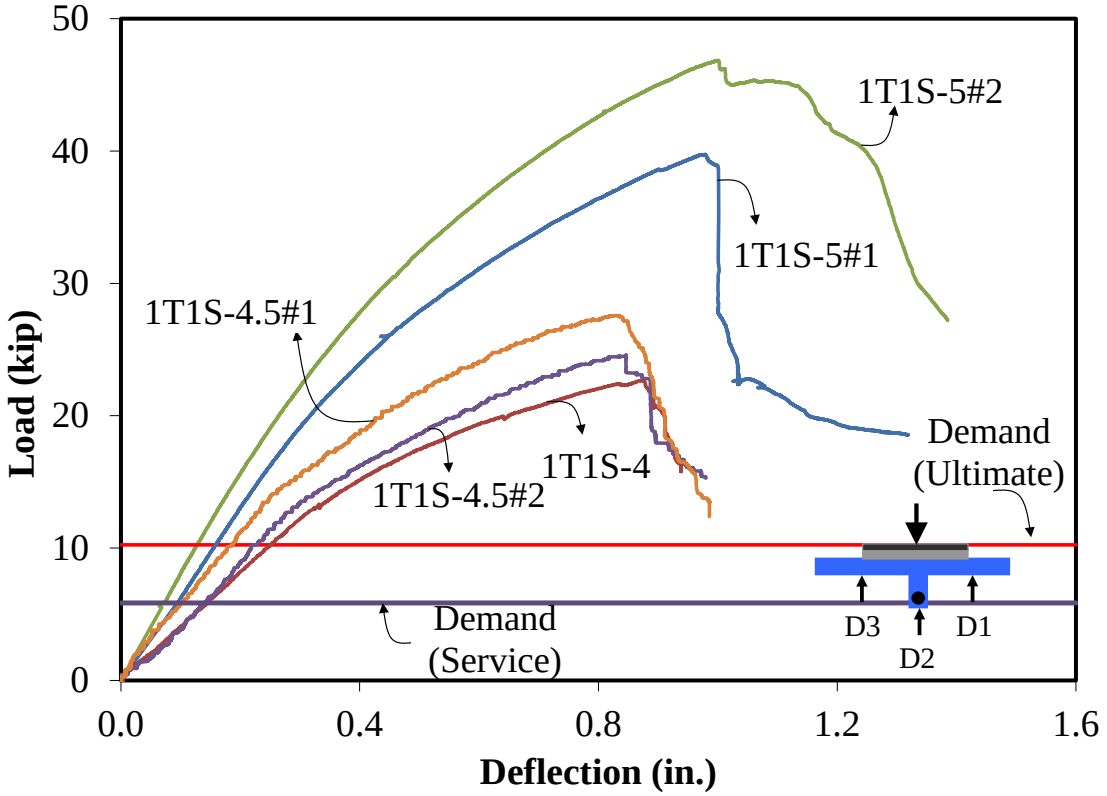

(c)

Figure 2.4 Flexure Tests of Specimens 1T1S: (a) Test Setup, (b) Failure Mode, and (c) Load-Deflection Responses (Note: Curves 1T1S-5#1 and #2 from Saleem 2011)

Figure 2.5 shows load-strain responses for Specimens 1T1S-4.5#1 and 1T1S-4, based on strain gauges attached at the mid-span to the rebar in the primary rib. Although yielding of rebar in both specimens occurs at a level much higher than the service load demand, it may generally be construed as a good indication of a fairly ductile behavior. It should be noted that in the face of dominant shear cracks, Xia et al. have demonstrated that the ductile behavior of these decks is more representative of the fiber pull-out mechanism in UHPC and the dowel action of the HSS bars rather than traditional yielding of steel reinforcement.

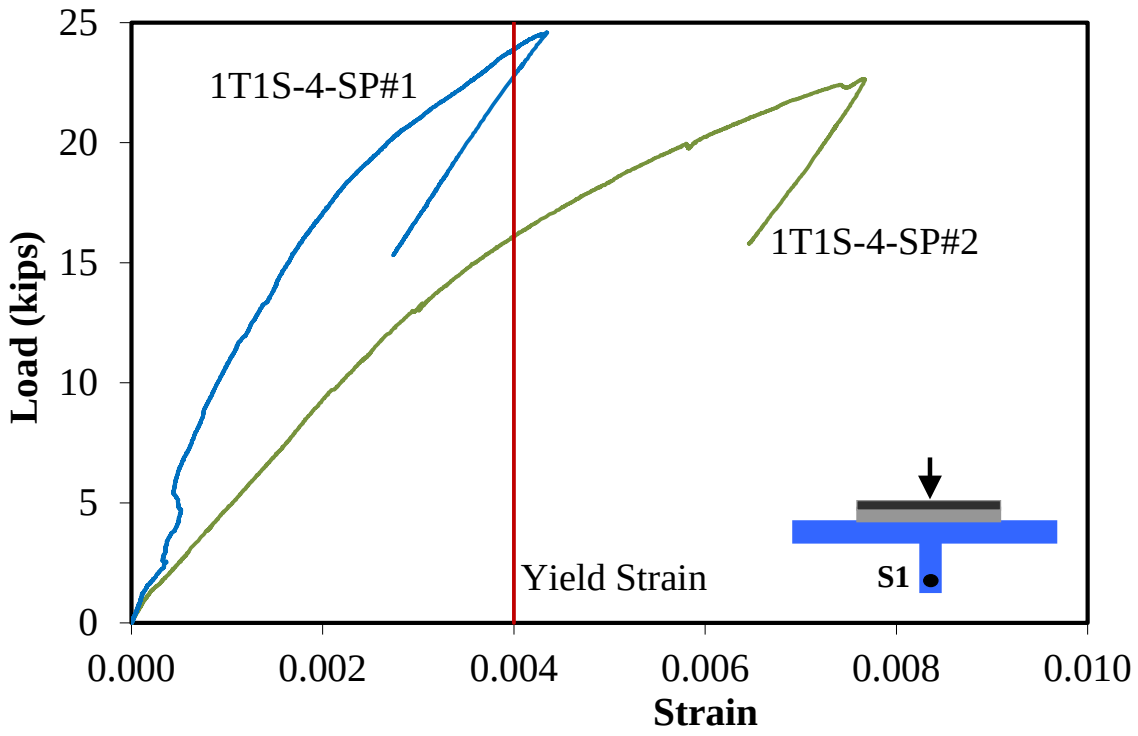

Figure 2.5 Load-Strain Response of Rebars in Specimens 1T1S

Several strain gauges were used to monitor the strain in UHPC. Results are presented in Appendix A.

2.2.4.1 Panel Action

Figure 2.6 shows the test setup, failure mode and load-deflection responses of the multi-rib simple-span specimen. Deflections are three recorded values (D1-D3) at mid-span, as shown in the figure inset. The failure mode was generally similar to that of single-rib simple-span specimens, in that it initiated with diagonal shear cracks near the supports, albeit mainly in the interior ribs. With the increase of the load, shear cracks grew both in width and length, especially in the center rib, leading to the failure accompanied by a considerable load drop.

As shown in Figure 2.6c, Specimen 4T1S showed an almost linear response up to about twice the service load deflection, while exhibiting a plastic behavior thereafter until failure. In comparison to the single-rib specimens (Figure 2.4c), the presence of multiple ribs helped increase the ductility of the proposed deck panel significantly through a considerable plastic deformation. This confirms earlier findings that failure of the proposed UHPC-HSS deck panel system is clearly ductile, despite the presence of dominant shear cracks.

For comparison, Figure 6c also includes the load-deflection response curves for the deeper specimen tested by Saleem (2011). Although specimen 4T1S-4 has a 20% shallower section and 28% less reinforcement, while its capacity is about 60% of Specimen 4T1S-5, it still exceeds its expected demand by at least 22%.

Load distribution among the ribs may be calculated based on mid-span deflections of each rib or mid-span strains in HSS bar in each rib. Using either approach, the load

distribution among the ribs is found as 33% for the center rib and 22% and 11% for the next two ribs. These factors are quite similar to those reported by Saleem et al. (2011).

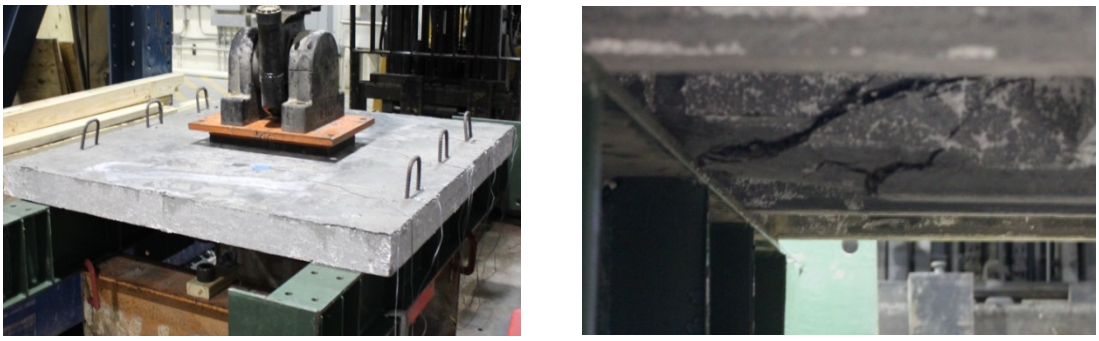

(a) (b)

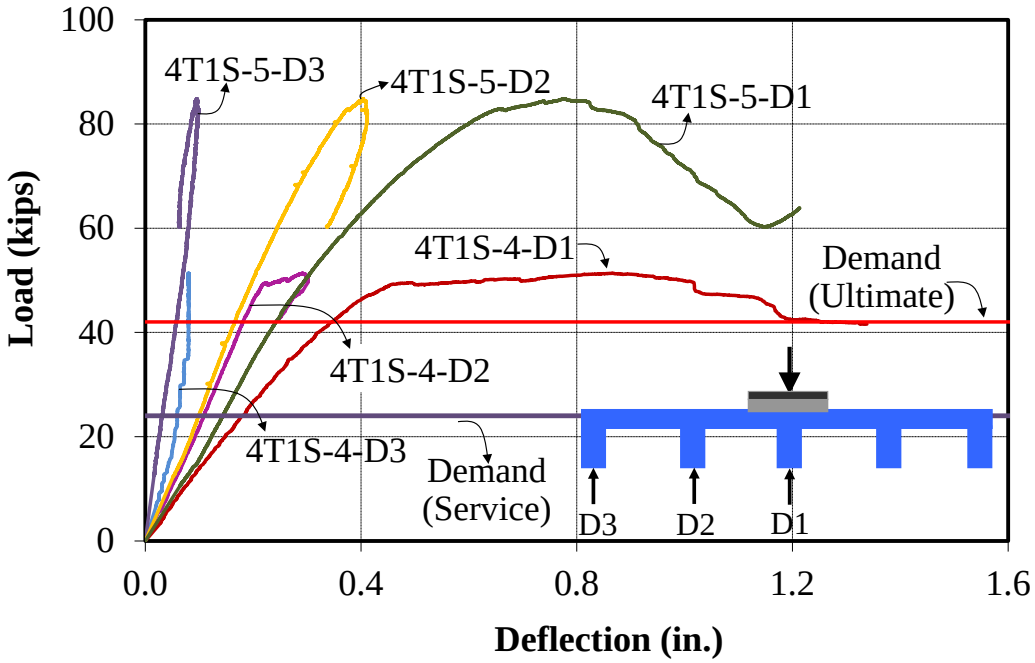

(c)

Figure 2.6 Tests of Specimens 4T1S: (a) Test Setup, (b) Failure Mode, and (c) Load-Deflection Responses (Note: Curves 4T1S-127-D1, D2, and D3 from Saleem 2011)

Figure 2.7 shows load-strain responses for Specimen 4T1S based on the strain gauges attached to the rebars in each of the primary ribs at the mid-span. The strain gauge in the exterior rib was damaged before reaching the ultimate load. Of the other two, the largest strain occurred in the rebar of the center rib, although it was still below the yield limit. As discussed earlier, one should note the sizeable displacement-based ductility of the deck system (Figure 2.6a); despite the apparent shear failure and the relatively low strain levels in the flexural reinforcement.

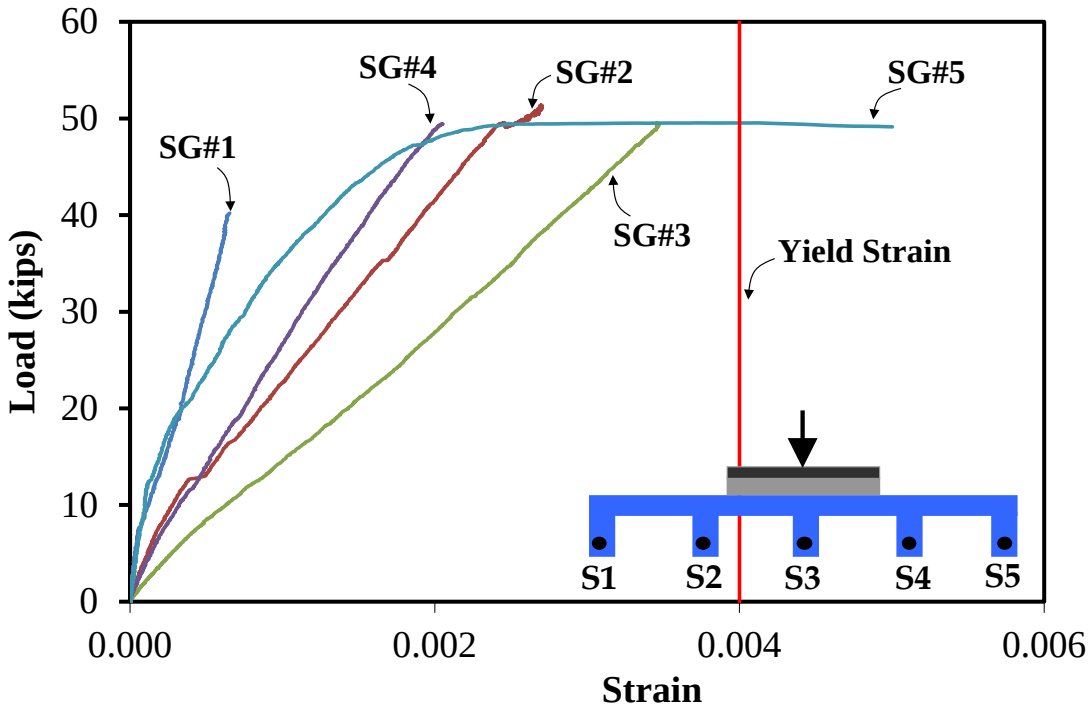

Figure 2.7 Load-Strain Response of Rebars in Specimen 4T1S

2.2.4.2 Punching Shear Behavior

Figure 2.8a shows the reserved punching shear test carried out on an exterior panel of Specimen 4T1S at the conclusion of its flexural test described above. The load was applied using the same loading plate on the slab between the first two ribs. Figure 8b shows the failure governed by major cracks in the primary ribs adjacent to the loading patch. No sign of punching shear, however, was observed on the top of the slab around the loading plate. Figure 8c shows the load-deflection responses. As shown in the figure inset, the deflections (D1-D3) were recorded at mid-span, under the loading patch and the two adjacent ribs. A sizeable deflection of 0.6 in. was measured in the middle of the panel right under the loading patch at the ultimate load of 42.49 kips. The ultimate load was about 17% lower than that observed in the first flexure test of the specimen. Clearly, the asymmetric loading did not allow full contribution of other ribs. The test was stopped after the load dropped to 37.32 kips due to excessive damage in the exterior rib.

Harris and Roberts-Wollmann (2005) proposed a modification to ACI equation for concrete breakout strength to predict the punching shear capacity of thin UHPC slabs

$$V_c = 0.38\, f_{ten} \frac{[(3h + a) \times (3h + b)] - (a \times b)}{\sqrt{h}} \qquad (2.1)$$

where f_{ten} = tensile strength of UHPC, h = thickness of the UHPC slab, and a and b = dimensions of the loading plate. Using a tensile strength of 1.1 ksi for a 10 in. × 20 in. loading plate, the punching shear capacity of the ¾ in. slab is calculated as 6.97 Kips, which is substantially lower than its experimentally measured capacity of 42.49 Kips. This explains why no sign of punching shear was observed in the slab, clearly because

the spacing of the primary ribs prevents a punching shear failure of the slab, and instead promotes one-way shear failure of primary ribs.

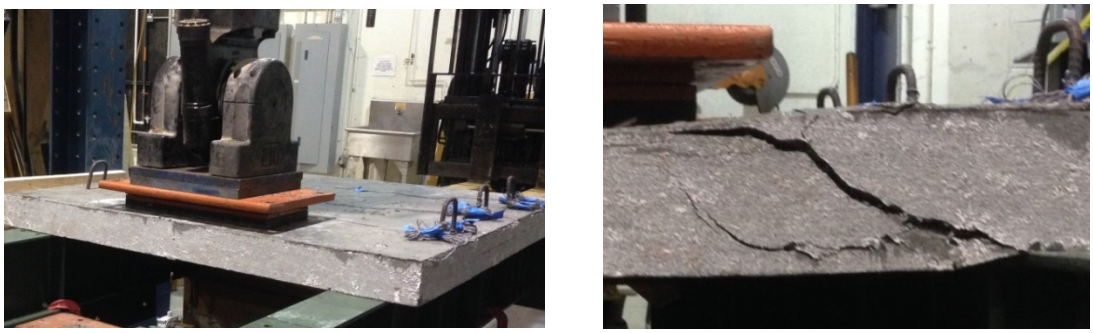

(a) (b)

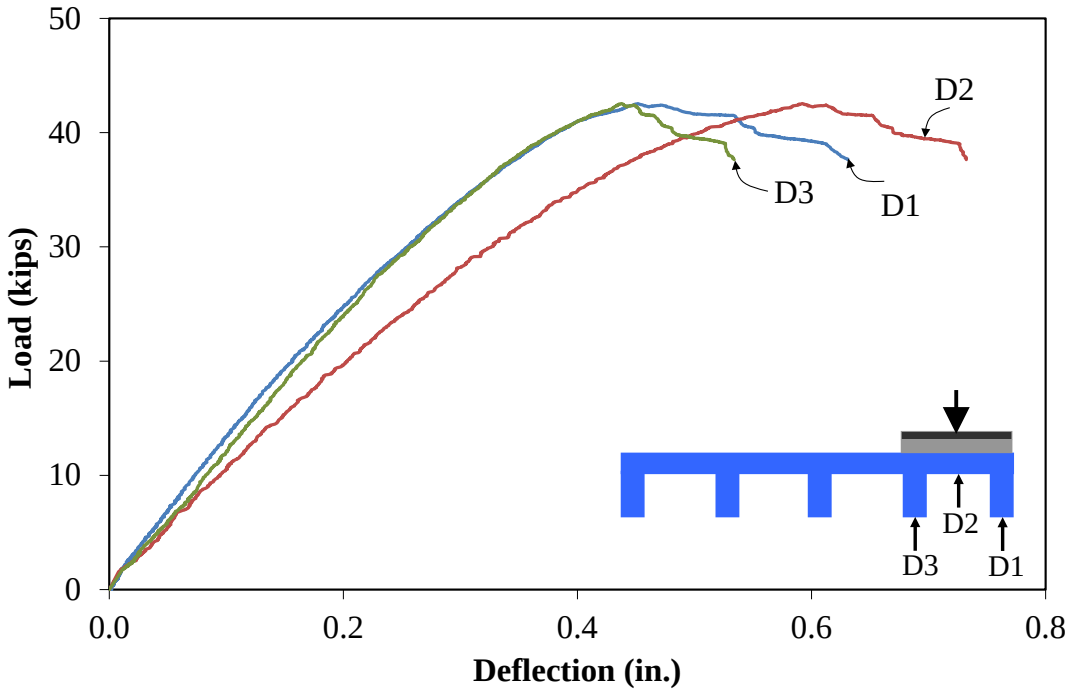

(c)

Figure 2.8 Punching Shear Test of Specimen 4T1S: (a) Test Setup, (b) Failure Mode, and (c) Load-Deflection Responses

2.2.4.3 Continuity Effects

The effects of continuity and negative moments were investigated using the single-rib two-span Specimen 1T2S. Figure 2.9 shows the test setup, deflected shape, and the failure mode, where diagonal cracks initiated near an exterior support in one span and propagated to the slab leading to the eventual failure. Minor shear cracks were also present in the other span, while some flexural cracks were observed on top of the slab over the interior support.

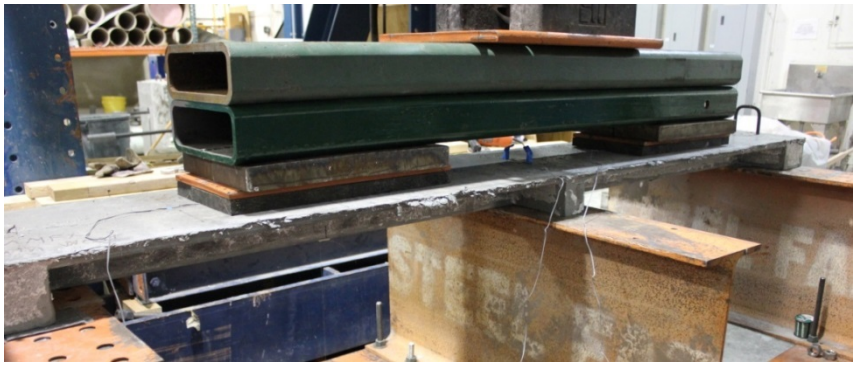

(a)

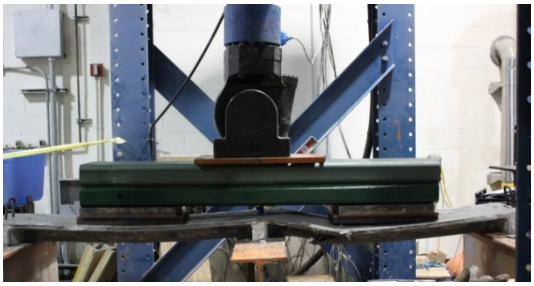

(b)

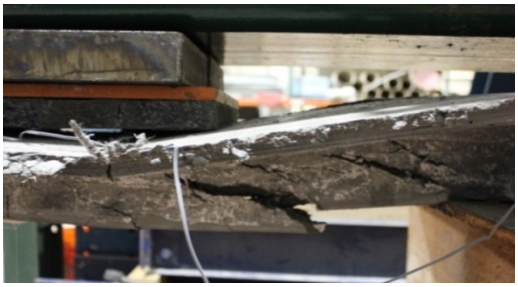

(c)

Figure 2.9 Flexure Tests of Specimen 1T2S: (a) Test Setup, (b) Deflected Shape, and (c) Failure Mode

Figure 2.10 shows the load-deflection response for the two measured mid-span displacements. Also shown for comparison are the load-deflection response curves for the deeper specimen tested by Saleem (2011). The comparison shows that although the new design has led to 18% reduction in the ultimate load, the capacity is still close to three times that of the expected demand, while the weight has been reduced by 37%. It is equally important to note the apparent high displacement-based ductility of the deck.

From the perspective of serviceability, the specimen showed a deflection of 0.07 in. at the service demand of 8.92 Kips. This corresponds to L/697, where L = center to center spacing of stringers, i.e., 4ft. Noting the continuity effect of typical decks spanning over multiple stringers, one can calculate a correction factor of 0.74 comparing the deflections of two-span and five-span decks under two wheel loads. As such, the corrected deflection of the proposed deck turns out to be L/942, which clearly meets the deflection limit of L/800.

Figure 2.11 shows the load-strain response of Specimen 1T2S, based on its measured rebar strains at both mid-spans. Similar to the load-displacement response, the strain in the north span was higher than that at the other span, where the gauge was damaged before reaching the ultimate load. As discussed earlier, the load-deflection behavior of the specimen was very ductile, while the rebar clearly did not reach its yield strain in either span.

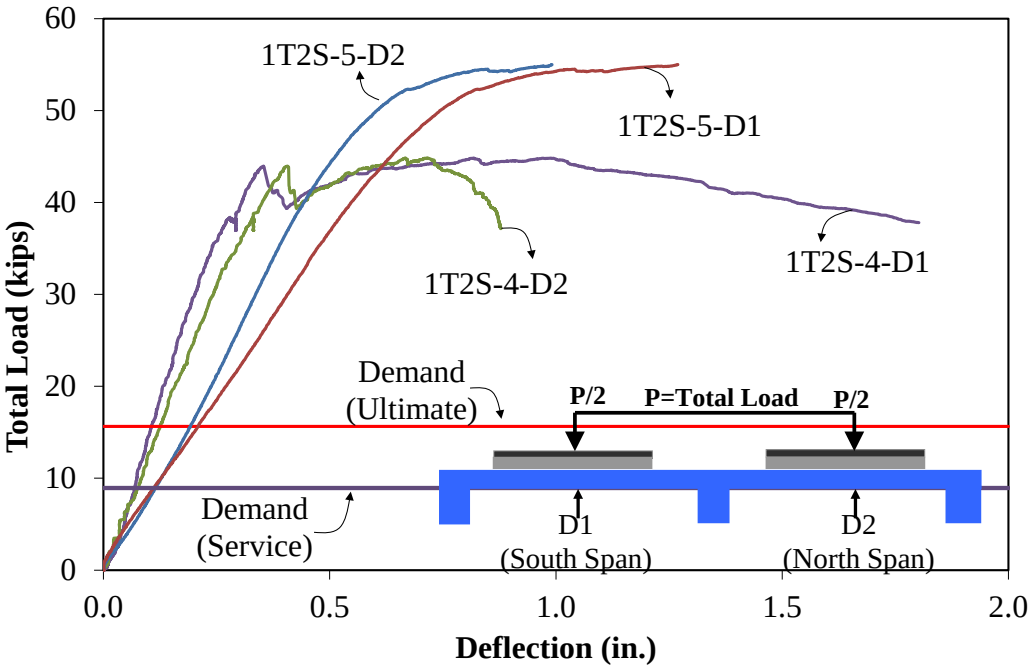

Figure 2.10 Load-Deflection Responses of Specimens 1T2S
(Note: Curves 1T2S-127-D1 & D2 from Saleem 2011)

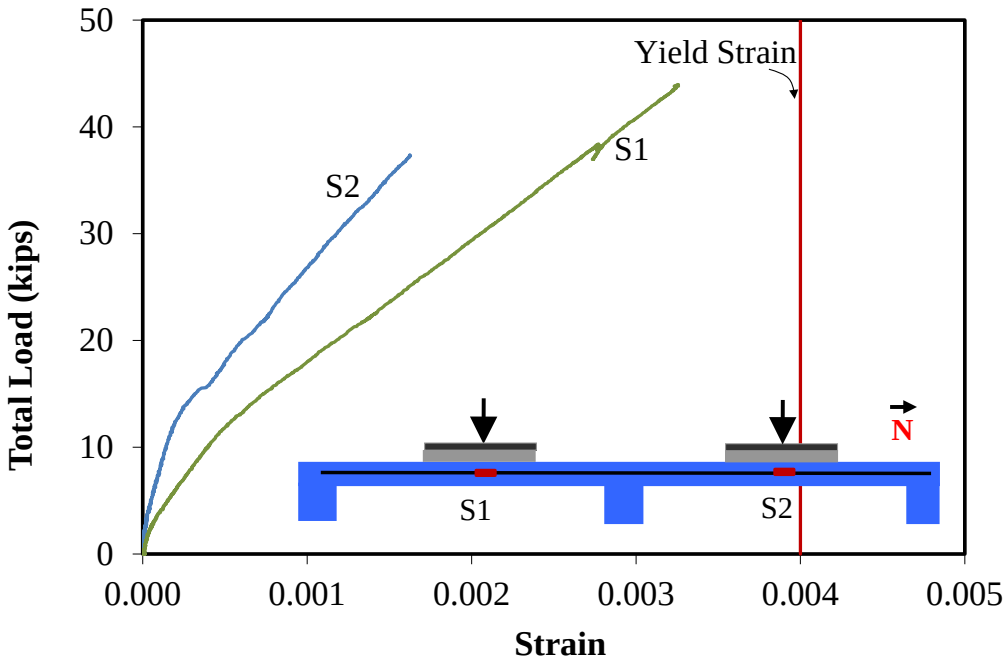

Figure 2.11 Load-Deflection Responses of Specimens 1T2S
(Note: Curves 1T2S-127-D1 & D2 from Saleem 2011)

2.3. Finite Element Modeling

2.3.1. General modeling

The numerical simulations were performed using the general-purpose finite element software package ABAQUS. This study includes the finite element analysis of three UHPC waffle deck specimens in T-section shape with single or multiple units in single or double span configurations. The dimensions of the specimens and the boundary conditions are exactly the same as the corresponding experimental tests in order to provide appropriate comparison between the finite element modeling outputs and experimental tests' results. A displacement control method was utilized for analyzing procedure. A 10×20" loading pad was modeled representing the HS 20 truck tire footprint. The displacement was assumed uniformly applied to the loading pad. Enhanced hexahedral 3D stress element with secondary order of accuracy was used to model the UHPC material. The element deletion option is on meaning that that the element will be removed from the stiffness matrix if it failed. In order to model the reinforcement, 3-node two-dimensional truss element type was used.

2.3.2. Material properties

2.3.2.1 UHPC Comprehensive strength

Comprehensive strength of the each specimen was modeled based on the compressive test results on 4 by 8 cylinders corresponding to each specimen. The compressive strength tests were carried out 28 days after the casting day.

2.3.2.2 **UHPC Comprehensive stress-strain behavior**

The stress-strain recommended by Aaleti was used in the modeling with a difference in peak stress value for the UHPC (value of stress at point A in Figure 2.12). The peak stress value was taken from the experimental tests results.

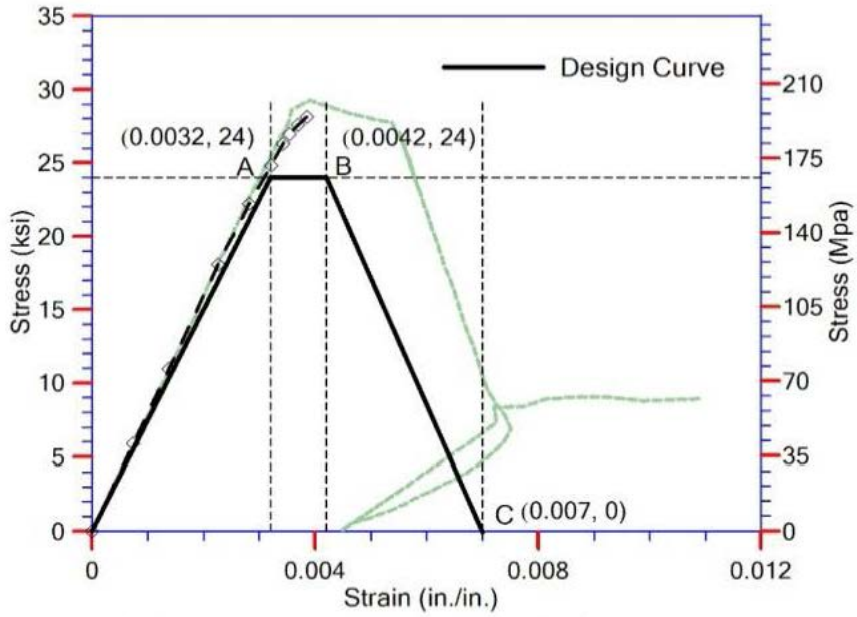

Figure 2.12 Stress-Strain Behavior of UHPC

2.3.2.3 **UHPC Tensile stress-strain behavior**

Different experimental methods were investigated to evaluate the tensile behavior of UHPC, including the flexural prism test, dog-bone test, split cylinder test and direct tension test (Graybeal, 2006). According to this study, the cracking tensile strength of UHPC is recommended as 1.3 ksi for steam-cured and 0.9 ksi for and untreated curing.

Graybeal (2006) recommended the cracking tensile strength of UHPC to be taken as 0.9-1.2 ksi. In this study, the Value of 1.0 ksi was used in the finite modeling.

2.3.2.4 UHPC Modulus of Elasticity and Poisson Ratio

Graybeal (2007) recommended a formula for calculating the modulus elasticity of UHPC:

$$E\,(psi) = 46{,}200\sqrt{f_c^{'}}\ \ (psi)$$

According to this formula, different modulus of elasticity was used for different specimens according to the corresponding test results; however the values were relatively close to each other. Some investigation was carried out on Poisson ratio of UHPC (Ahlborn, 2008). The Poisson ratio was taken as 0.2 in the finite element modeling.

2.3.2.5 HSS Material Properties

Figure 2.13 presents the stress-strain curve for HSS which is taken from the manufacturer data sheet.

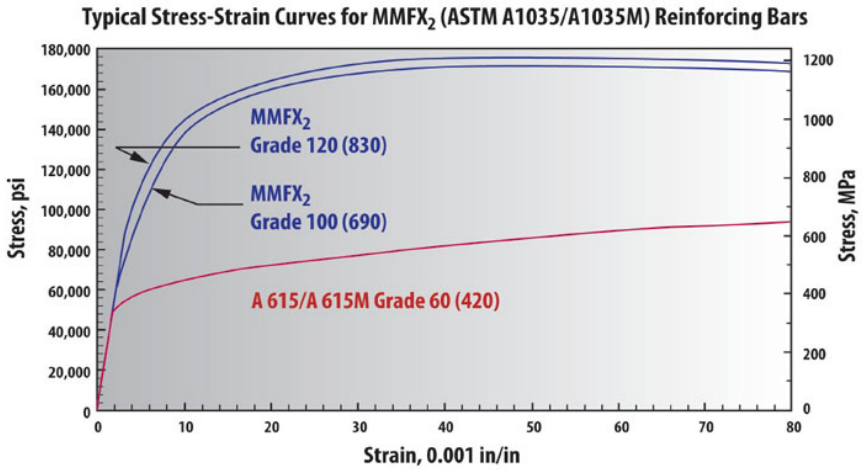

Figure 2.13 Stress-Strain Behavior of HSS (MMFX)

2.3.3. Modeling and Results for 1T1S Specimen

Figure 2.14 shows the geometry and mesh of the Specimen 1T1S. The boundary condition is presented in Figure 2.15. As seen in the figure, the boundary conditions on the support are modeled by constraining the lines on both ends. In one side three degrees of displacement are constrained to model a pin support; on the other side two degrees are constrained to model a roller support.

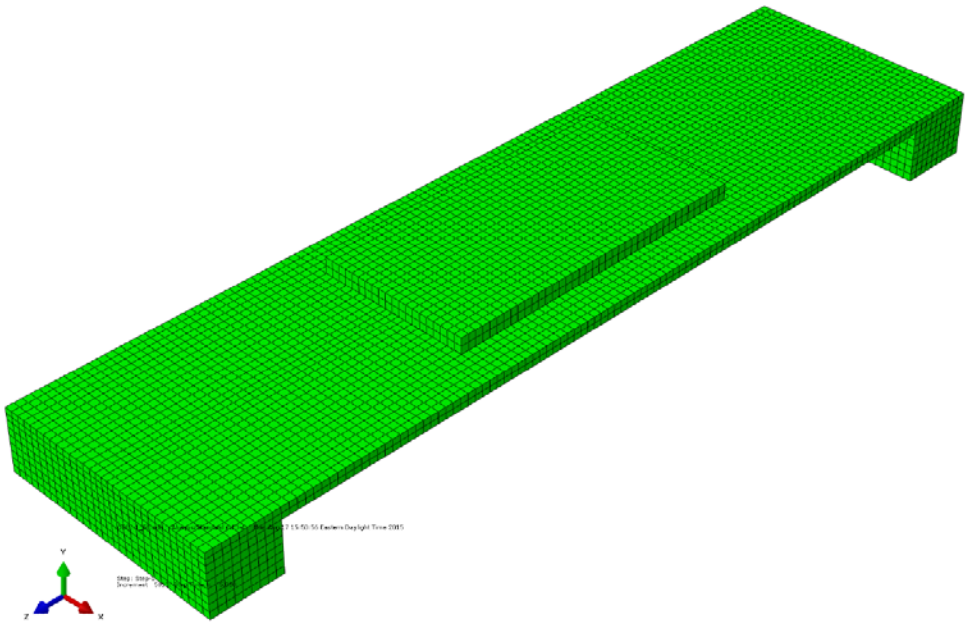

Figure 2.14 Geometry and Mesh of Specimen 1T1S

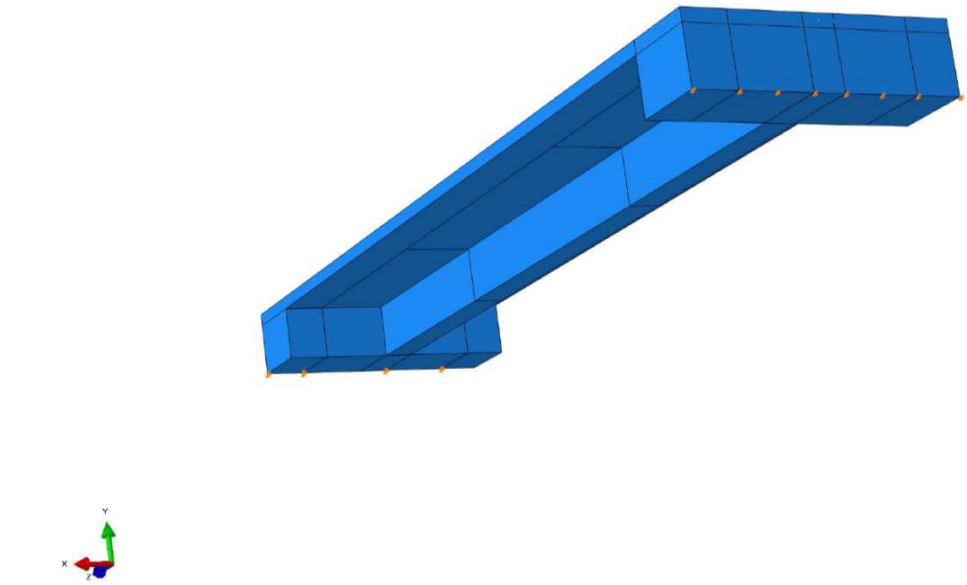

Figure 2.15 Boundary Conditions of Specimen 1T1S

Figure 2.16 shows the deflected model as compared to the tested specimen. As seen in the figure, the failure mode is the beam shear crack next to the supports which determined the good consistency in the modes of failure between the FE model and the tested specimen. The Load-Deflection response of the specimen is shown in Figure 2.17 which is compared to the corresponding experimental test.

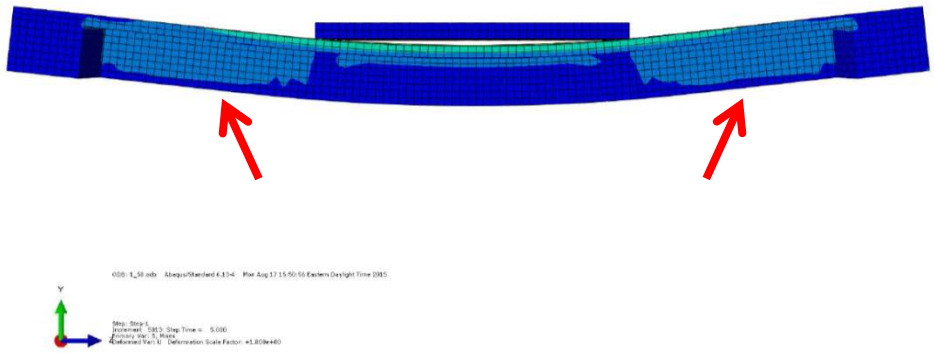

(a)

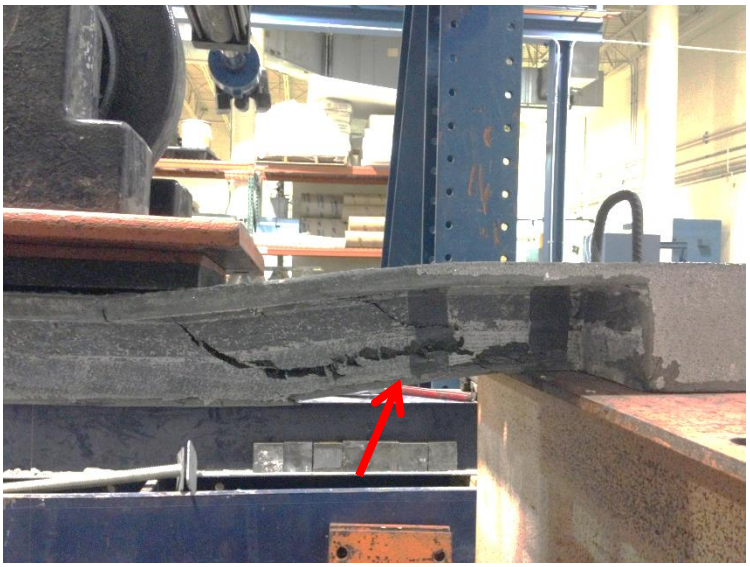

(b)

Figure 2.16 Failure Modes and Deflected shape of the Specimen 1T1S, (a) FE Modeling, and (b) Failure Mode in Experimental Test

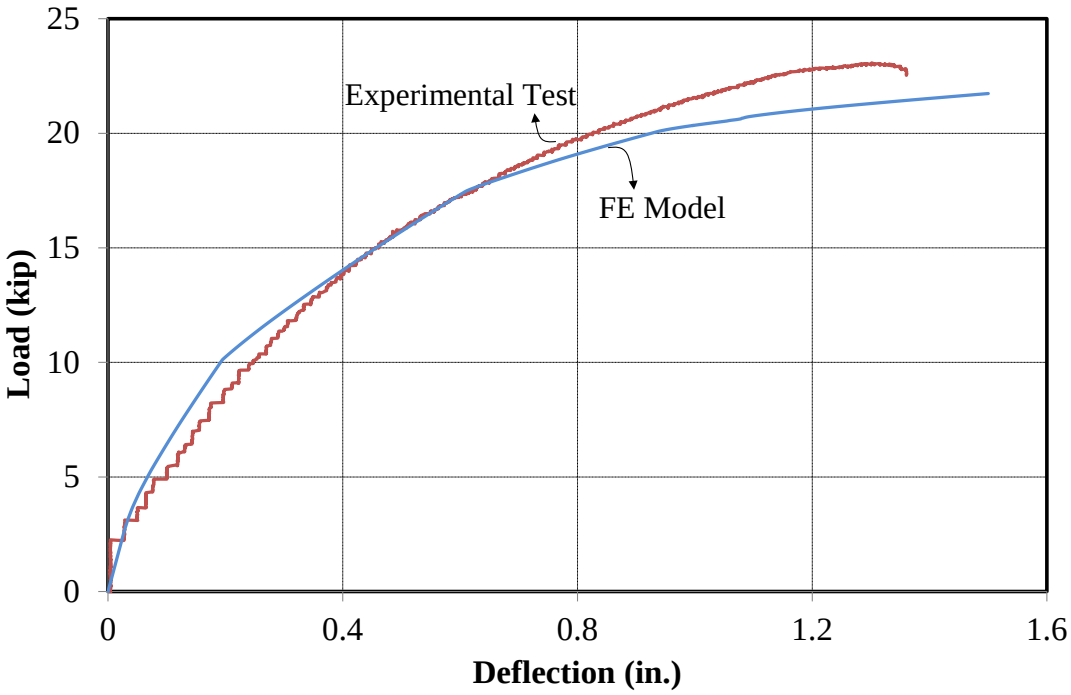

Figure 2.17 Load-Deflection Response of Model 1T1S

It can be noticed that the finite element results showed a good agreement with the tests results although the model underestimate the load capacity for 1.34 kips which may be results from the value for the shear strength made in the model.

2.3.4. Modeling and Results for Specimen 1T2S

The finite element model of Specimen 1T2S is shown in Figure 2.18.

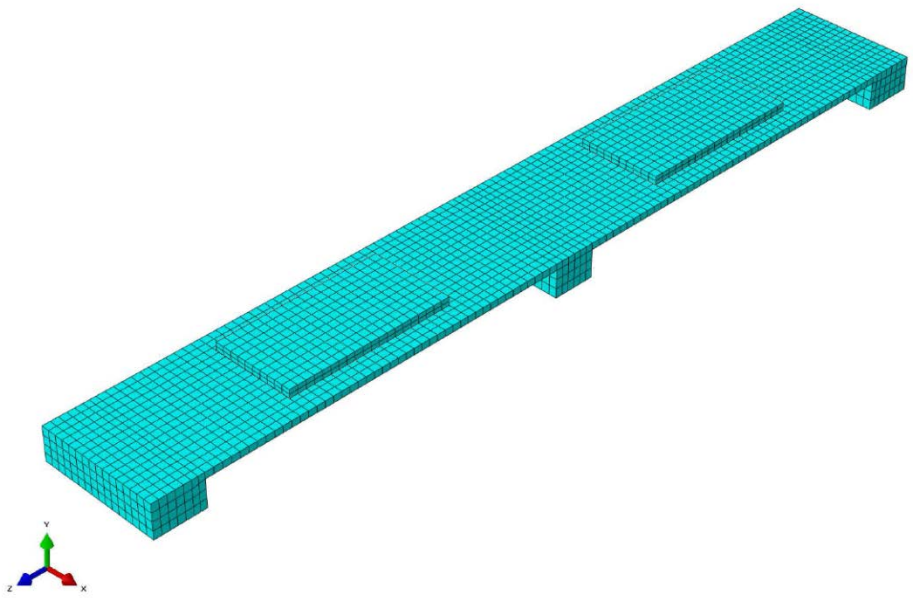

Figure 2.18 Finite Element Model of Specimen 1T2S

The deflected shape of the specimen along with the failure mode is presented in Figure 2.19. The top view and side view of the model is shown in separate figures in Figure 2.20 and 2.21, respectively. Figure 2.22 which illustrate the load-deflection response of the specimen comparing to its counterpart in the experimental tests.

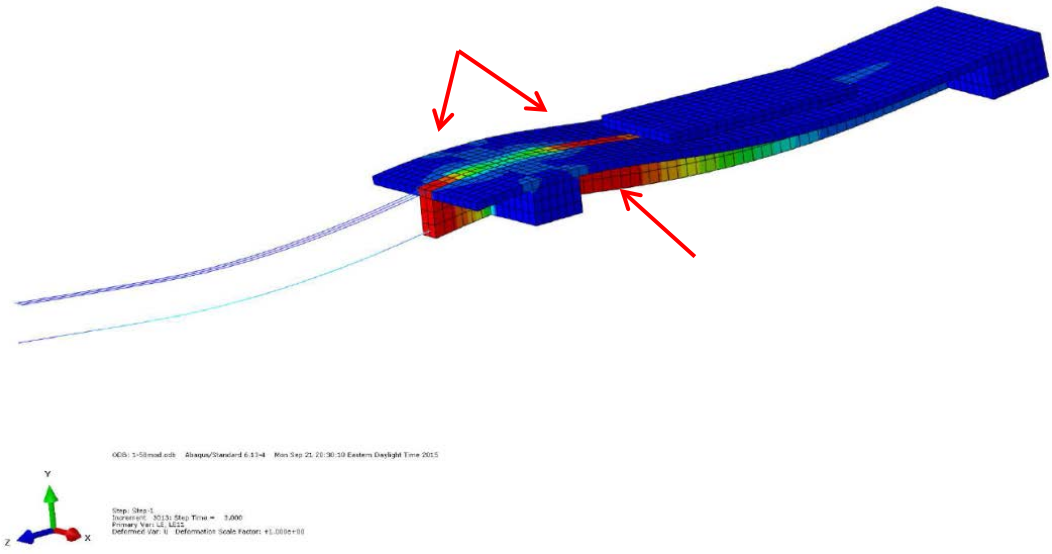

(a)

(b)

Figure 2.19 Failure Modes and Deflected shape of the Specimen 1T2S, (a) FE Modeling, and (b) Failure Modes in Experimental Test

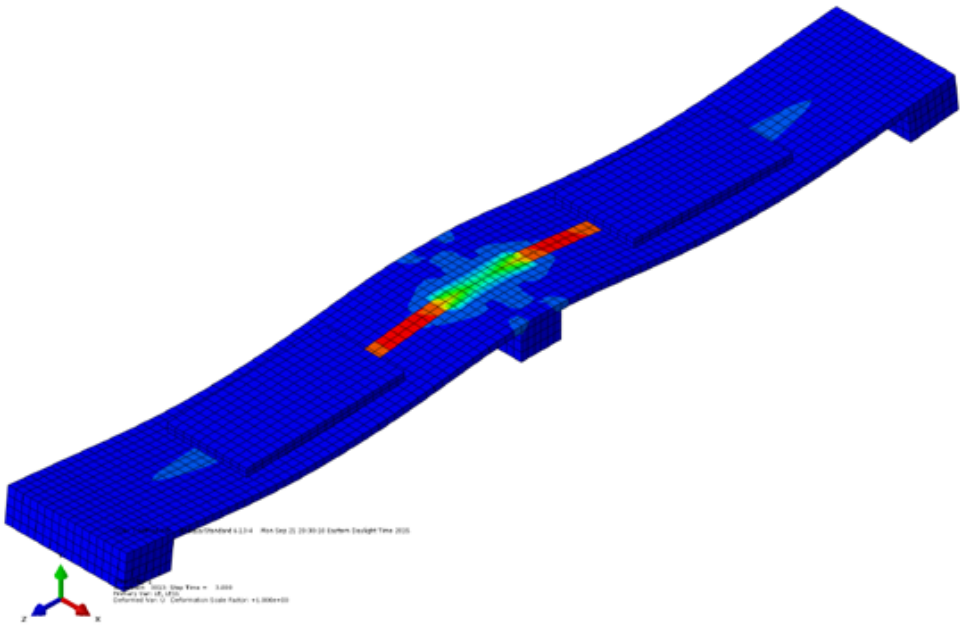

Figure 2.20 Top View of the Deformed Model

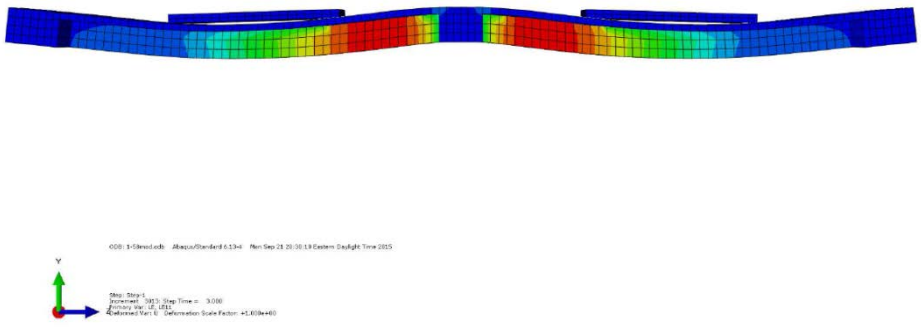

Figure 2.21 Side View of the Deformed Model

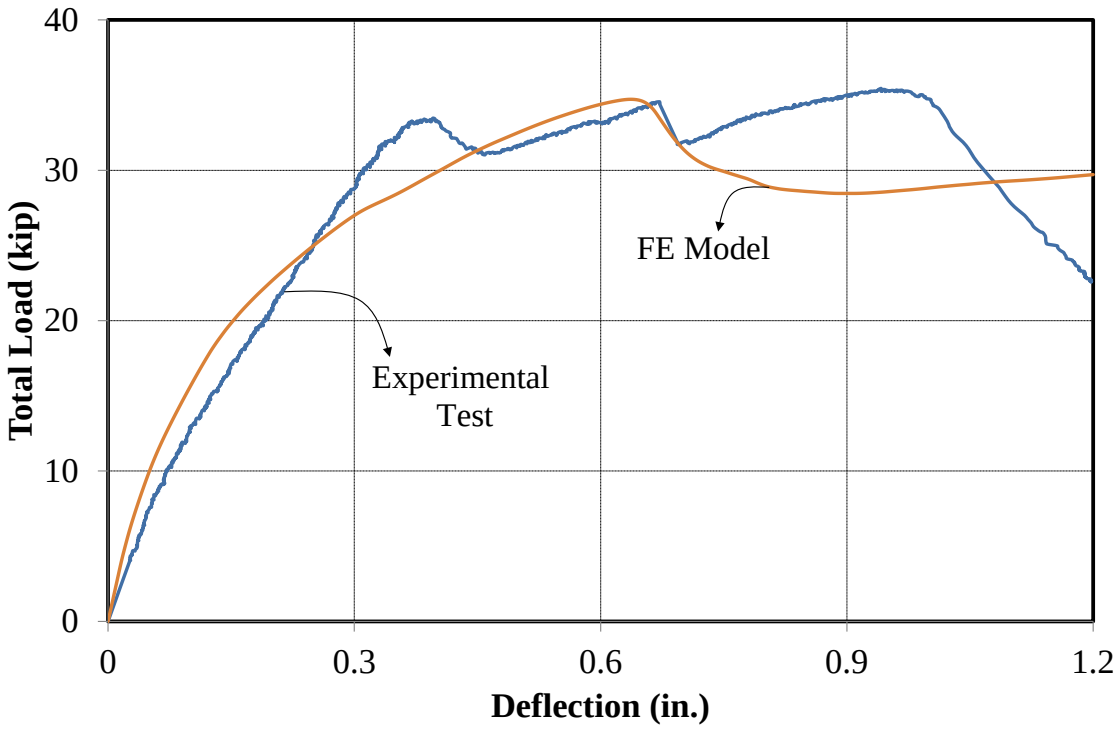

Figure 2.22 Load-Deflection Response of Specimen 1T2S

Figure 2.22 shows a good agreement between the result of the finite element model and the experimental test. Also, the FE model estimates the maximum load so consistent to the experiments.

2.3.5. Modeling and Results for Specimen 4T1S

The finite element model of Specimen 4T1S is shown in Figure 2.23 followed by the deflected shape of the specimen along with the failure mode in Figure 2.24. Figure 2.25 shows the failure mode and shear cracks on the main ribs. Similar cracks are detected on the transverse ribs shown in Figure 2.26. In each case, the finite element results are compared to the corresponding experimental specimen.

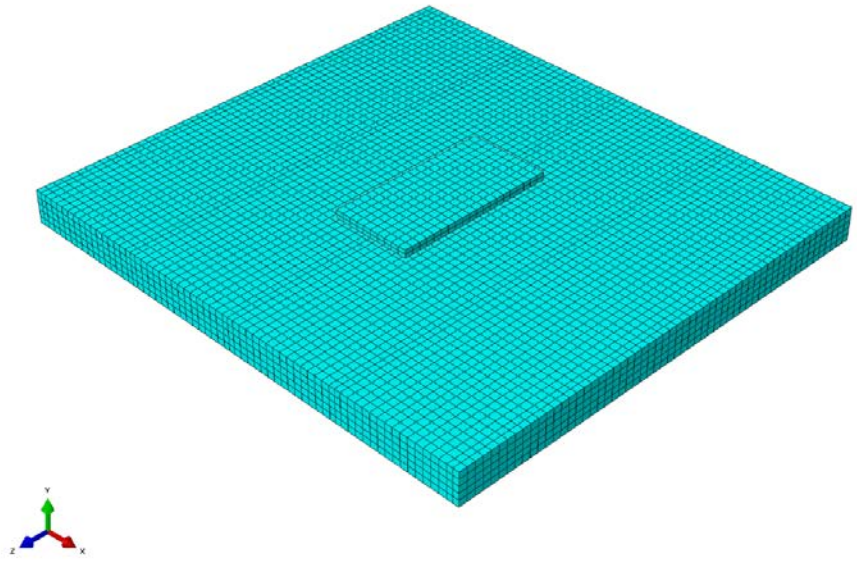

(a)

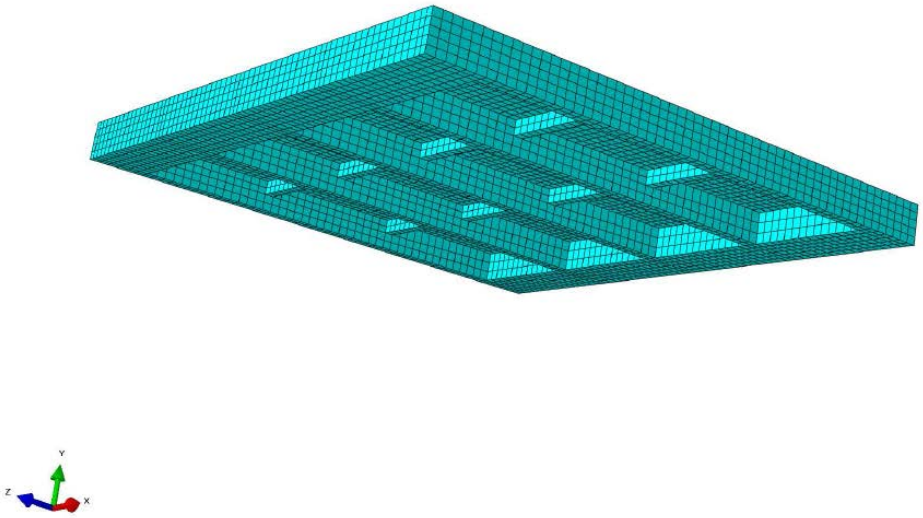

(b)

Figure 2.23 Finite Element Modeling of Specimen 4T1S, (a) Geometry and Mesh, and (b) Modeling of the Main and Transverse Ribs

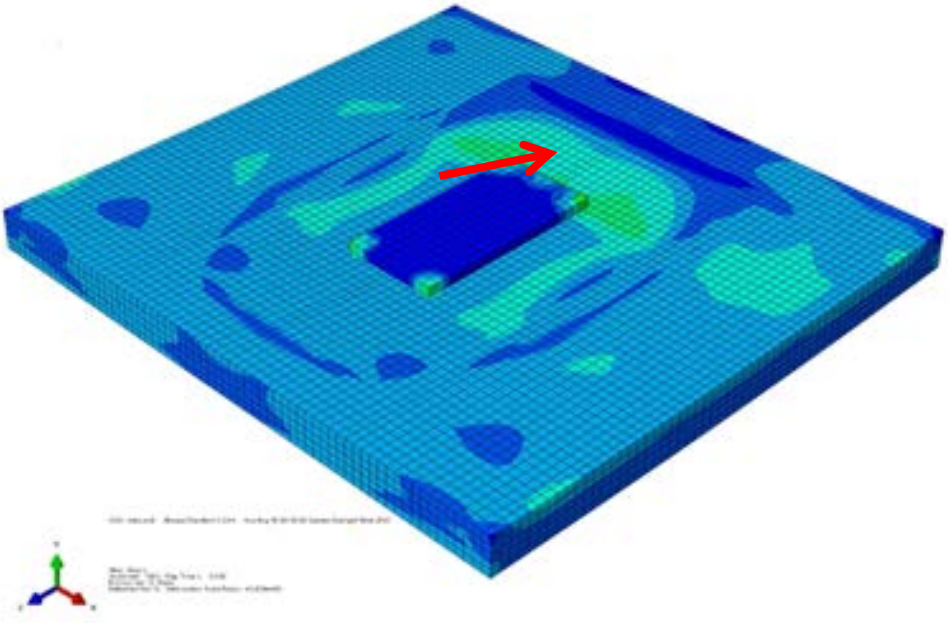

(a)

(b)

Figure 2.24 Failure Modes and Deflected shape of the Specimen 4T1S, (a) FE Modeling, and (b) Failure Modes in Experimental Test

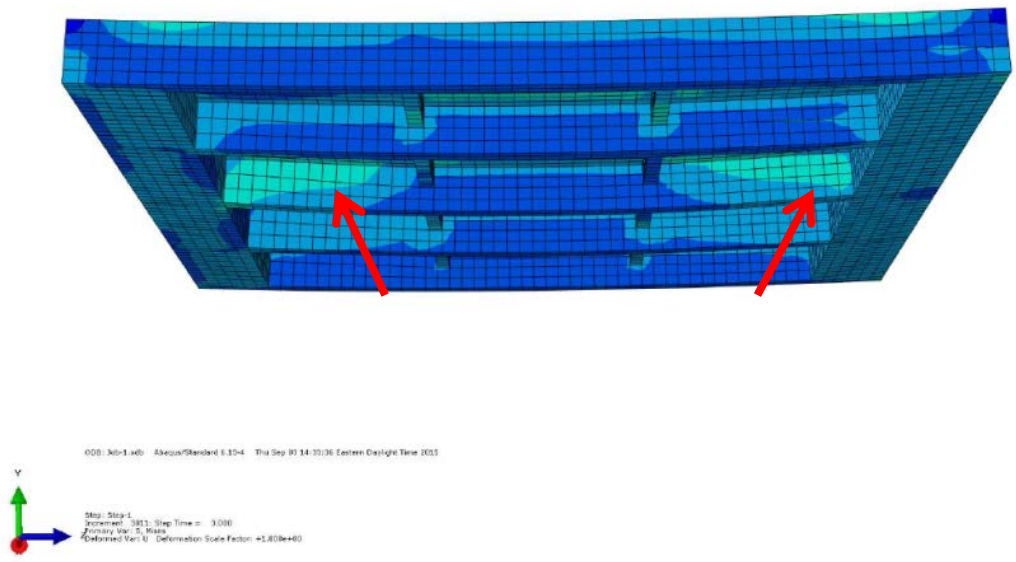

(a)

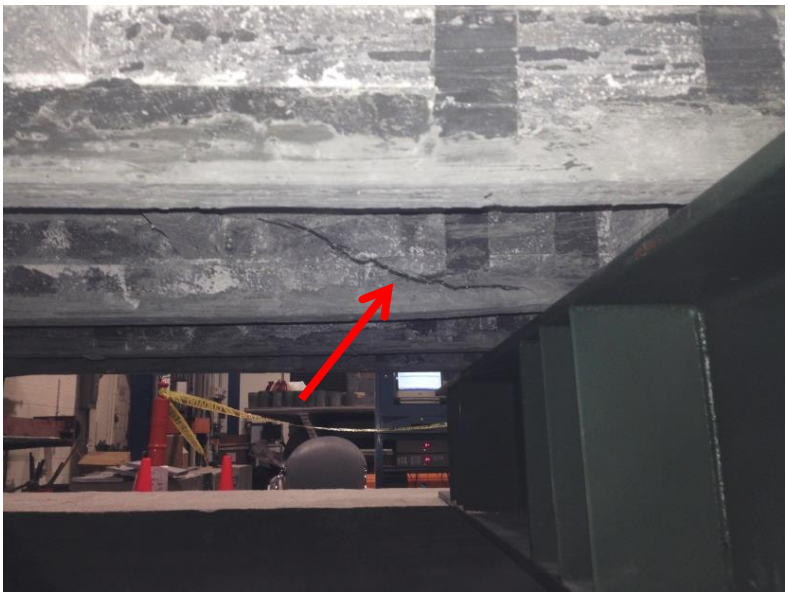

(b)

Figure 2.25 Beam Shear Cracks on the Main Ribs, (a) FE Modeling, and (b) Experimental Test

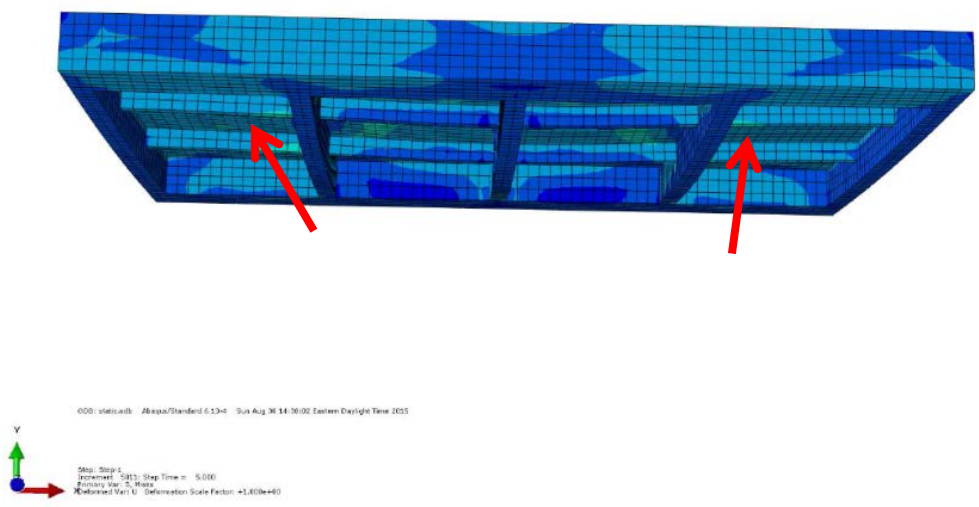

(a)

(b)

Figure 2.26 Beam Shear Cracks on the Transverse Ribs, (a) FE Modeling, and (b) Experimental Test

Figure 2.27 shows the load-deflection response of the finite element modeling of Specimen 4T1S. According to the figure, the finite element model was able to estimate the overall behavior of the experimental specimen.

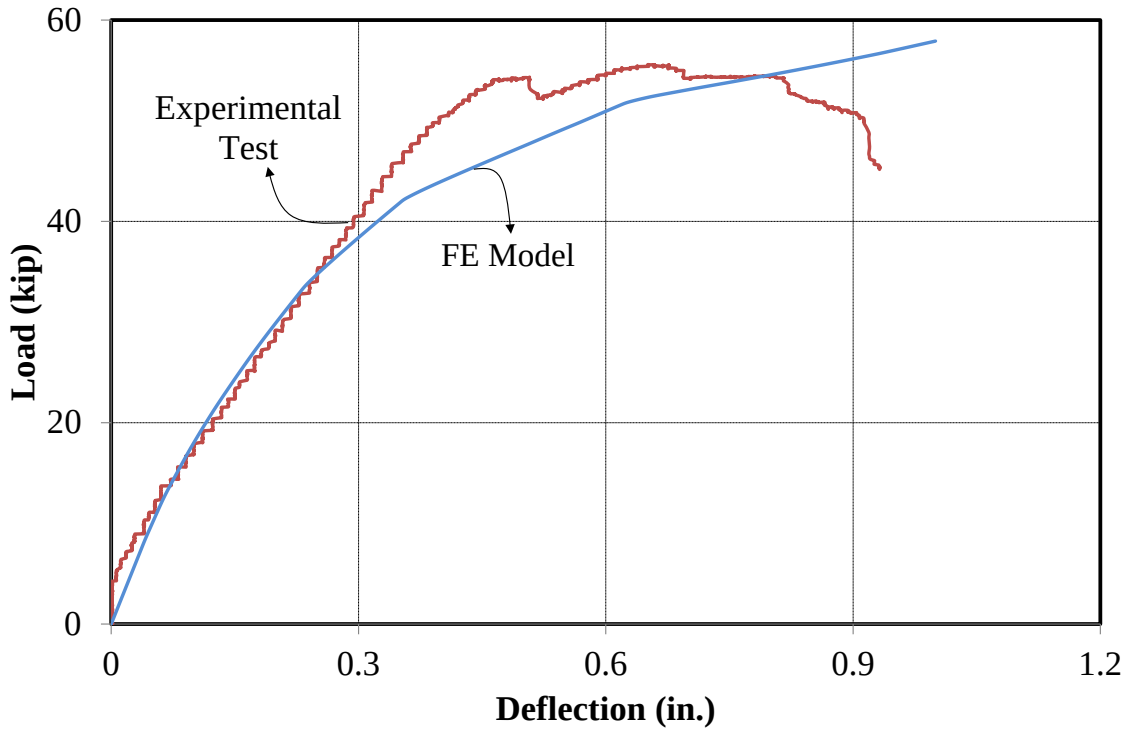

Figure 2.27 Load-Deflection Response of Specimen 4T1S

2.4. Conclusion

A comprehensive experimental study was carried out to develop an optimized lightweight bridge deck system primarily for movable bridges, while it is expected to have extended applications in other bridge deck replacement and widening projects. The objective of the research was to reduce the weight of a recently developed low-profile asymmetric waffle UHPC slab reinforced with HSS rebars. A weight limit of 21 psf was imposed on the bridge deck with a stringer spacing of 4 ft. In a two-step optimization process, both the size and the reinforcement of the deck were modified, reducing the weight by over 37%. Test results showed that the optimized section can suitably meet the

load demand, ductility, and serviceability requirements, while staying within the weight limits for movable bridges.

The main conclusions of this study are as follows:

1. The proposed deck system fails in a clearly ductile manner, despite its apparent shear failure and in the absence of consistent yielding in steel reinforcement.
2. The proposed deck system is not susceptible to punching shear of its thin slab, due to the arrangement of the primary and secondary ribs, which promotes one-way shear of the primary ribs instead.
3. The load distribution for the center rib in the optimized deck is about 33%, very similar to that observed for the original deeper deck.
4. All decks configuration were modeled and finite element analysis was performed to compare the load-deflection responses from the tests with the outcomes of finite element models to examine the ability of the model to predict the overall and components behavior of the decks. The results showed a good agreement between the experimental and analytical results especially. Moreover, the models captured the initial stiffness and estimated the ultimate load, appropriately.

3. A NOVEL UHPC-CFRP WAFFLE DECK PANEL SYSTEM FOR ACCELERATED BRIDGE CONSTRUCTION

3.1. Introduction

At an average age of 42 years, 10% of the nation's 607,380 bridges are posted for load restrictions, with an additional 15% considered structurally deficient or functionally obsolete (ASCE 2013). While there are major concerns with decks in 75% of structurally deficient bridges, often weight and geometry of the deck further limit the load rating and functionality of the bridge. Traditional deck systems and construction methods usually lead to prolonged periods of traffic delays, limiting options for transportation agencies to replace or widen a bridge, especially in urban areas. To address these challenges, as part of its "Highways for LIFE" program, the Federal Highway Administration has promoted accelerated bridge construction using prefabricated elements (Culmo, 2011). One such application was demonstrated in the implementation of a prefabricated ultra-high performance concrete (UHPC) waffle deck system with field-cast UHPC connections (Heimann, 2013), as developed by Aaleti et al. (2011).

Originally developed in the 1990's, UHPC has prevailed as an effective construction material for bridge applications around the world (Hajar et al., 2003). It is composed of high-strength cementitious material, steel fibers, ground quartz, and super plasticizer (Habel et al., 2006) with high compressive and post-cracking tensile strengths and excellent durability (Graybeal, 2011). UHPC makes an ideal material where self-weight is a concern. It has also been recommended as a durable riding surface (Shann,

2012). In order to take full advantage of its high strength, it is more beneficial to combine UHPC with high-strength reinforcement.

As an alternative to open grid steel decks for movable bridges (Mirmiran et al., 2009), Saleem et al. (2011) developed a low-profile asymmetric waffle deck made of UHPC reinforced with high-strength steel (HSS) bars. The asymmetry comes from the arrangement of primary and secondary ribs, respectively perpendicular and parallel to the direction of traffic. Saleem et al. (2011) showed the feasibility of a 5-inch thick UHPC waffle deck with No. 7 HSS bars through a series of tests with single and multiple ribs, and in simple or two-span configurations. The system was further modified by Ghasemi et al. (2015), limiting its overall depth to only 4 inch with No. 5 HSS bars, effectively reducing its weight to below 21 psf, while still meeting the strength and ductility demands for a 4 ft. typical stringer spacing.

Fiber reinforced polymer (FRP) is another advanced material with high strength-to-weight ratio and excellent corrosion resistance. An FRP deck weighs 80% less than a comparable reinforced concrete deck (Mu et al., 2006). Chen and El-Hacha (2011) proposed a hybrid UHPC-FRP beam, made up of a pultruded glass FRP hollow box section with a cast-in-place UHPC layer on top and a carbon FRP sheet bonded along its soffit. Saleem (2011) conducted experiments on a hollow core UHPC deck made with pultruded carbon FRP tubes. Both systems showed potential for combining the excellent properties of FRP and UHPC. Frostlechner (2012) studied flexural behavior of a thin-walled UHPC-GFRP hollow rectangular section, and subsequently made a strong case for

combining UHPC with FRP shapes or FRP reinforcement to fully utilize the benefits of the two advanced materials.

The present study expands the work of Aaleti et al. (2011) and Heimann (2013) on UHPC waffle deck with mild steel reinforcement and the work of Saleem et al. (2011) on low-profile UHPC waffle deck with HSS reinforcement, by (a) significantly reducing the depth and weight of the panels, and (b) replacing the steel reinforcement with carbon FRP (CFRP) bars. It is believed that not only the ultra-high strength of UHPC is best matched with the high strength of CFRP reinforcement for an efficient system, but more importantly, the ductile behavior of UHPC can help mask the linear elastic response of CFRP reinforcement and result in an overall ductile system. This is the first time that UHPC and CFRP reinforcement are combined in an ultra-lightweight super shallow waffle deck for bridge applications. The issues of consideration from the design and constructability perspectives include strength and stiffness, bond and development length for the reinforcement, punching shear and panel action. A series of experiments are conducted to help address these issues for the development of this new type of bridge deck.

3.2. Experimental Work

As depicted through a three-dimensional perspective in Figure 3.1, the proposed waffle deck consists of a very thin slab with primary ribs perpendicular to the direction of traffic, and shallower and less frequent secondary ribs in the direction of traffic. In order to study the behavior of the deck, two groups of specimens were investigated; single-rib and multi-rib specimens. The experiments also aimed at finding the optimal depth of the

panels. Given the size of the specimens, it was important to assess the bond and development length of CFRP bars with UHPC, and if needed, provide appropriate anchorage device.

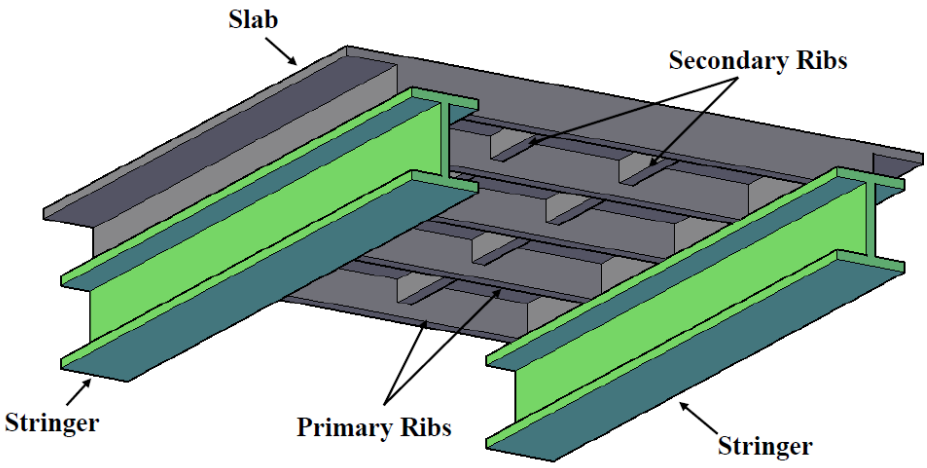

Figure 3.1 Schematic of the Proposed UHPC Waffle Deck System

3.2.1. Test Matrix and Specimen Preparation

Table 3.1 shows the test matrix for this study with two groups of specimens made and tested in two consecutive phases. The specimen names include number of ribs (T), number of spans (S), specimen depth and sample number (if more than one). Group 1 consisted of four single-rib specimens tested in a simple-span configuration, with two identical samples for each of the two depths of 4 and 5 inch (see Figure 3.2). Group 2 included three specimens, all with the same depth of 4 inch, but in three different configurations; single-rib simple-span, single-rib two-span, and multi-rib simple-span (see Figure 3.3). The multi-rib specimen featured 2¾ inch deep transverse ribs to help with load distribution among primary ribs. For comparison, the table also shows three

groups of UHPC waffle deck specimens with HSS reinforcement tested in previous studies (Saleem et al. 2011, Ghasemi et al., 2015).

Table 3.1 Test Matrix

Group	Specimen Name	Test Phase	Overall Depth (in.)	Rib Spacing (in.)	Slab Thickness (in.)	Unit Weight (psf)	28-Day UHPC Compressive Strength (ksi)	Flexural Reinforcement	
								Slab	Primary Rib
UHPC-CFRP									
CFRP-1	1T1S-4#1	1	4	15	¾	18.80	24	No. 3	No. 4
	1T1S-4#2	1					24		
	1T1S-5#1	1	5			21.30	24		
	1T1S-5#2	1					24		
CFRP-2	1T1S-4#3	2	4	15	¾	18.80	27		
	4T1S-4	2					27		
	1T2S-4	2					26		
UHPC-HSS									
HSS-0[1]	1T1S-5#1	0	5	12	1¼	32.37	18	No. 4	No. 7
	1T1S-5#2	0					27		
	4T1S-5	0					26		
	1T2S-5	0					22		
HSS-1[2]	1T1S-4½#1	1	4½	15	¾	21.72	24	No. 3	No. 5
	1T1S-4½#2	1					24		
HSS-2[2]	1T1S-4	2	4	15	¾	20.26	27		
	4T1S	2					27		
	1T2S	2					25		

[1] Taken from Saleem et al. (2011).

[2] Taken from Ghasemi et al. (2015).

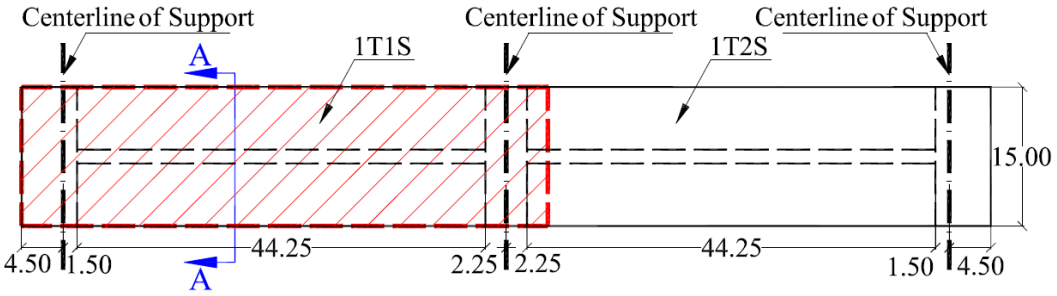

(a)

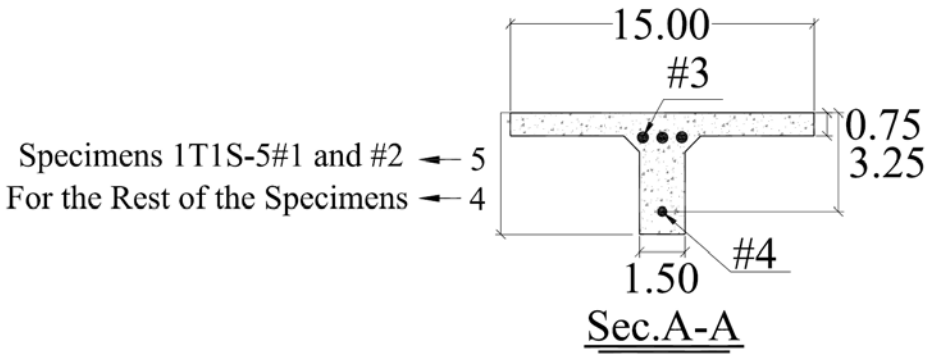

*All measurements are in inch.

(b)

Figure 3.2 Schematics Single-Rib Specimens in Simple-Span or Two-Span Configurations: (a) Plan View, and (b) Section

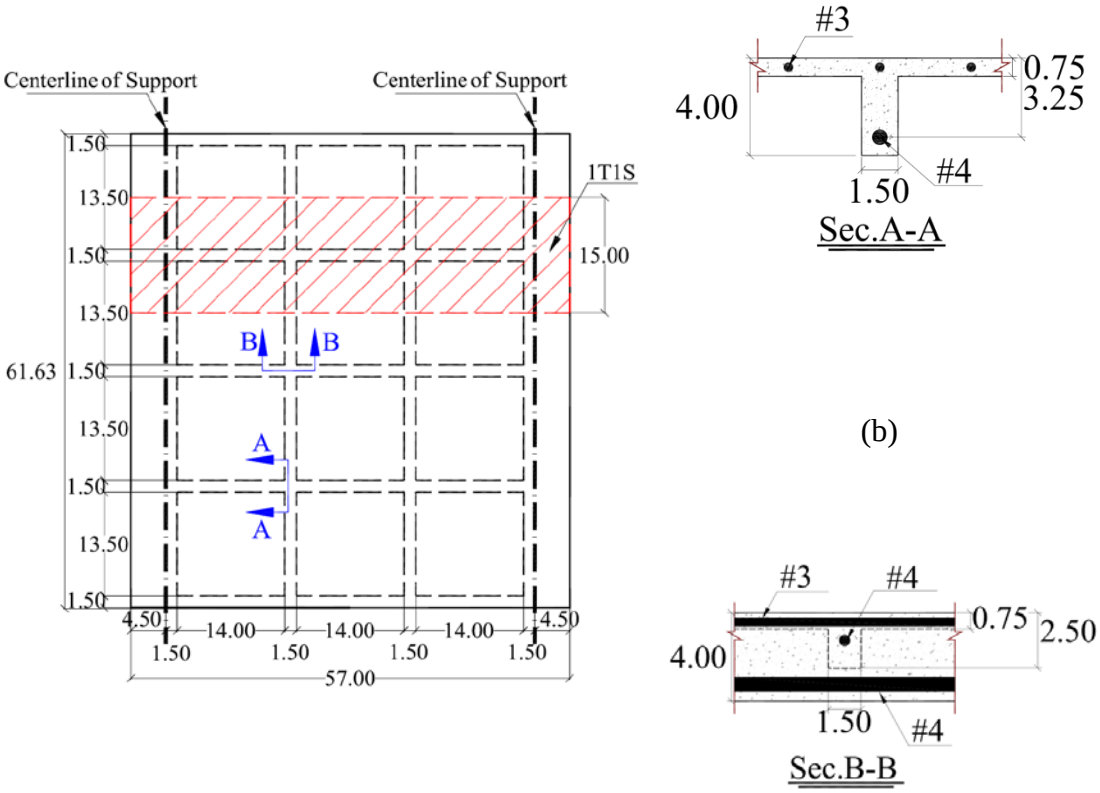

*All measurements are in inch.

Figure 3.3 Schematics of Multi-Rib Simple-Span Specimen: (a) Plan View, and (b) and (c) Sections

Ductal®, a commercially available UHPC product, made by Lafarge North America, was used in this study. It is composed of a premix powder (cement, silica fume, ground quartz and sand), water, superplasticizer, and 2% metallic fibers by volume. The fibers were ½ inch long with a tensile strength of 406 ksi. Six different batches of UHPC were mixed for casting the specimens in formwork made of Styrofoam and timber (see

Figure 3.4). All specimens were air cured in the laboratory for a period of 28 days. Two companion

4 × 8 inch cylinders were used to measure the average 28-day compressive strength of each batch, as shown in Table 3.1.

(a)

(c)

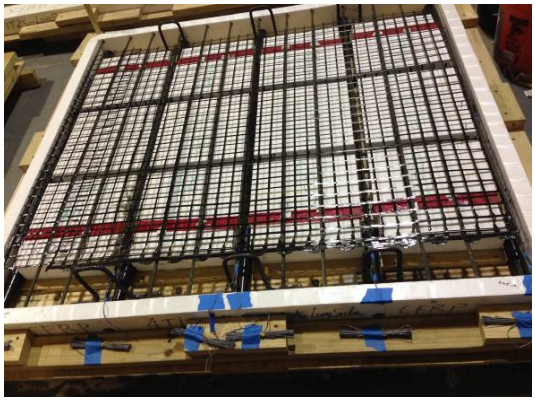

(b)

(d)

Figure 3.4 Specimen Preparation: (a) and (b) Formwork, and (c) and (d) Casting

A C-grid CFRP mesh made by Chomarat of Anderson, SC, was used in the thin slab to improve its load-carrying capacity (see Figure 4b). The mesh has an elastic modulus of 34083 ksi and an ultimate strain of 0.76%. ASLAN 200 CFRP bars made by Hughes Brothers of Seaward, NE, were used as primary reinforcement. A clear cover of ½ inch was maintained for all bars. Table 3.2 lists the geometric and material properties of CFRP bars.

Table 3.2 Geometric and Material Properties of CFRP Bars

Nominal Diameter (in)	**Cross-Sectional Area[1] (in.^{2})**	**Nominal Cross-Sectional Area[2] (in.^{2})**	**Tensile Strength (ksi)**	**Modulus of Elasticity (psi 10^6)**	**Ultimate Strain (%)**
3	0.121	0.110	315	18	1.75
4	0.201	0.196	300	18	1.67

Note: As reported by the manufacturer.

[1] Cross-sectional area determined by immersion testing, as per ASTM D7205, Section 11.2.5.

[2] Cross-sectional area used in tensile strength calculations.

Figure 3.5 shows the anchorage for the main CFRP bars in the specimens of Group 1 as a series of wrapped unidirectional E-glass fiber fabric (SikaWrap Hex 100G), made by Sika Corp. of Lyndhurst, NJ. The GFRP wrap was impregnated using Sikadur 32 Hi-Mod epoxy resin by the same manufacturer, for a total thickness of ¾-inch. The end surface of the wrap was then ground to facilitate monitoring of the bar slippage. As seen in Figure 3.5b, the anchorage was found insufficient to prevent the slippage of

CFRP bar. Therefore, for specimens of Group 2, a more elaborate anchorage system was adopted from Schesser et al. (2013), consisting of a grout-filled steel tube. The tube was sized according to ASTM Standard D7205M (2011) with a 10-inch length, 1½-inch outside diameter and ¼-inch wall thickness. The tube was filled with Bustar, an expansive grout made by Demolition Technologies of Greenville, AL. A wooden frame was made to ensure proper alignment of CFRP bars during the grouting process (Figure 3.6a). A gauge length of ¾-inch was used for the bars, with at least ¼-inch of the bar exposed at each end (Figure 3.6b) to help measure slippage. The ancillary tests, as will be described later, showed no bar slippage for this anchorage system.

(a)

(b)

Figure 3.5 Simple End Anchorage System for CFRP Bars in Phase 1: (a) Grinded End, and (b) Slippage of CFRP Bar

The preliminary design of specimens was conducted using a finite element model. The required live load demands, shown in Table 3.3, were calculated using the equivalent strip method and the deck slab design table (AASHTO LRFD 2013) for each group of

specimens based on the specimen width, load factors, multiple presence factors, dynamic load allowance, and the loading configuration. It should be noted that a similar approach was used by Aaleti and Sritharan (2014) for the design of their UHPC waffle deck system.

(a)

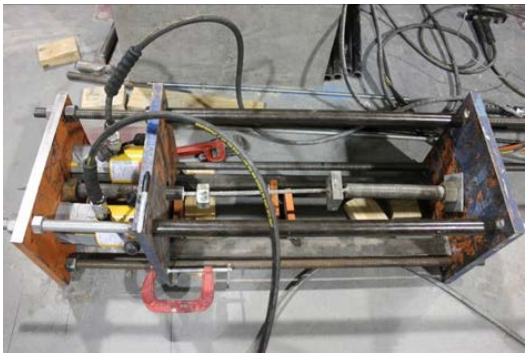

(c)

(b)

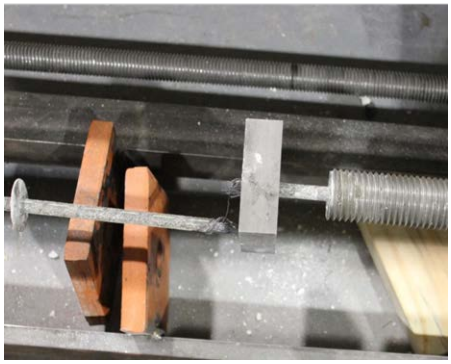

(d)

Figure 3.6 Anchorage System for CFRP Bars in Phase 2: (a) Casting of Expansive Grout, (b) Close-up View, (c) Ancillary Test Setup, and (d) Failure of CFRP Bar

3.2.2. Test Setup and Instrumentation

Figure 3.7a shows the test setup with one of the 1T1S specimens resting on two W24×76 stringers placed at 4 ft. on center on W12×16 floor beams with 3 ft. spacing. This arrangement was designed to simulate the typical superstructure of a movable

bridge. The loading patch of an HS20 truck dual-tire wheel (AASHTO LRFD 2013) was simulated using a 10 × 20 inch steel plate over a neoprene pad. Except for the punching shear test, the loading patch was placed at the center of the span and aligned in the direction of traffic. The simple-span specimens were subjected to a single load at their mid-span (Figures 3.7a and 3.7c), while two equal loads were applied concurrently in the middle of both spans in two-span specimen (Figure 3.7b). At the conclusion of its flexure test, the multi-rib specimen was tested for punching shear in between the first and second ribs with the same loading patch (Figure 3.7d).

Several strain gauges were used to monitor responses of CFRP bars and UHPC at critical locations. String pots were also used to measure deflections of the specimen under each rib. Loading was applied using a 230 kips capacity hydraulic actuator, at an average rate of 0.03 mm/min. The data was recorded at a frequency of 1 Hz, and tests were stopped at around 30% load drop, unless preceded by a clear sign of failure.

Ancillary tests were conducted to assess the performance of anchorage system in CFRP bars of Group 2. Figure 3.6c shows the self-reacting test frame with two 60 kips hydraulic jacks controlled by a single hydraulic pump. The frame was assembled with three 1 inch thick plates of 16 × 24 inch and four No.7 high-strength steel threaded rods.

(a)

(c)

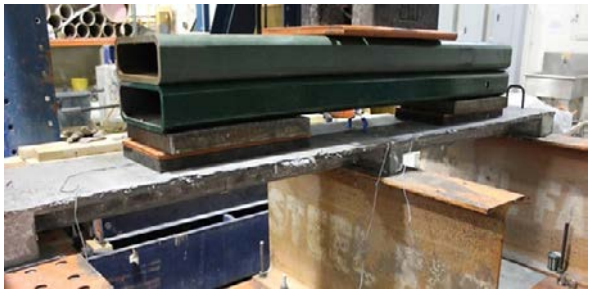

(b)

(d)

Figure 3.7 Setup for Flexure Tests of (a) Specimen 1T1S, (b) Specimen 1T2S, (c) Specimen 4T1S, and (d) Punching Shear Test of Specimen 4T1S

3.2.3. Test Results and Discussion

Table 3.3 shows a summary of test results for the two groups of specimens, as well as results from prior experiments on the UHPC waffle decks with HSS reinforcement (Saleem et al. 2011, and Ghasemi et al. 2015). The table shows the required live load demand for each group of specimens, along with capacity/demand ratio and capacity/demand per unit weight of the deck panel for each specimen. All specimens met their respective demand loads. In the following sections, test results are grouped together for discussion of each performance metric.

Table 3.3 Summary of Test Results

Group	Specimen Name	Overall Depth (in.)	Service Load Deflection (in.)	Ultimate Deflection (in.)	Ultimate Load (kip)	Demand Load (kip)	Capacity/ Demand	Capacity/ Demand per Unit Weight
UHPC-CFRP								
CFRP-1	1T1S-4#1	4	0.54	1.19	16.77	10.25	1.6	0.09
	1T1S-4#2		0.48	1.06	17.15		1.7	0.09
	1T1S-5#1	5	0.37	1.03	21.49		2.1	0.10
	1T1S-5#2		0.35	0.97	19.56		1.9	0.09
CFRP-2	1T1S-4	4	0.45	1.03	18.66		1.8	0.10
	4T1S-4		0.50	0.83	51.26	42.04	1.2	0.06
	1T2S-4		0.19	0.80	26.75	15.65	1.7	0.09
UHPC-HSS								
HSS-0[1]	1T1S-5#1	5	0.06	0.98	40.02	8.21	4.9	0.15
	1T1S-5#2		0.1	0.98	46.99		5.7	0.18
	4T1S-5		0.19	0.79	84.98	34.17	2.5	0.08
	1T2S-5		0.9	1.26	55.08	12.52	4.4	0.14
HSS-1[2]	1T1S-4½#1	4½	0.1	0.83	27.65	10.25	2.7	0.12
	1T1S-4½#1		0.14	0.87	24.73		2.4	0.11
HSS-2[2]	1T1S-4	4	0.15	0.91	22.71		2.2	0.11
	4T1S-4		0.18	0.87	51.48	42.04	1.2	0.06
	1T2S-4		0.07	0.87	44.96	15.65	2.9	0.14

[1] Taken from Saleem et al. (2011).
[2] Taken from Ghasemi et al. (2015).

3.2.3.1 Anchorage of CFRP Bars

Ancillary tests showed the adequacy of steel tube for the anchorage of CGRP bars, as evident by the rupture of the bar with no slippage (Figure 3.6d). On the other hand, the simple GFRP wraps in specimens of Group 1 did not provide adequate anchorage, leading to premature slippage of the CFRP bars (Figure 3.5b), and affecting the overall deflection (Figure 3.8a) and failure mode of deck specimens. The bar slippage was observed in specimens of Group 1 at about half the ultimate load or 80% of the demand load. Based on data from Table 3.3, the average service-level deflection of Specimens 1T1S-102 in Group 1 was about 15% higher than the similar specimen in Group 2. Also, specimens of Group 1 showed a pronounced shear anchorage failure (Figure 3.8b), as compared to the shear-flexure cracks in similar specimen in Group 2 (Figure 3.8c). The tubular anchorage system effectively increased the stiffness and capacity of the deck, and decreased the corresponding deflection. This behavior was quite similar to that observed for UHPC waffle deck specimens in previous studies with HSS reinforcement that were effectively anchored using 180^{o} hooks (Saleem et al. 2011, and Ghasemi et al., 2015).

(a)

(b) (c)

Figure 3.8 Flexure Test and Failure Mode of Specimens 1T1S, (a) Deflected Shape of Specimen 1T1S, (b) Close of View of Beam Shear Crack, and (c) Shear Crack at the Edge of the Loading Pad

3.2.3.2 Flexural Behavior

Figure 3.9 shows the load-deflection responses of the two groups of single-rib simple-span specimens (1T1S) with different depths. For comparison, one response curve is shown for a similar 4-inch deep specimen with HSS reinforcement (Ghasemi et al. 2015). The difference in the latter part of the responses for the two identical 5-inch deep specimens may be attributed to the slippage of the bars occurring at two different load levels of 21.60 and 19.11 kips, respectively, and rather prematurely due to the ineffective

wrapping of CFRP bars in Group 1. Although all specimens clearly exceeded the required demand load, both the stiffness and capacity of the specimen with HSS reinforcement are higher than those with CFRP. On the other hand, Table 3 shows that UHPC decks with CFRP reinforcement provide a more optimal design solution, given their lower capacity/demand ratio and capacity/demand per unit weight of the deck. Table 3.3 also shows measured deflections for each specimen at the levels of service and ultimate loads. The ratio of these two deflection levels indirectly suggests a reasonable ductility for each deck specimen. Figure 3.10 shows load-strain responses of 1T1S specimens, based on strain gauges attached at the mid-span to the CFRP bar in the primary rib. The figure shows a maximum strain of 0.8%, which is less than half of the rupture strain of CFRP bars. As such, ductile behavior of the specimens is attributed mainly to the dowel action of CFRP bars and the fiber pull-out mechanism in UHPC.

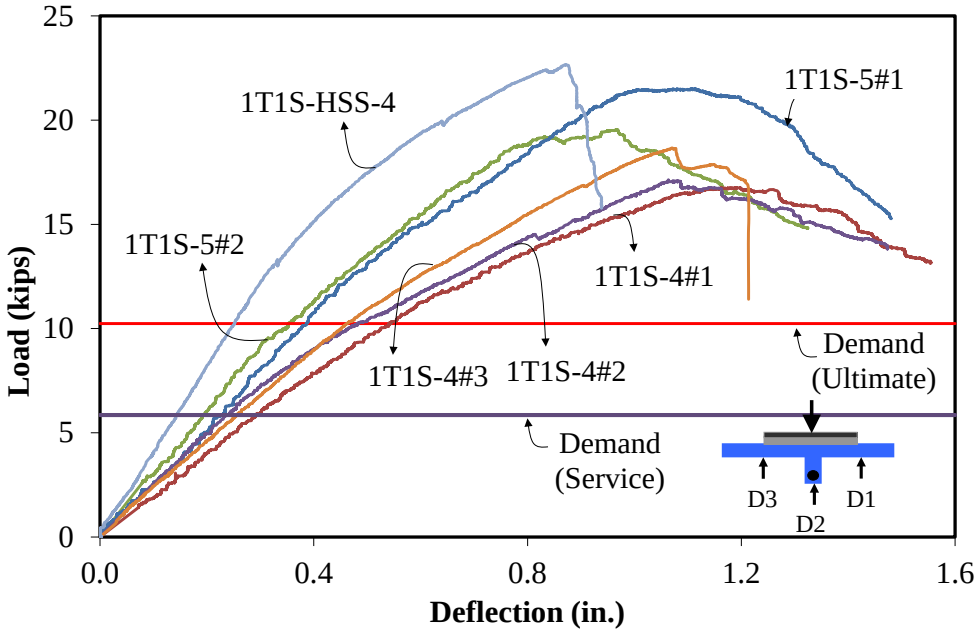

Figure 3.9 Load-Deflection Responses of Specimens 1T1S

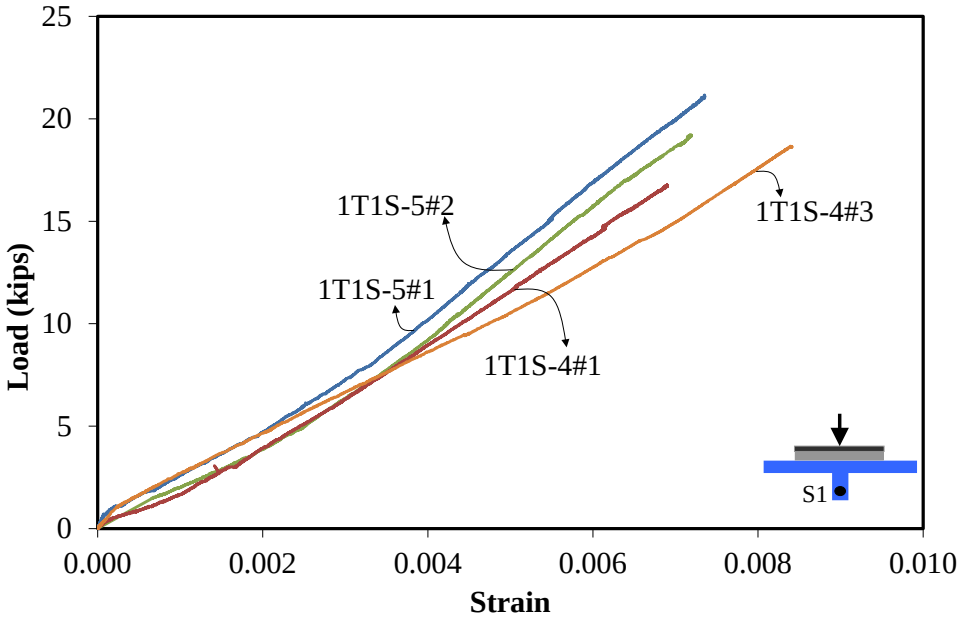

Figure 3.10 Load-Strain Responses of CFRP Bars in Specimens 1T1S

Additional strain gauges were attached to the top surface of the UHPC slab and to the web of the section in order to capture the strain in the UHPC. Test results are shown in **Appendix A**.

3.2.3.3 Panel Action

Figure 3.11 shows the top and bottom views of the multi-rib simple-span Specimen 4T1S after its flexural test, shown in Figure 3.7c. The failure mode was similar to that observed for single-rib specimens. The cracks appeared in the main ribs under the loading patch, and grew in length and width until failure. Figure 3.12 shows the load-deflection responses under each rib for the same specimen. The failure load at 51.26 kips was about 20% higher than the ultimate demand of 41.81 kips. The ductility and plastic deformation, on the other hand, were considerably larger than that observed for the

single-rib specimens. The reason for higher load capacity may be attributed to the presence of additional ribs and their participation in carrying the load through panel action.

For comparison, Figure 3.12 also shows the response curves under each rib for a similar 4 inch deep multi-rib specimen with HSS reinforcement (Ghasemi et al., 2015). It is clear both from the figure and from Table 3.3 that the capacity of the multi-rib specimen is the same with either type of HSS or CFRP reinforcement, while the panel with CFRP bars seems more flexible. Load distribution among the ribs may be calculated based on mid-span deflections of each rib or mid-span strains in CFRP bar in each rib. Using either approach, the load distribution among the ribs is found as 33% for the center rib and 22% and 11% for the next two ribs. These factors are quite similar to those for UHPC-HSS specimens, as reported by Saleem et al. (2011) and Ghasemi et al. (2015).

Figure 3.13 shows load-strain responses of the multi-rib specimen, based on strain gauges attached at the mid-span to the CFRP bar in each rib. The figure shows a maximum strain of 0.6% in the center rib, higher than that observed in single-rib specimens, but still about half of the rupture strain of CFRP bars. Again, the apparent ductile behavior of the specimen may be attributed to the dowel action of CFRP bars and the fiber pull-out mechanism in UHPC. It is clear from both deflection and strain responses in Figures 3.12 and 3.13 that side ribs lose their effectiveness beyond service loads.

(a) (b)

Figure 3.11 Failure Modes in Specimen 4T1S: (a) Top View, and (b) Bottom View

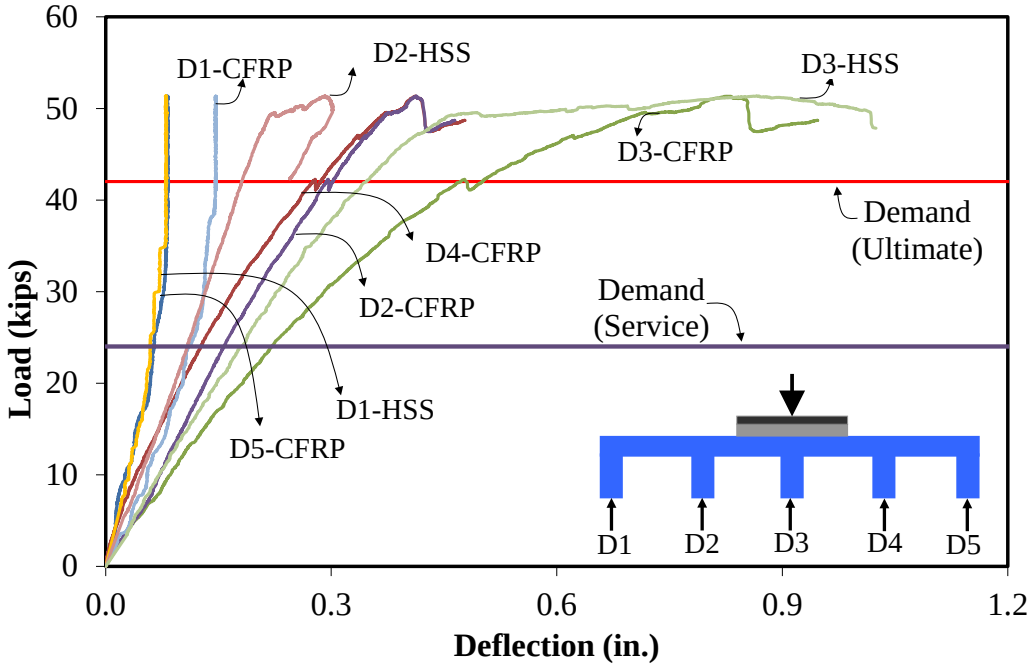

Figure 3.12 Load-Deflection Responses under Each Rib of Specimen 4T1S

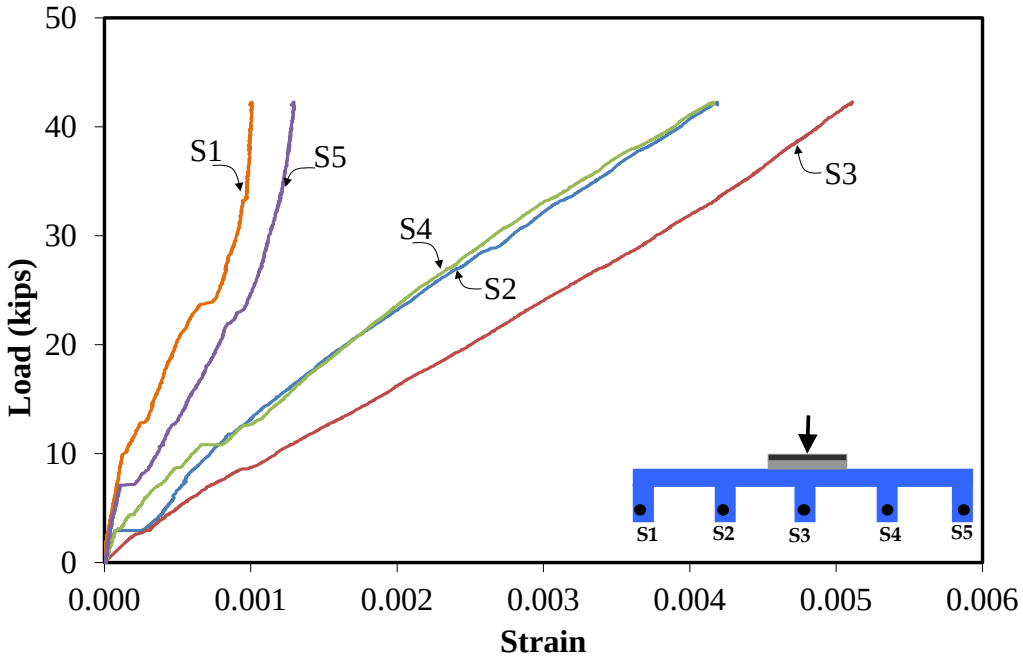

Figure 3.13 Load-Strain Responses of CFRP Bars in Each Rib of Specimen 4T1S

3.2.3.4 Punching Shear

Figure 3.14 shows the punching test and failure mode for Specimen 4T1S at the conclusion of its flexure test, where only the center rib was damaged. The failure was marked by major shear cracks forming in the two ribs adjacent to the loading patch, with no sign of punching. The load-deflection responses under each rib are shown in Figure 3.15, with the maximum deflection occurring right under the loading patch in between the two loaded ribs. It should be noted that the capacity of the specimen under the asymmetric punching was 32.15 kip, which is only 60% of its capacity under symmetric flexural loading (51.25 kip), primarily because of lack of contribution from adjacent ribs that were either damaged or away from the loading patch. Figure 3.15 also shows the response curves of a similar 4-inch-deep multi-rib specimen with HSS reinforcement

(Ghasemi et al., 2015), with clearly higher stiffness and capacity, as compared to UHPC-CFRP deck.

Harris and Roberts-Wollmann (2005) developed an equation which predicts the punching shear capacity of thin UHPC slabs as a modification to the ACI Committee 318 (2011) equation for concrete breakout strength, as

$$V_c = 0.38\, f_{ten} \frac{[(3h + a) \times (3h + b)] - (a \times b)}{\sqrt{h}} \qquad (3.1)$$

where f_{ten} = tensile strength of UHPC, h = thickness of the top thin UHPC slab, and a and b = dimensions of the loading patch. Using a tensile strength of 7.6 MPa for a 254 × 508 mm loading patch, the punching shear capacity of the 19 mm slab may be calculated as 31 kN, which is considerably lower than its measured capacity of 143 kN. This comparison justifies the earlier observation that the specimen did not fail in punching shear.

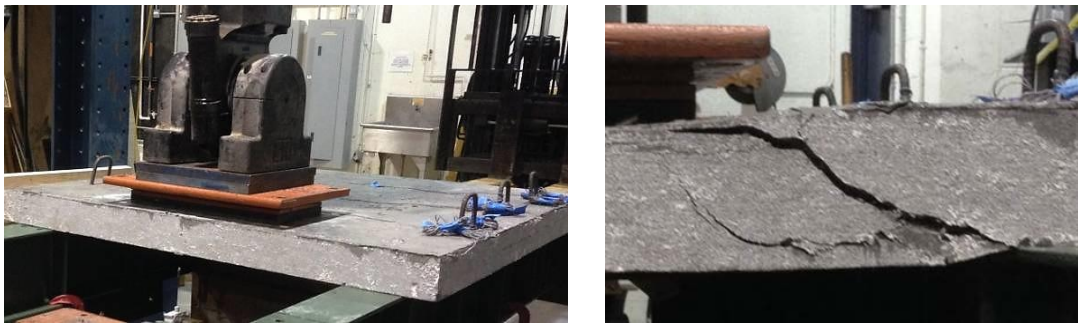

(a) (b)

Figure 3.14 Punching Shear Test and Failure Mode in Specimens 4T1S

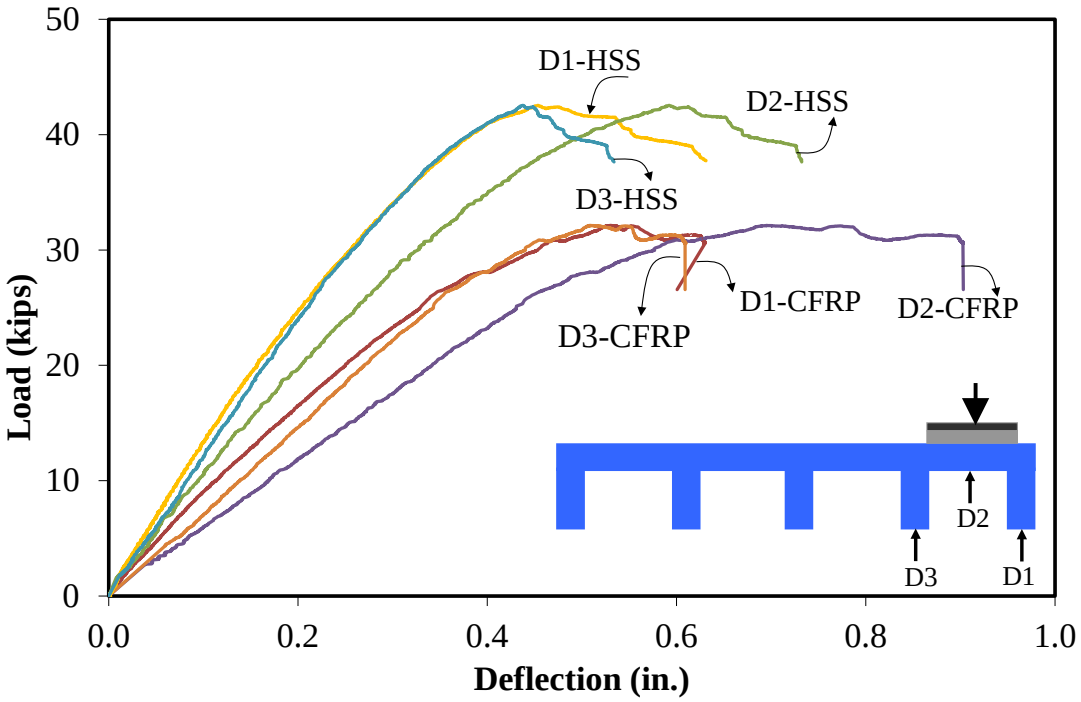

Figure 3.15 Load-Deflection Responses of Specimen 4T1S in Punching Shear

3.2.3.5 Continuity Effect

The behavior of the deck system in negative moment region was investigated by testing a single-rib two-span specimen, as shown in Figure 3.16. Shear in the main ribs near the support was seemingly the predominant mode of failure, similar to that observed in simple-span specimens. The shear cracks initiated in the web in one span and moved towards the top slab. Figure 3.17 shows the load-deflection responses of the specimen along with those of a similar specimen with HSS reinforcement tested in previous studies earlier by Ghasemi et al. (2015). At 26.75 kips, the capacity of the specimen with CFRP reinforcement was 70% higher than the required demand of 15.65 kips, although only 60% of the capacity of similar specimen with HSS reinforcement (i.e., 44.96 kips). Both

types of reinforcement resulted in a ductile response for the deck. It is also noteworthy that the capacity of Specimen 1T2S was 26.75 kips or 43% higher than that of Specimen 1T1S at 18.66 kips, which may be attributed to the continuity effect. Figure 3.18 shows the load-strain responses of CFRP bar at the middle of both spans. The maximum strain is about 1/3 of the rupture strain of CFRP bar.

Table 3.3 lists the deflection of Specimen 1T2S at the level of service load as 0.19 inch, which corresponds to L/254, where L = center to center spacing of stringers, which was 4 ft. Considering a modification factor of 0.74 comparing the deflections of two-span and five-span decks under two wheel loads, the modified deflection becomes L/343, which is about twice the deflection limit of L/800 (AASHTO LRFD 2013). It should be noted that continuity effect remains constant beyond five spans. It is also noteworthy that UHPC deck with HSS reinforcement has a modified deflection of L/914.

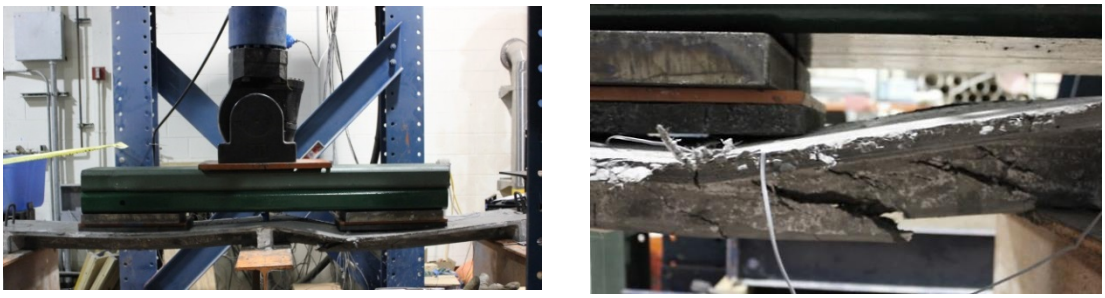

(a) (b)

Figure 3.16 Failure Mode of Specimen 1T2S: (a) Deflected Shape, and (b) Shear Crack

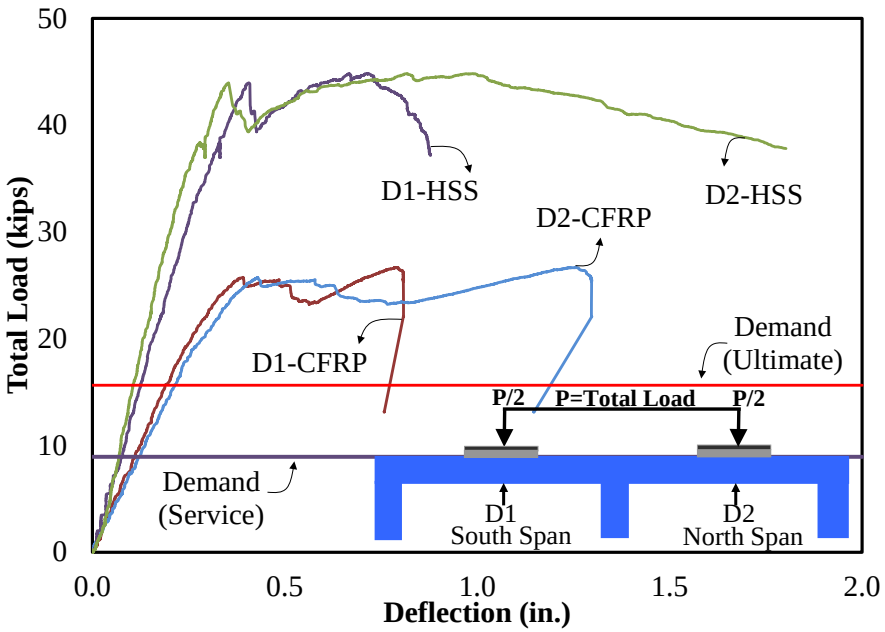

Figure 3.17 Load-Deflection Responses of Specimens 1T2S

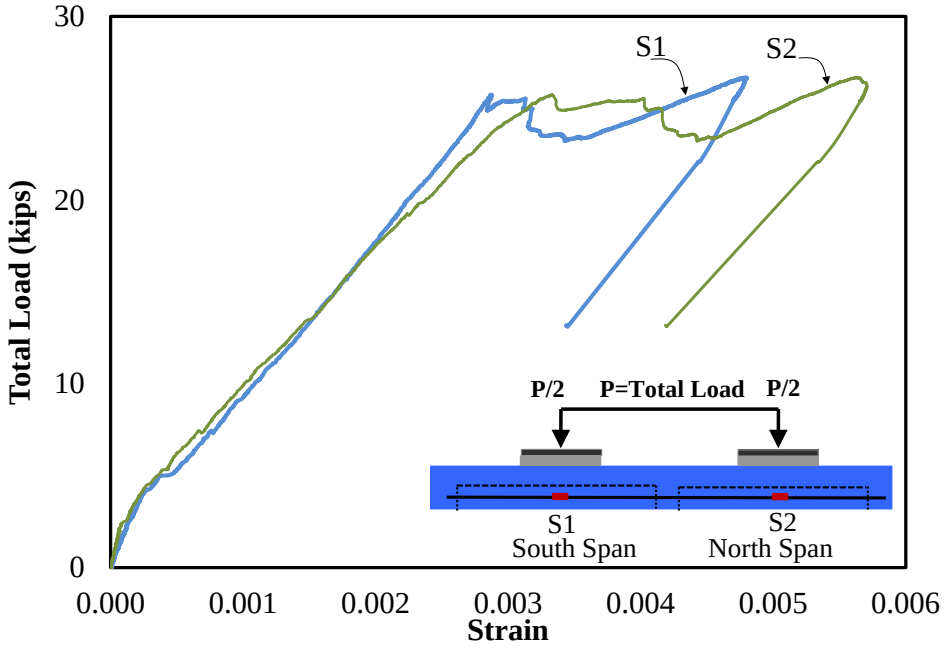

Figure 3.18 Load-Strain Responses of CFRP Bar in Specimen 1T2S

3.3. Finite Element Modeling

3.3.1. General Modeling

Similar to Section 2.3, all UHPC-CFRP specimens were modeled in ABAQUS finite element software. The geometry and material input is the same as explained in Section 2.3.1. The material properties for CFRP bars are shown in Table 3.2, taken from manufacturer data sheet.

3.3.2. Modeling and Results for 1T1S Section

The Geometry, mesh and boundary conditions of 1T1S-CFRP are the same as Section 2.3.3. Figure 3.19 shows the deflected model as compared to the tested specimen. As seen in the figure, the failure mode is the beam shear crack next to the supports which determined the good consistency in the modes of failure between the FE model and the tested specimen. The Load-Deflection response of the specimen is shown in Figure 3.20 which is compared to the corresponding experimental test. It can be noticed that the finite element results showed a good agreement with the tests results although the model underestimate the load capacity for 1.75 kips which may be a result for the value for the shear strength in the modeling.

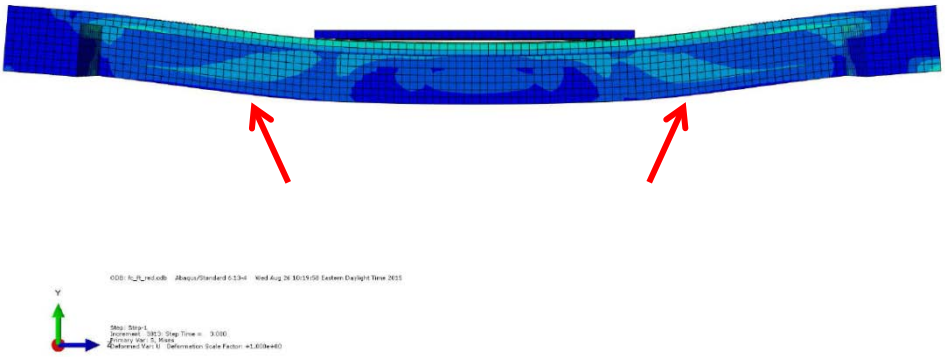

(a)

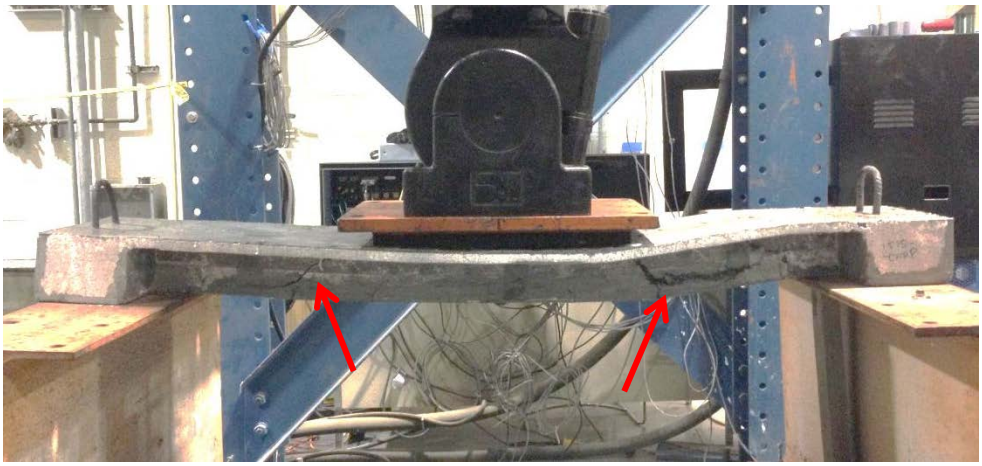

(b)

Figure 3.19 Failure Modes and Deflected shape of the Specimen 1T1S, (a) FE Modeling, and (b) Failure Mode in Experimental Test

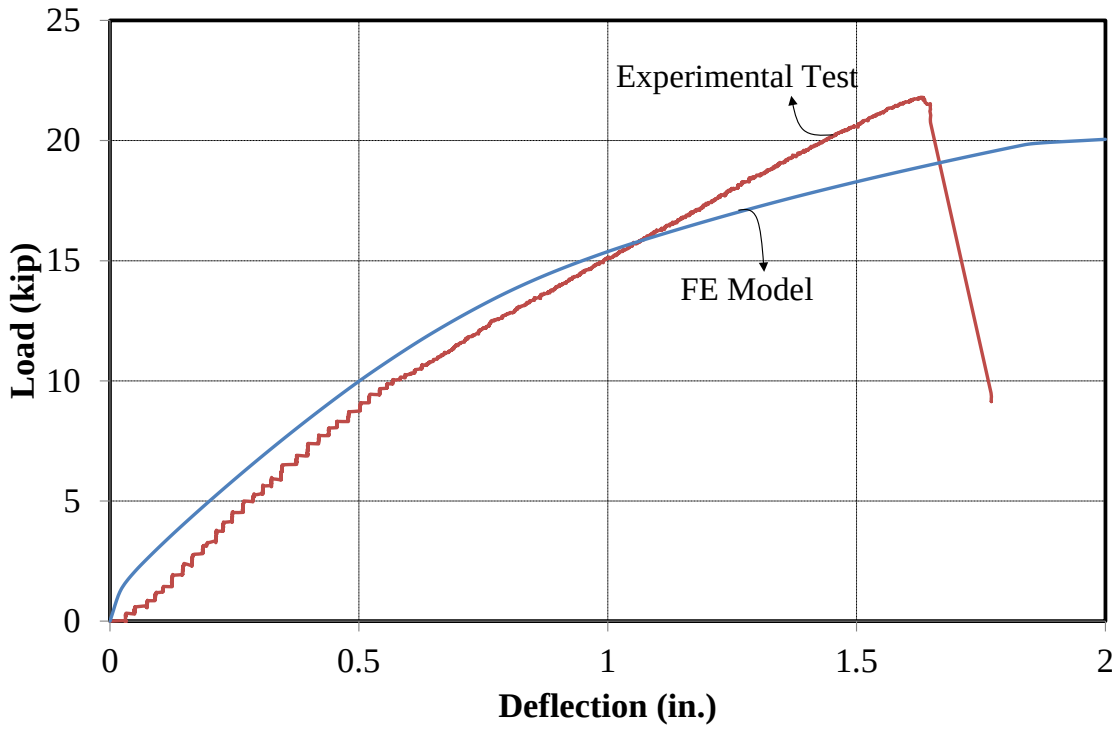

Figure 3.20 Load-Deflection Response of Model 1T1S

3.3.3. Modeling and Results for 1T2S Section

The finite element model for 1T2S specimens is the same as described in Section 2.3.4. The deflected shape of the specimen along with the failure mode is presented in Figure 3.21. The top view and side view of the model is shown in separate figures in Figure 3.22 and 3.23, respectively. Figure 3.24 which illustrate the load-deflection response of the specimen comparing to its counterpart in the experimental tests.

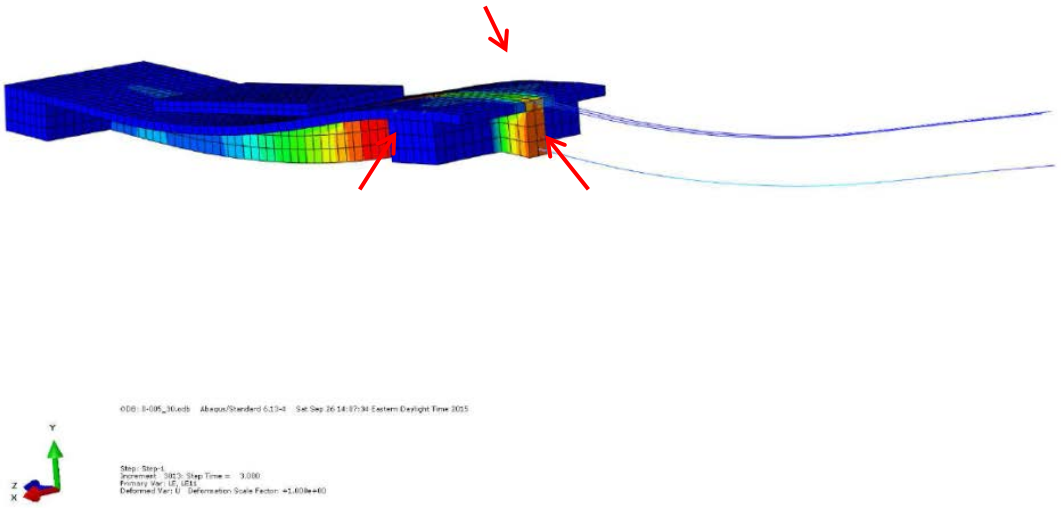

(a)

(b) (c)

Figure 3.21 Failure Modes and Deflected shape of the Specimen 1T2S, (a) FE Modeling, (b) Crack on the Slab, and (c) Shear Cracks on the Web

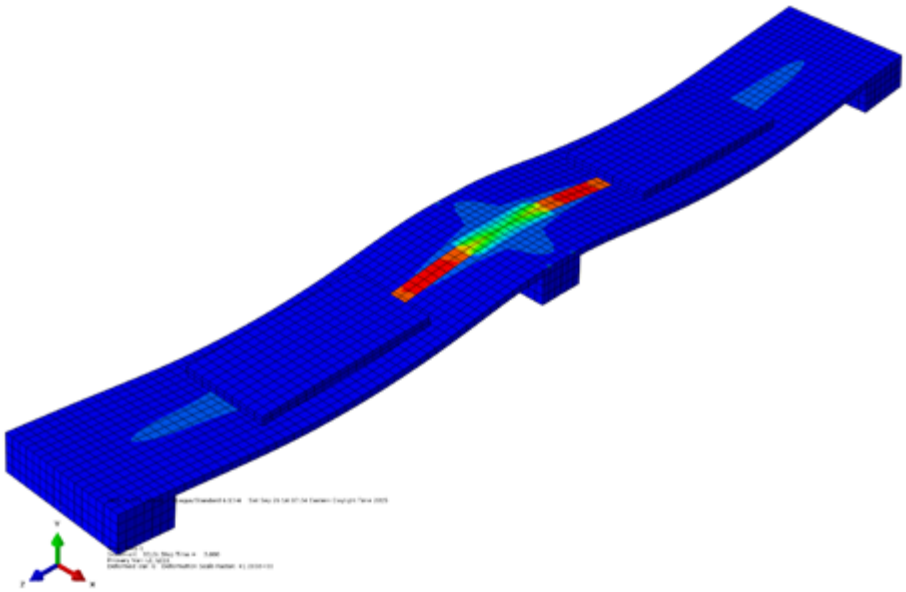

Figure 3.22 Top View of the Deformed Model

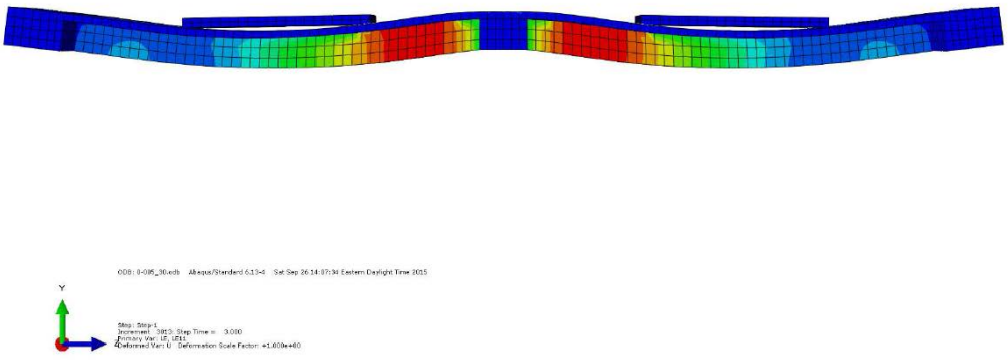

Figure 3.23 Side View of the Deformed Model

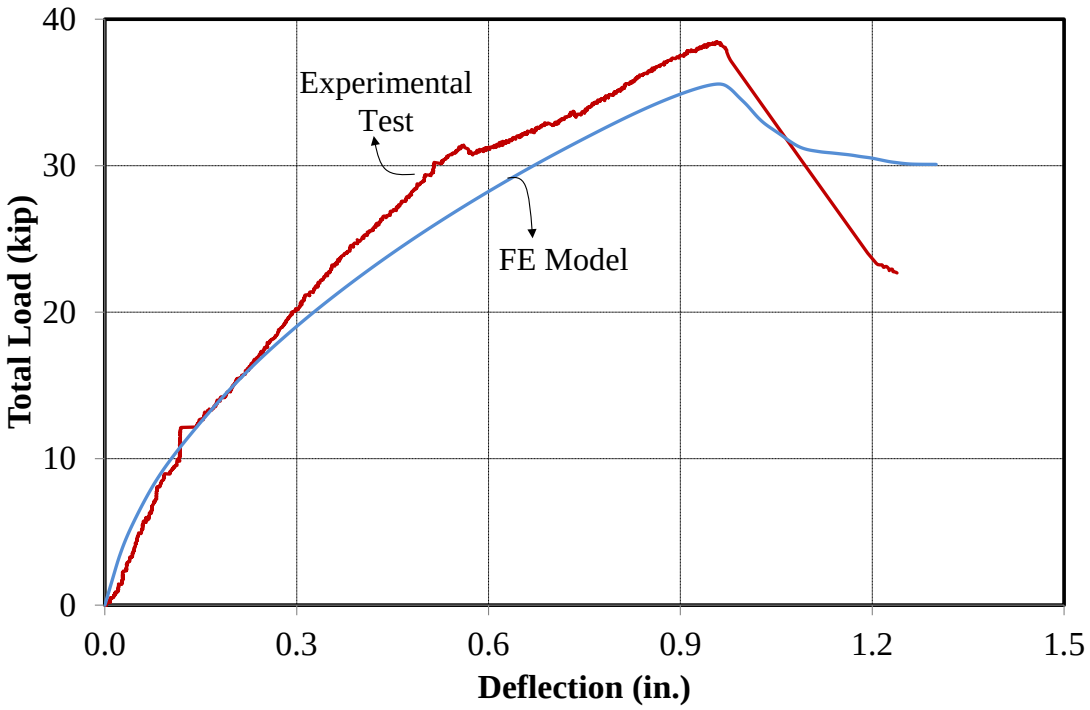

Figure 3.24 Load-Deflection Response of Specimen 1T2S

Although the Figure underestimate the maximum load for about 7% , it still shows a good agreement with the result of the experiments.

3.3.4. Modeling and Results for 4T1S Section

The finite element model for Specimen 4T1S is the same as described in Section 2.3.5. Following the same procedure, Figure 3.25 Shows the failure mode and cracks on the slab. The shear cracks on the main ribs are illustrated in Figure 3.26. Similar cracks are detected on the transverse ribs shown in Figure 3.27. In each case, the finite element results are compared to the corresponding experimental specimen.

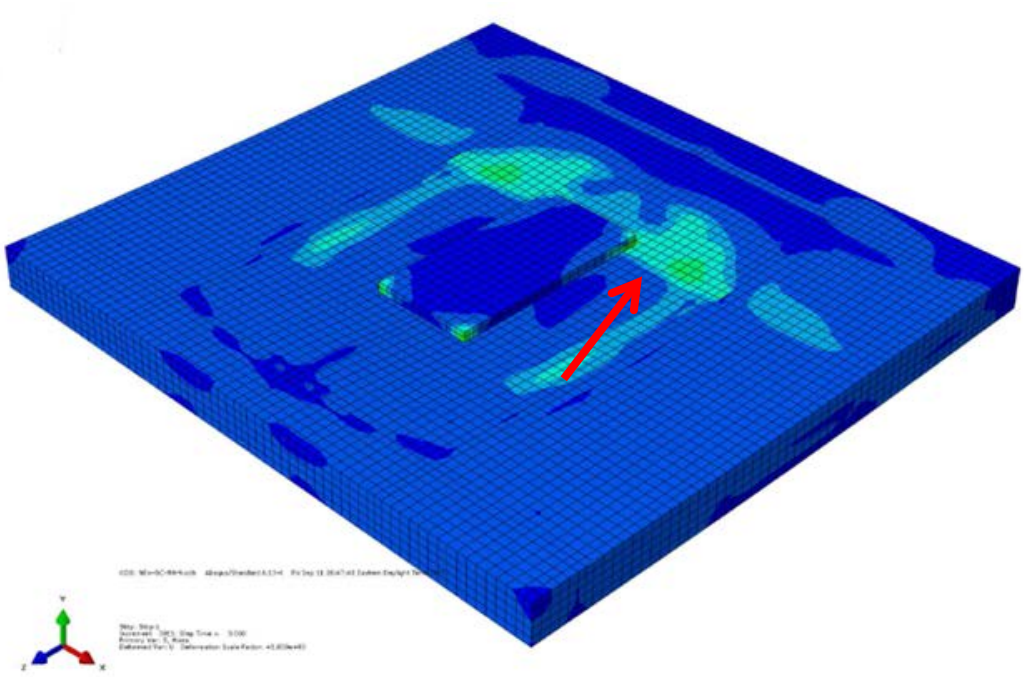

(a)

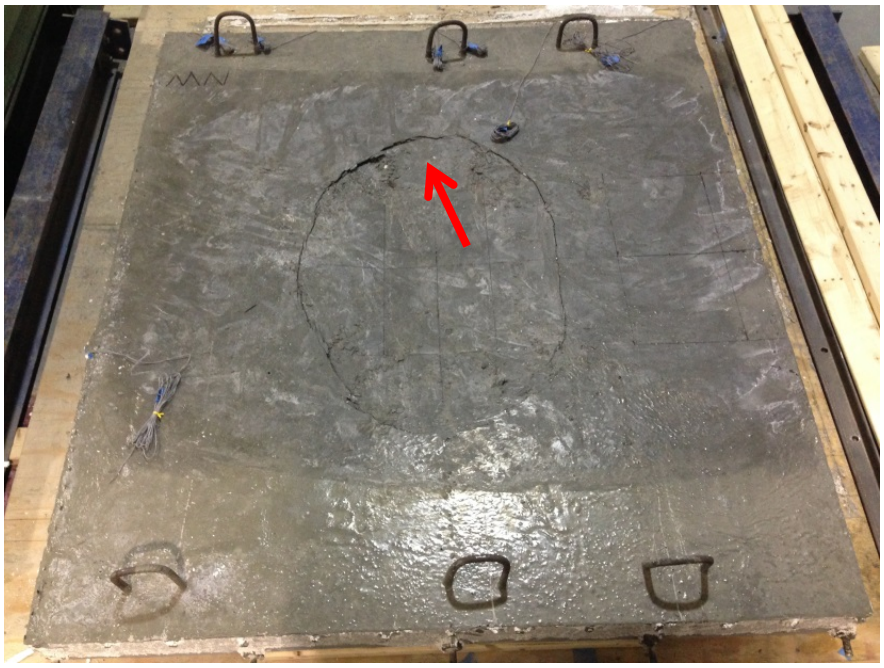

(b)

Figure 3.25 Failure Modes and Deflected shape of the Specimen 4T1S, (a) FE Modeling, and (b) Failure Modes in Experimental Test

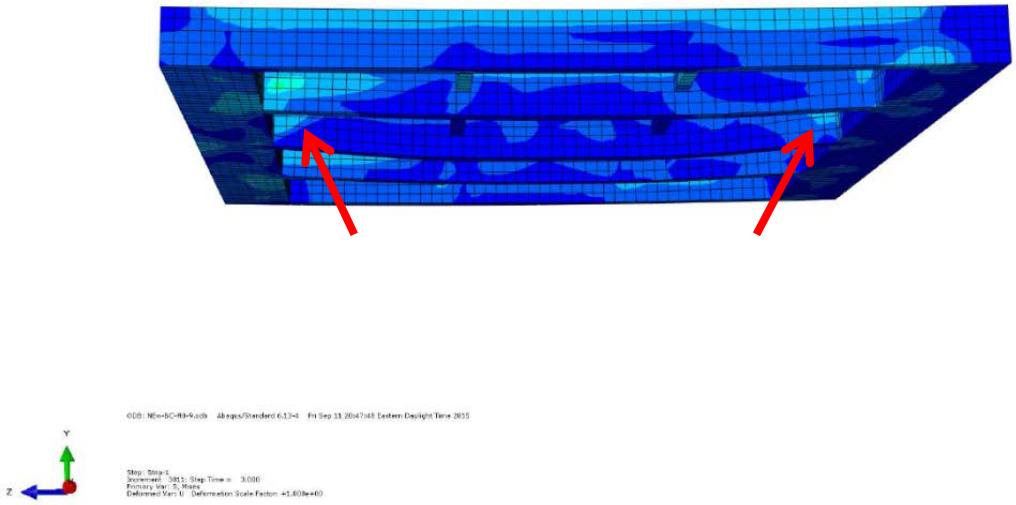

(a)

(b)

Figure 3.26 Beam Shear Cracks on the Main Ribs, (a) FE Modeling, and (b) Experimental Test

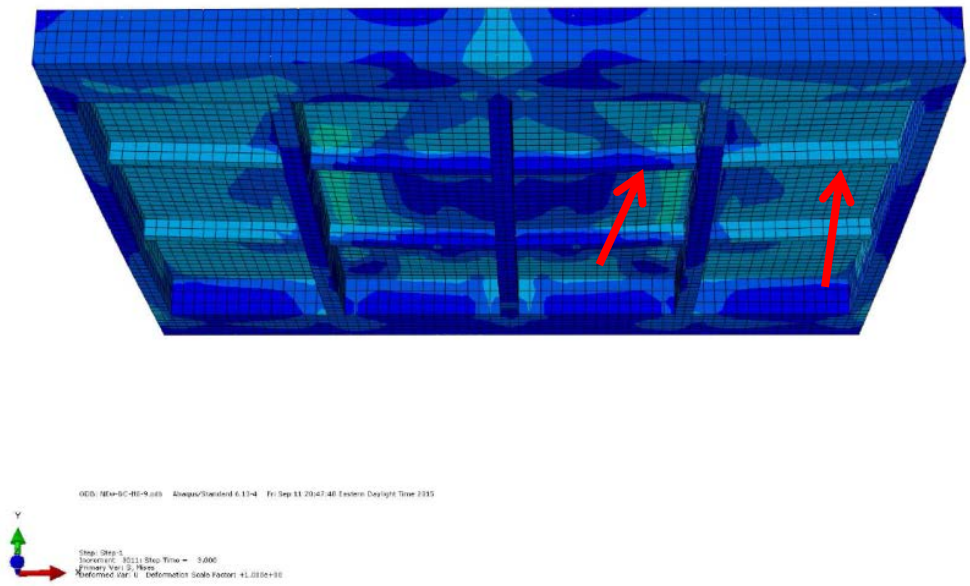

(a)

(b)

Figure 3.27 Beam Shear Cracks on the Transverse Ribs, (a) FE Modeling, and (b) Experimental Test

Figure 3.28 shows the load-deflection response of the finite element modeling of Specimen 4T1S. According to the figure, the finite element model was able to estimate the overall behavior of the experimental specimen.

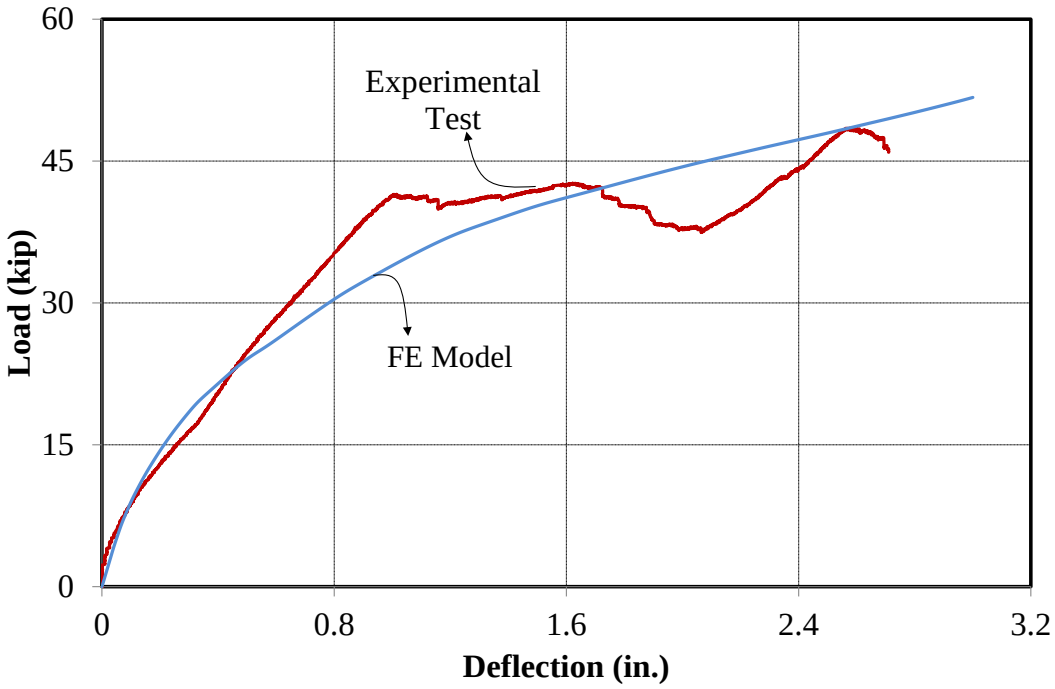

Figure 3.28 Load-Deflection Response of Specimen 4T1S

3.4. Conclusion

An innovative deck system is proposed for accelerated bridge construction, using ultra high performance concrete (UHPC) in the form of an ultra-lightweight super-shallow waffle slab reinforced with carbon fiber reinforced polymer (CFRP) bars. The novel combination of the two advanced materials leads to a deck panel with only 4 inch overall depth and only 18.80 psf self-weight, while still meeting the load demands for a 4 ft. typical stringer spacing. In this study, seven specimens with two different overall

depths, with single or multiple ribs, and in simple or two-span configuration were tested in two consecutive phases. The following conclusions can be drawn from this study:

- The experiments confirmed the feasibility of the proposed deck system, and its comparable performance to a similar deck using high-strength steel reinforcement.
- The proposed deck is not susceptible to punching shear of its thin slab, due to the arrangement of the primary and secondary ribs, which promotes one-way shear of the primary ribs instead.
- The proposed deck system fails in a ductile manner, despite its apparent shear failure and in the absence of yielding of the reinforcement. The ductility stems from dowel action of CFRP bars and the fiber pull-out of UHPC.
- Load distribution among the ribs, whether calculated based on deflections or strains, are quite similar to those for UHPC-HSS specimens. The load distribution for the center rib is 33%, with the next two adjacent ribs at 22% and 11%, respectively.
- All UHPC-CFRP decks were modeled in ABAQUS. The finite element simulation output was compared to the load-deflection responses from the test. It appears that the results between the experimental and analytical were so close in both the initial stiffness and the estimated ultimate load.

4. ACCELERATED PAVEMENT TESTING

4.1. Introduction

Based on static testing conducted in the lab, the UHPC waffle deck system has shown great promise as a viable alternative to open grid steel decks. In order to evaluate the long-term performance of the UHPC deck panels under field conditions, it was decided to test the system at the Accelerated Pavement Testing (APT) facility in Gainesville under the Heavy Vehicle Simulator (HVS). It is proposed that four lightweight bridge deck panels and their connections to each other and the stringers be tested under the dynamic impact of wheel load as described in this chapter.

4.2. Experimental Work

Due to the geometry and configuration of the testing pit, the depth of the deck section needed to be 5 inch, which is different from the optimized depth of 4 inch as described in previous chapters. In order to have a better understanding of the behavior of the section with 5-inch depth under HVS loading, six laboratory specimens were built for the purpose of sizing through static tests with single and multiple ribs in simple and double span configurations. The results of recent tests were then compared to those of previous tests, as described in the following sections.

4.2.1. Test Matrix and Specimen Preparation

Table 4.1 shows the test matrix for this study. The specimen names include number of ribs (T), number of spans (S), specimen depth and sample number (if more than one). All specimens have the same depth of 5 inch, but in three different configurations, single-rib simple-span, single-rib two-span, and multi-rib simple-span (see Figures 2.1, 2.2, 3.2, and 3.3). The multi-rib specimen featured 2¾-inch-deep transverse ribs to help with load distribution among primary ribs. For comparison, the table also shows all UHPC waffle deck specimens with HSS and CFRP reinforcement tested in all previous studies (Saleem et al. 2011, Ghasemi et al., 2015).

4.2.2. Test Setup and Instrumentation

The test setup and instrumentation is similar to Sections 2.2.2, 2.2.3, and 3.2.2.

4.2.3. Test Results and Discussion

Table 4.2 shows a summary of test results for the current studies along with the results from prior experiments on the UHPC waffle decks with HSS and CFRP reinforcement (Saleem et al. 2011, and Ghasemi et al., 2015). The table shows the required live load demand for each group of specimens, along with capacity/demand ratio and capacity/demand per unit weight of the deck panel for each specimen. In the following sections, test results for each group of specimens are presented.

Table 4.1 Test Matrix

Group	Specimen Name	Test Phase	Overall Depth (in.)	Rib Spacing (in.)	Slab Thickness (in.)	Unit Weight (psf)	28-Day UHPC Compressive Strength (ksi)	Flexural Reinforcement	
								Slab	Primary Rib
UHPC-CFRP									
CFRP-3	1T1S-5	3	5	15	1	24.22	24	No. 3	No. 6
	4T1S-5	3	5	15	1		25	No. 3	No. 6
	1T2S-5	3	5	15	1		24	No. 3	No. 6
UHPC-HSS									
HSS-3	1T1S-5	3	5	15	1	26.13	22	No. 3	No. 6
	4T1S-5	3	5	15	1		23	No. 3	No. 6
	1T2S-5	3	5	15	1		22	No. 3	No. 6
UHPC-CFRP									
CFRP-1[2]	1T1S-4#1	1	4	15	¾	18.80	24	No. 3	No. 4
	1T1S-4#2	1					24		
	1T1S-5#1	1	5			21.30	24		
	1T1S-5#2	1					24		
CFRP-2[2]	1T1S-4#3	2	4	15	¾	18.80	27		
	4T1S-4	2					27		
	1T2S-4	2					26		
UHPC-HSS									
HSS-0[1]	1T1S-5#1	0	5	12	1¼	32.37	18	No. 4	No. 7
	1T1S-5#2	0					27		
	4T1S-5	0					26		
	1T2S-5	0					22		
HSS-1[2]	1T1S-4½#1	1	4½	15	¾	21.72	24	No. 3	No. 5
	1T1S-4½#2	1					24		
HSS-2[2]	1T1S-4	2	4	15	¾	20.26	27		
	4T1S	2					27		
	1T2S	2					25		

Table 4.2 Summary of Test Results

Group	Specimen Name	Graph Labels	Overall Depth (in.)	Service Load Deflection (in.)	Ultimate Deflection (in.)	Ultimate Load (kip)	Demand Load (kip)	Capacity/ Demand	Capacity/ Demand per Unit Weight
UHPC-CFRP									
CFRP-3	1T1S-5	CFRP-5#3	5	0.23	1.76	21.80	8.14	2.68	0.11
	4T1S-5	CFRP-5#3		0.64	2.71	48.48	52.13	0.93	0.04
	1T2S-5	CFRP-5#3		0.12	1.24	38.45	17.45	2.20	0.09
UHPC-HSS									
HSS-3	1T1S-5	HSS-5#3	5	0.076	1.71	23.07	8.14	2.83	0.11
	4T1S-5	HSS-5#3		0.21	0.93	55.59	52.13	1.07	0.04
	1T2S-5	HSS-5#3		0.084	1.20	35.45	17.45	2.03	0.08
UHPC-CFRP									
CFRP-1[2]	1T1S-4#1	CFRP-4#1	4	0.54	1.19	16.77	10.25	1.6	0.09
	1T1S-4#2	CFRP-4#2		0.48	1.06	17.15		1.7	0.09
	1T1S-5#1	CFRP-5#1	5	0.37	1.03	21.49		2.1	0.10
	1T1S-5#2	CFRP-5#2		0.35	0.97	19.56		1.9	0.09
CFRP-2[2]	1T1S-4	CFRP-4#3	4	0.45	1.03	18.66		1.8	0.10
	4T1S-4	CFRP-4#3		0.50	0.83	51.26	42.04	1.2	0.06
	1T2S-4	CFRP-4#3		0.19	0.80	26.75	15.65	1.7	0.09
UHPC-HSS									
HSS-0[1]	1T1S-5#1	HSS-5#1	5	0.06	0.98	40.02	8.21	4.9	0.15
	1T1S-5#2	HSS-5#2		0.1	0.98	46.99		5.7	0.18
	4T1S-5	HSS-5#1		0.19	0.79	84.98	34.17	2.5	0.08
	1T2S-5	HSS-5#1		0.9	1.26	55.08	12.52	4.4	0.14
HSS-1[2]	1T1S-4½#1	HSS-4½#1	4½	0.1	0.83	27.65	10.25	2.7	0.12
	1T1S-4½#1	HSS-4½#2		0.14	0.87	24.73		2.4	0.11
HSS-2[2]	1T1S-4	HSS-4	4	0.15	0.91	22.71		2.2	0.11
	4T1S-4	HSS-4		0.18	0.87	51.48	42.04	1.2	0.06
	1T2S-4	HSS-4		0.07	0.87	44.96	15.65	2.9	0.14

[1] Taken from Saleem et al. (2011) and [2] Taken from Ghasemi et al. (2015).

4.2.4. Flexural Behavior

Similar to Sections 2.2.4 and 3.2.2, the flexural behavior of Specimens 1T1S was assessed. Figures 4.1 and 4.2 show the test setup, failure mode, and load-deflection responses of single-rib simple-span specimens for UHPC-HSS and UHPC-CFRP, respectively. Similar to previous experiments, failure was initiated by minor web shear cracks near supports. Minor flexural cracks were also present near mid-span without having any impact on the overall failure. Shear cracks gradually widened as testing progressed, eventually leading to a load drop and failure of the deck panel.

Figure 4.3 shows the load-deflection responses of the single-rib simple-span specimens for both HSS and CFRP reinforcement compared to all previous specimens of the current research projects. The load capacity is normalized to the corresponding ultimate demand load for each specimen according to the data presented in Table 4.2. As seen in the figure, in all of the specimens, the capacity exceeded the ultimate demand load. The 5-inch deep specimens seem to be more flexible as compared to their counterparts in previous phases. This may be attributed to the larger clear span of 5-ft., in contrast to the 4-ft. span in previous phases. Although the overall depth was also changed proportionally, not all thicknesses were sized for the larger span.

Figures 4.4 and 4.5 show the load-strain responses for all specimens 1T1S with HSS reinforcement and CFRP reinforcement, respectively. As expected, there is great similarity between the results of this phase and those of previous phases.

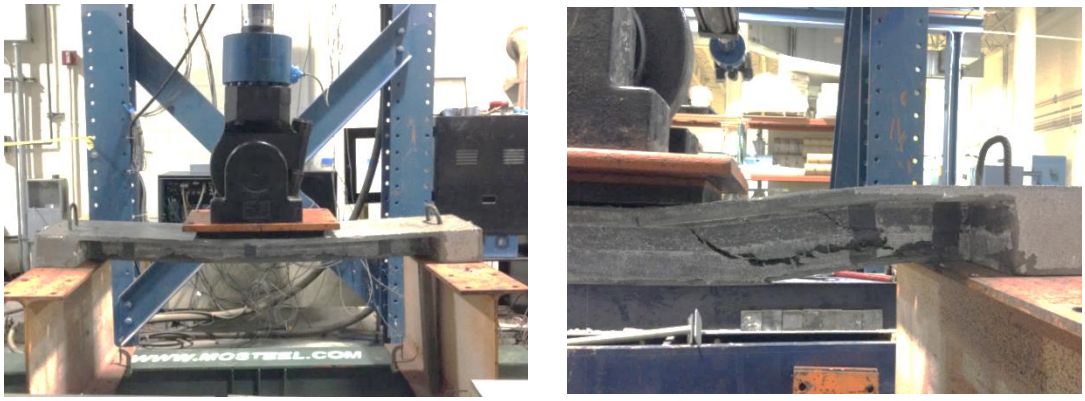

(a) (b)

Figure 4.1 Flexure Test and Failure Mode of Specimens 1T1S-HSS, (a) Deflected Shape of Specimen 1T1S, and (b) Beam Shear Crack

(a) (b)

Figure 4.2 Flexure Test and Failure Mode of Specimens 1T1S-CFRP, (a) Deflected Shape of Specimen 1T1S, and (b) Beam Shear Crack

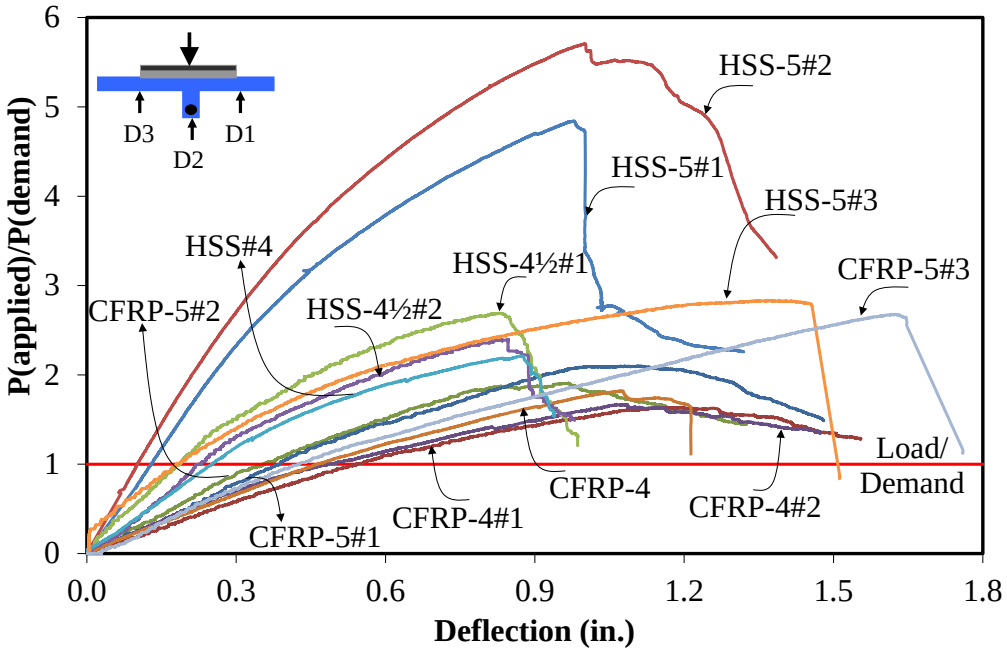

Figure 4.3 Load-Deflection Responses of all Specimens 1T1S

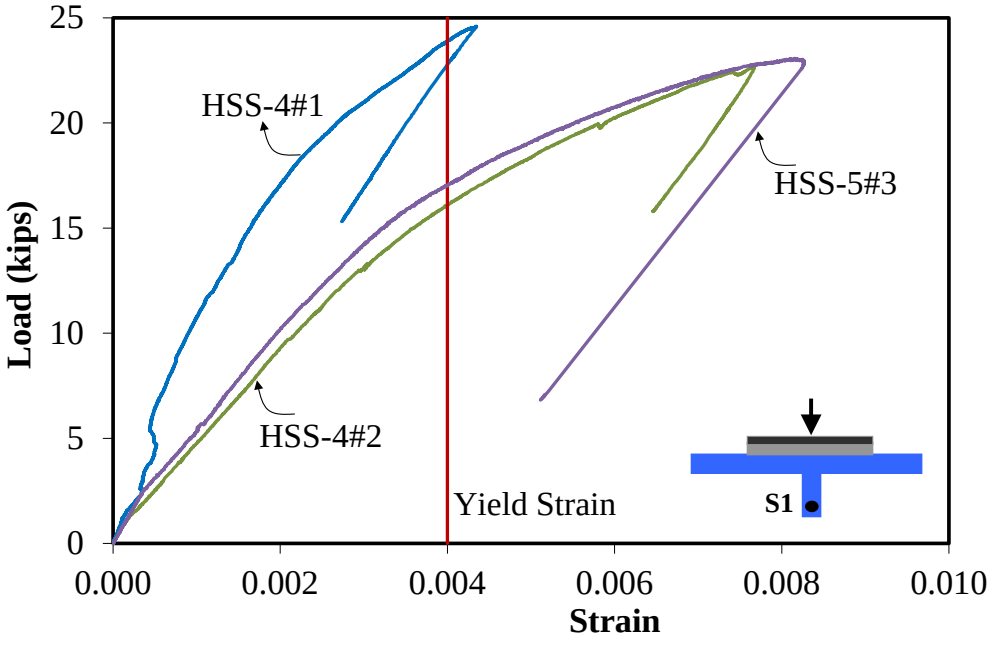

Figure 4.4 Strain Responses of HSS Bars in Specimens 1T1S

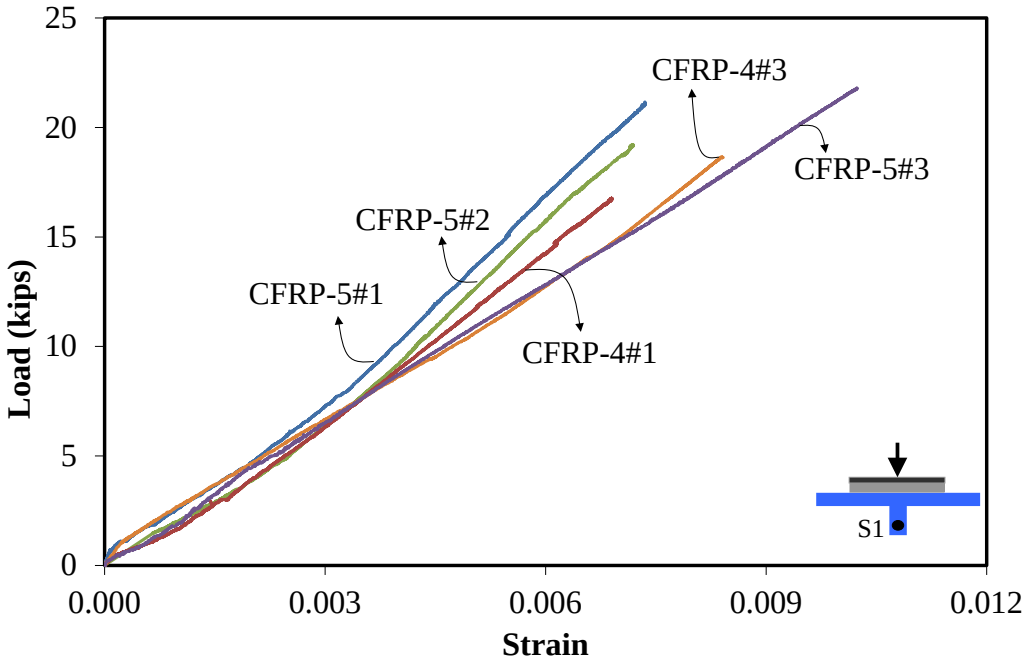

Figure 4.5 Strain Responses of CFRP Bars in Specimens 1T1S

Additional strain gauges were attached to the top surface of the UHPC deck and to the web in order to capture the strain in the UHPC. The results are shown in **Appendix B**.

4.2.5. Panel Action

Performance of Specimens 4T1S was evaluated similar to Sections 2.2.4.1 and 3.2.3.3. Figure 4.6 shows the top and bottom views of the multi-rib simple-span Specimen 4T1S after its flexural test for Specimen 4T1S-HSS. Test results for Specimen 4T1S-CFRP are illustrated in Figure 4.7. The failure mode was similar to that observed for single-rib specimens of this phase and the previous multi-ribs simple-span specimens.

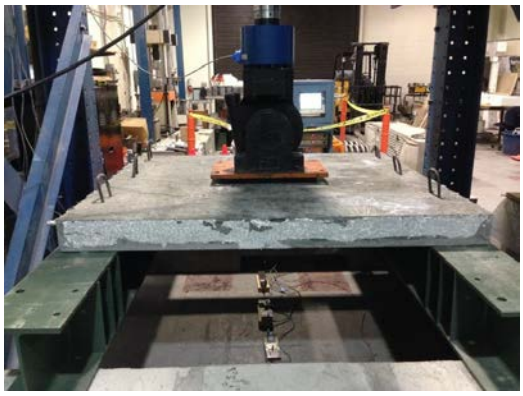

(a)

(b)

(c)

(d)

Figure 4.6 Flexure Test and Failure Mode of Specimens 4T1S-HSS, (a) Test Setup, (b) Beam Shear Crack, (c) Cracks on the Slab, and (d) Cracks on the Top Slab

(a)

(b)

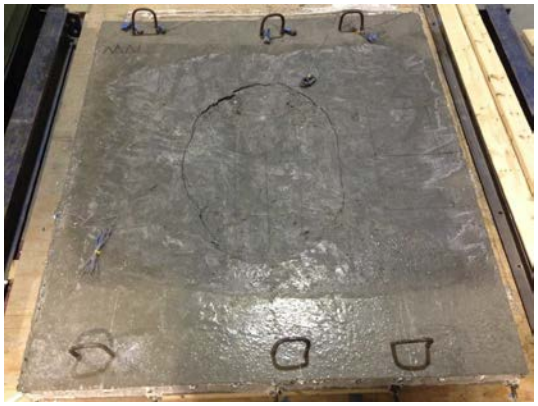

(c)

Figure 4.7 Flexure Test and Failure Mode of Specimens 4T1S-CFRP, (a) Test Setup, (b) Beam Shear Crack, and (c) Cracks on the Top of the Slab

For comparison, Figure 4.8 shows the response curves under each rib for current Specimens 4T1S with both types of reinforcement (i.e., either HSS or CFRP) along with all previous specimens in a normalized load capacity basis. The panel with CFRP bars seems to be more flexible, as expected. Also, the 5 inch deep panel with CFRP bars did not meet the ultimate demand load criteria. Only the load-deflection response of the middle rib (D3) is shown in the figure for all specimens to avoid cluttering the graph.

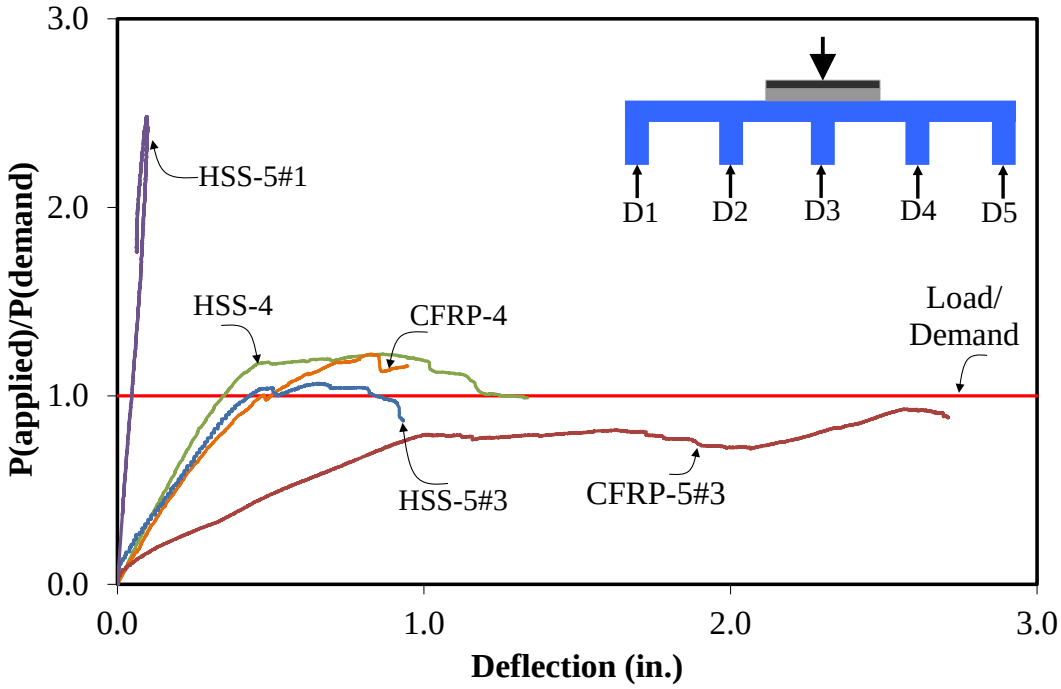

Figure 4.8 Load-Deflection Responses of all Specimens 4T1S

Figure 4.9 shows load-strain responses for all Specimens 4T1S with HSS reinforcement based on strain gauges attached at the mid-span to the rebar in the primary rib. The results are considerably similar to previous phases. Similar results are shown for all Specimens 4T1S with CFRP reinforcement in Figure 4.10.

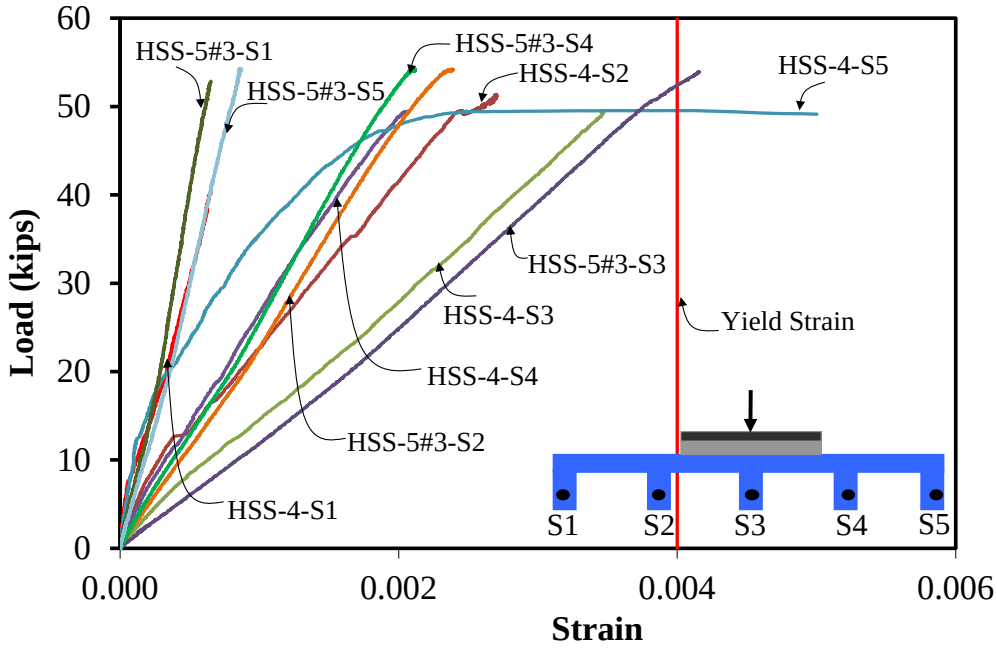

Figure 4.9 Load-Strain Responses of all Specimens 4T1S-HSS

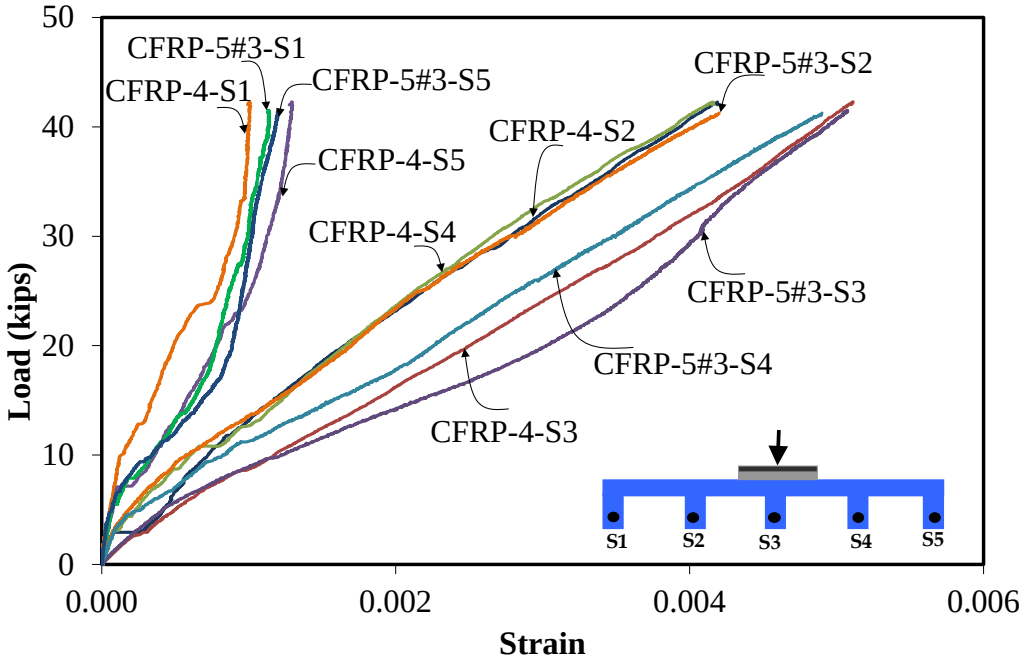

Figure 4.10 Load-Strain Responses of all Specimens 4T1S-CFRP

4.2.6. Punching Shear Behavior

Similar to Sections 2.2.4.2 and 3.2.3.4 the punching shear behavior of the Specimens 4T1S with both types of reinforcement was assessed on the same specimens 4T1S after flexural tests. Figure 4.11 shows the punching shear test carried out on exterior panel of Specimen 4T1S-HSS. The load-deflection response of the punching shear test is presented in Figure 4.12.

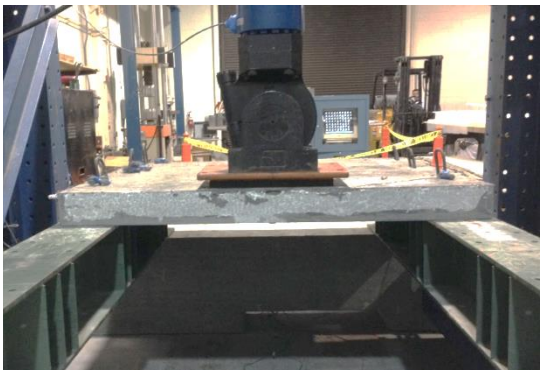

(a)

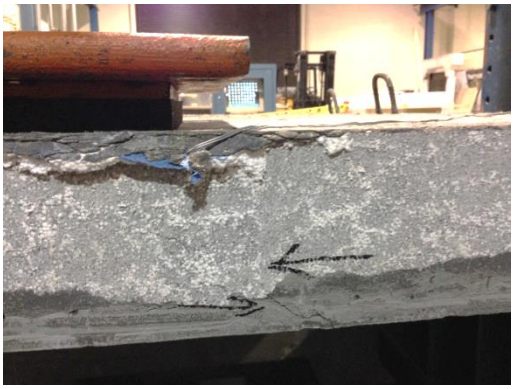

(b)

(c)

Figure 4.11 Punching Shear Test of Specimen 4T1S: (a) Test Setup, (b) Beam Shear Crack, and (c) Cracks on the Top of the Slab

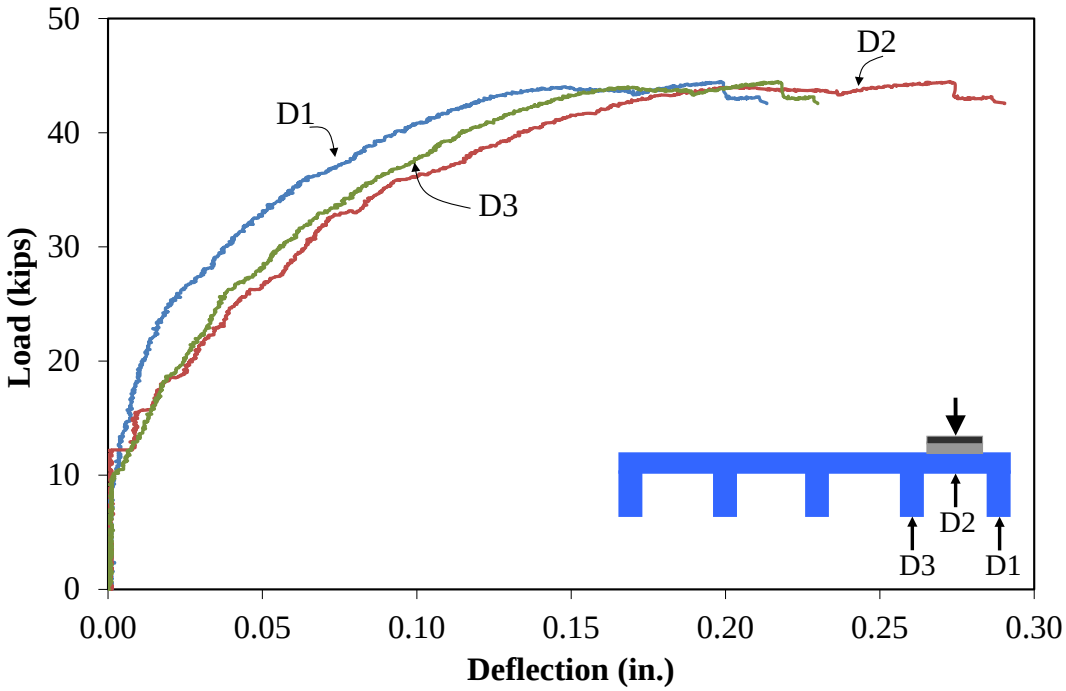

Figure 4.12 Load-Deflection Responses of Specimen 4T1S-HSS

Similar studies have been carried out on Specimen 4T1S-CFRP. The corresponding results are shown in Figures 4.13 and 4.14.

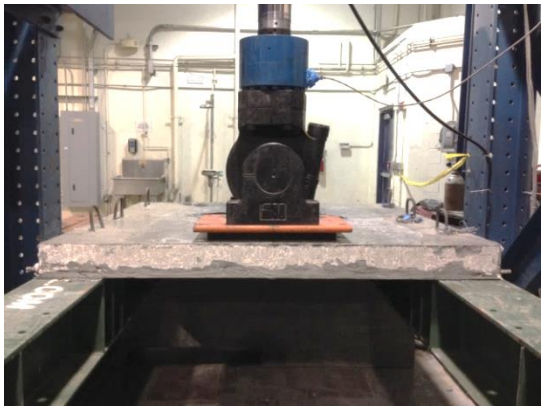

(a)

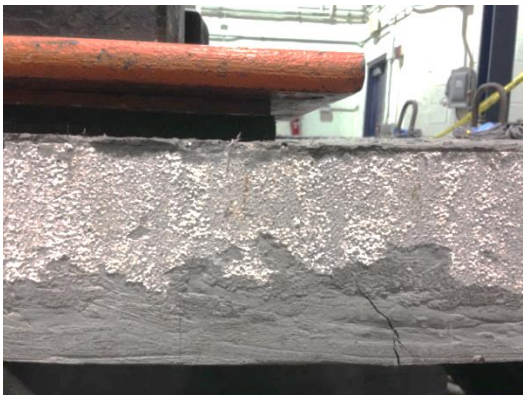

(b)

(c)

Figure 4.13 Punching Shear Test of Specimen 4T1S: (a) Test Setup, (b) Beam Shear Crack, and (c) Cracks on the Top of the Slab

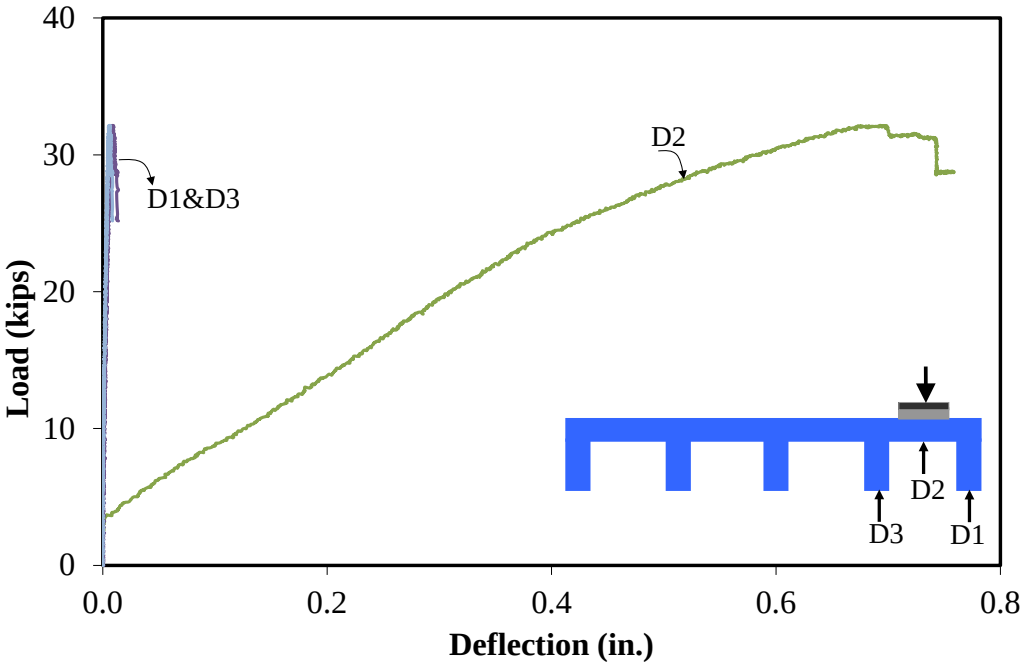

Figure 4.14 Load-Deflection Responses of Specimen 4T1S-CFRP

4.2.7. Continuity Effects

The effects of continuity and negative moments were investigated using the single-rib two-span Specimen 1T2S. Figures 4.15 and 4.16 show the test setup, deflected shape and the failure mode, where diagonal cracks initiated near an exterior support in one span, and propagated to the slab leading to the eventual failure for Specimens 1T2S-HSS and 1T2S-CFRP. Minor shear cracks were also present in the other span, while some flexural cracks were observed on top of the slab over the interior support. Major flexural cracks on interior support at the face of the northern span of the specimens occurred (see Figure 4.16.d).

(a)

(b) (c)

Figure 4.15 Flexure Tests of Specimen 1T2S-HSS: (a) Test Setup, (b) Deflected Shape, and (c) Failure Mode

(a)

(b)

(c)

(d)

Figure 4.16 Flexure Tests of Specimen 1T2S-CFRP: (a) Test Setup, (b) Deflected Shape, (c) Failure Mode (Beam Shear Crack), and (d) Flexural Crack on the Interior Support

For comparison, Figure 4.17 shows the two mid-spans response curves for current Specimens 4T1S with both types of reinforcement along with all previous specimens. The responses are normalized based on load capacity. All specimens meet the ultimate demand load capacity. The figure clearly shows that the ultimate capacity of the

current 5-inch-deep specimens with both types of reinforcement is similar while the UHPC-CFRP specimen seemed to be more flexible.

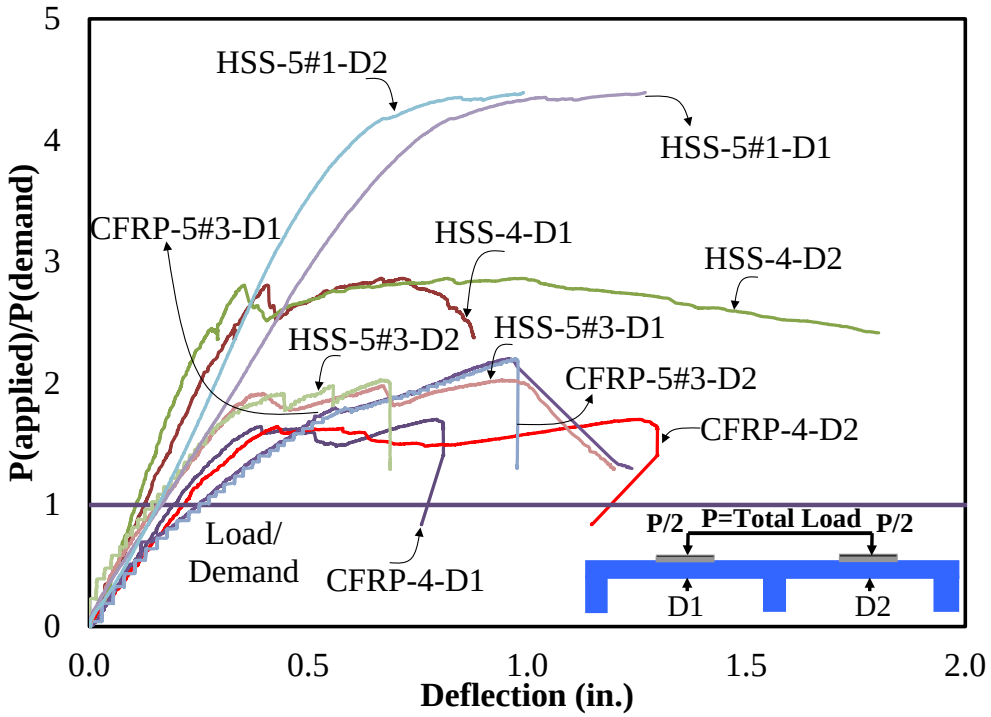

Figure 4.17 Load-Strain Responses of All Specimens 1T2S

Figure 4.18 shows load-strain responses for all Specimens 1T2S with HSS reinforcement based on strain gauges attached at the mid-span to the rebar in the middle of the primary ribs. Contrary to previous specimens with HSS reinforcement, the main bar in the span with maximum deflection yielded.

Figure 4.19 shows load-strain responses for all Specimens 1T2S with CFRP reinforcement based on strain gauges attached at the mid-span to the rebar in the middle rib.

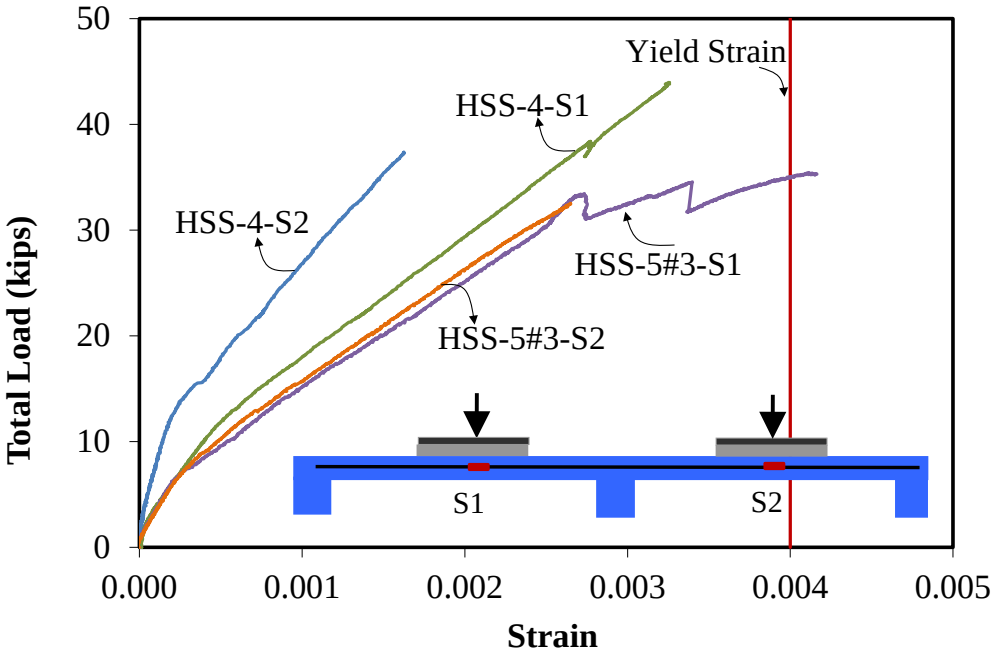

Figure 4.18 Load-Strain Responses of All Specimens 1T2S-HSS

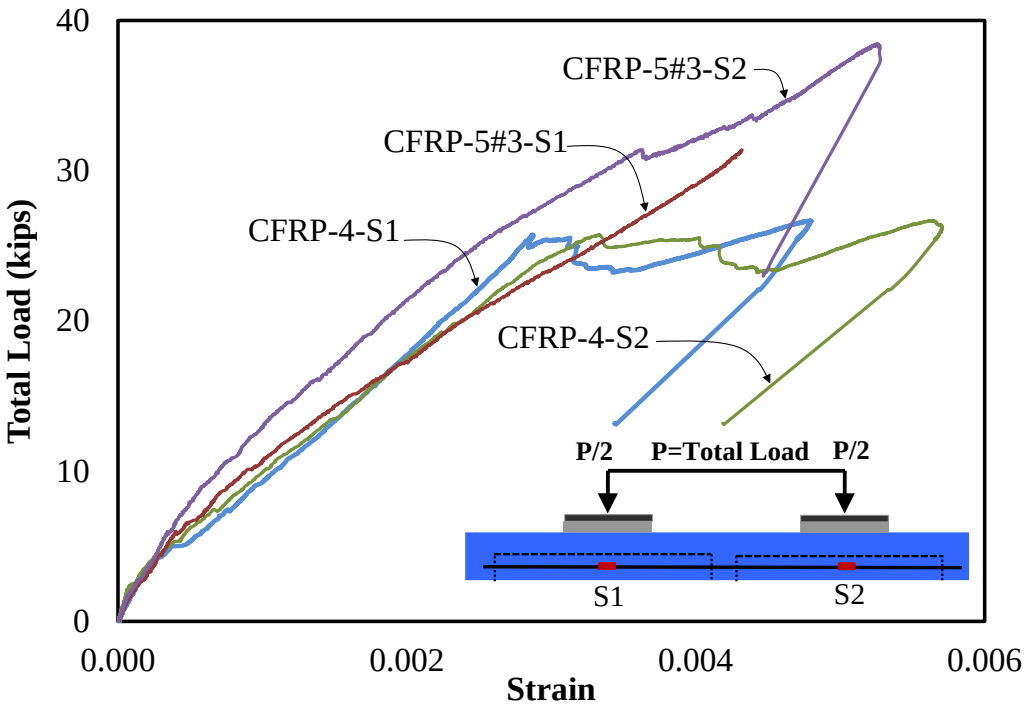

Figure 4.19 Load-Strain Responses of All Specimens 1T2S-CFRP

4.2.8. Accelerated Pavement Testing under Heavy Vehicle System

According to Figures 4.7 (c), 4.11 (c), and 4.12 (c) the punching shear cracks occurred on the slab for both Specimens 4T1S-HSS and 4T1S-CFRP. Also, according to Figure 4.8, Specimen 4T1S-CFRP did not meet the ultimate demand load criteria. Therefore, for the final slabs which will be tested under HVS, the thickness of the slab and the amount of CFRP reinforcement were both increased.

In the following pages, the overall testing diagram and the arrangement of the four deck panels are shown along with the schematic details of each deck system. Figure 4.20 shows the test setup and layout plan of the waffle decks. As seen in this figure, the bridge deck consists of four deck panels sitting on two support beams of W10×39. All panels have a depth of 5 in. and a transverse length of 6 ft., with center-to-center spacing

of the stringers as 5 ft. and a panel width of 5 ft. in the direction of traffic. The dimensions and components of the panels are illustrated in Figures 4.21 to 4.24.

Figure 4.25 shows the connections between the panels containing three different types of details based on the type of the reinforcement of each panel. Figure 4.26 shows the loading plan. As seen in the figure, a 16-kip wheel (based on HS-20 truck loading) will be applied to the decks. Figure 4.27 shows the location of the block-outs, representing the connections between waffle deck panels and the supporting stringers. The loading path of the wheel is shown in Figure 4.28.

The instrumentation plans are shown in Figures 4.29 and 4.30. As seen in Figure 4.29, three types of string pots were planned to measure the deflections at critical locations, including mid-span deflections, relative deflections of the panels, and global deflection of the bridge, as well as transverse deflections. The locations of strain gauges are shown in Figure 4.30. The strain gauges were placed at the mid-span of the bar in the middle rib, where maximum positive moments were intended to occur, and locations under top and bottom flanges of the supporting stringers at mid-span.

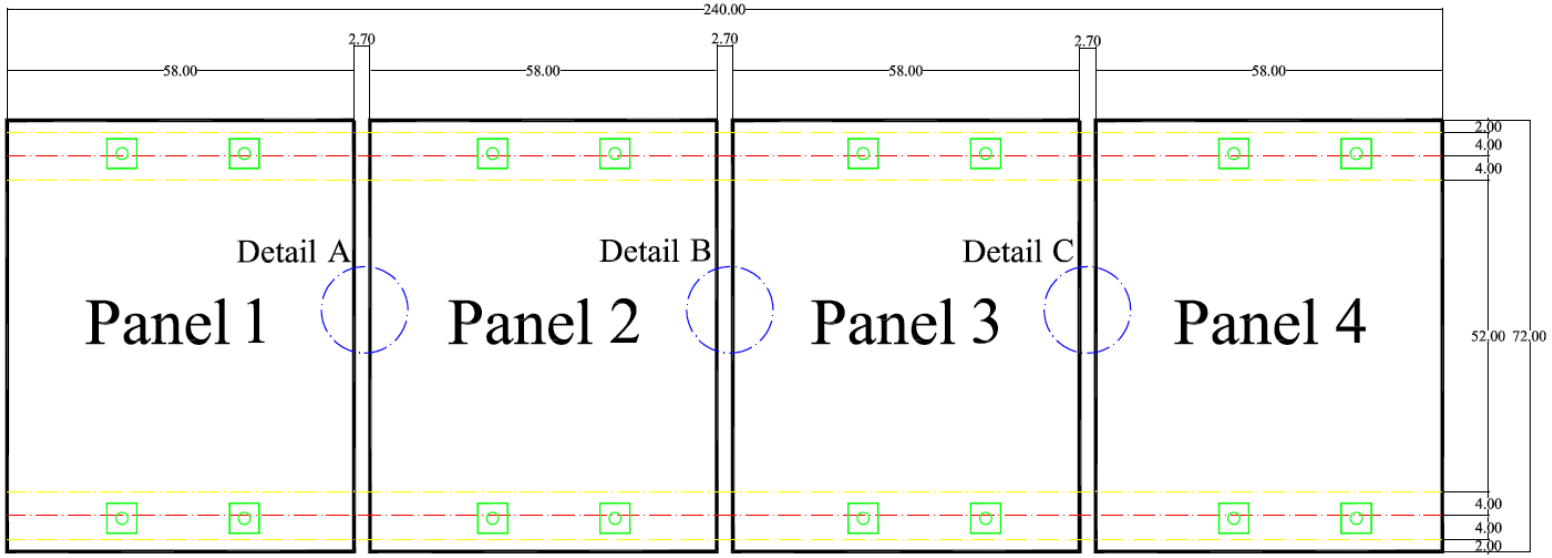

Figure 4.20 Panels Layout

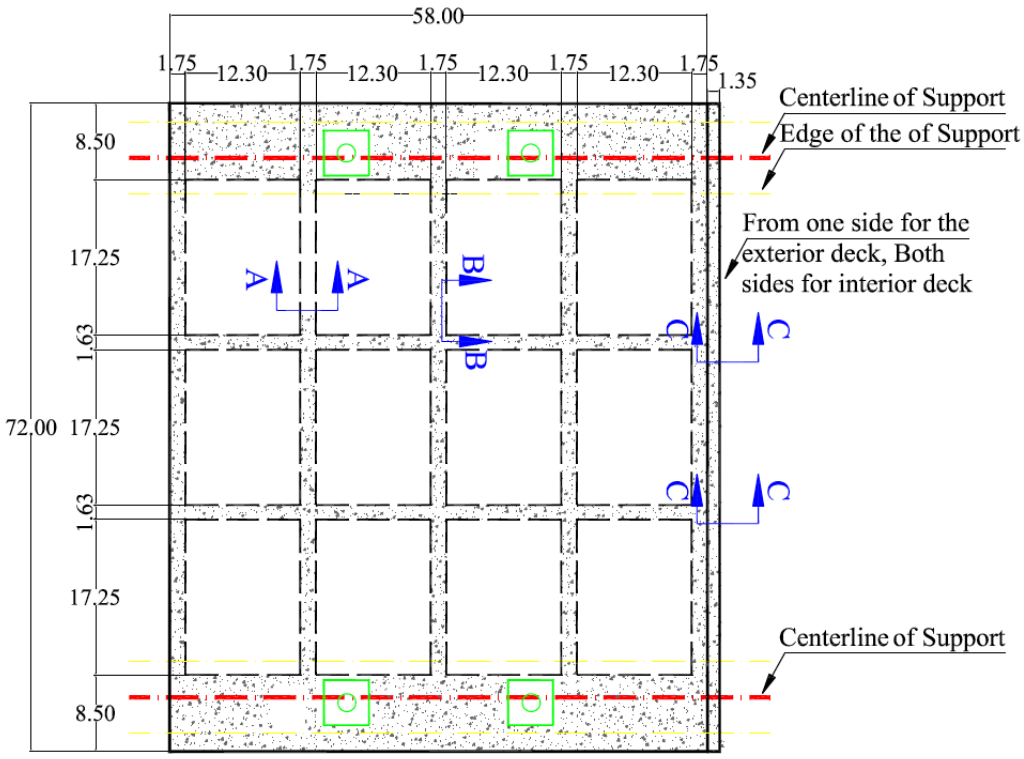

Figure 4.21 Panel 1 (UHPC-HSS)

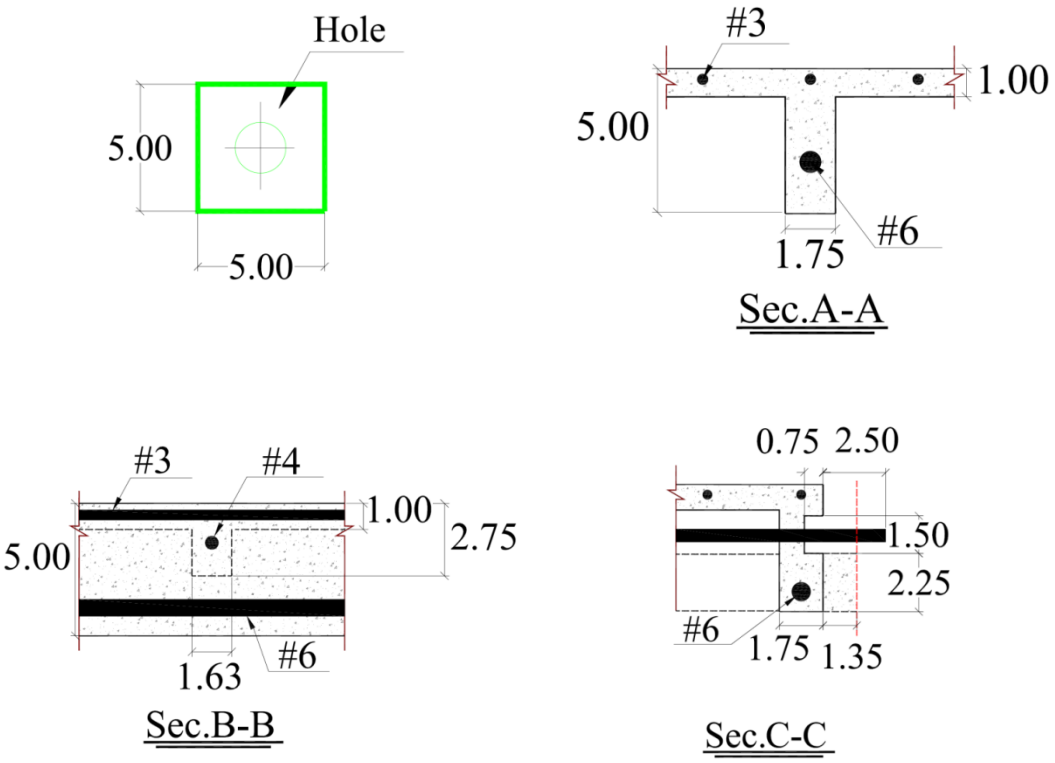

Figure 4.22 Detail of Panel 1 (UHPC-HSS)

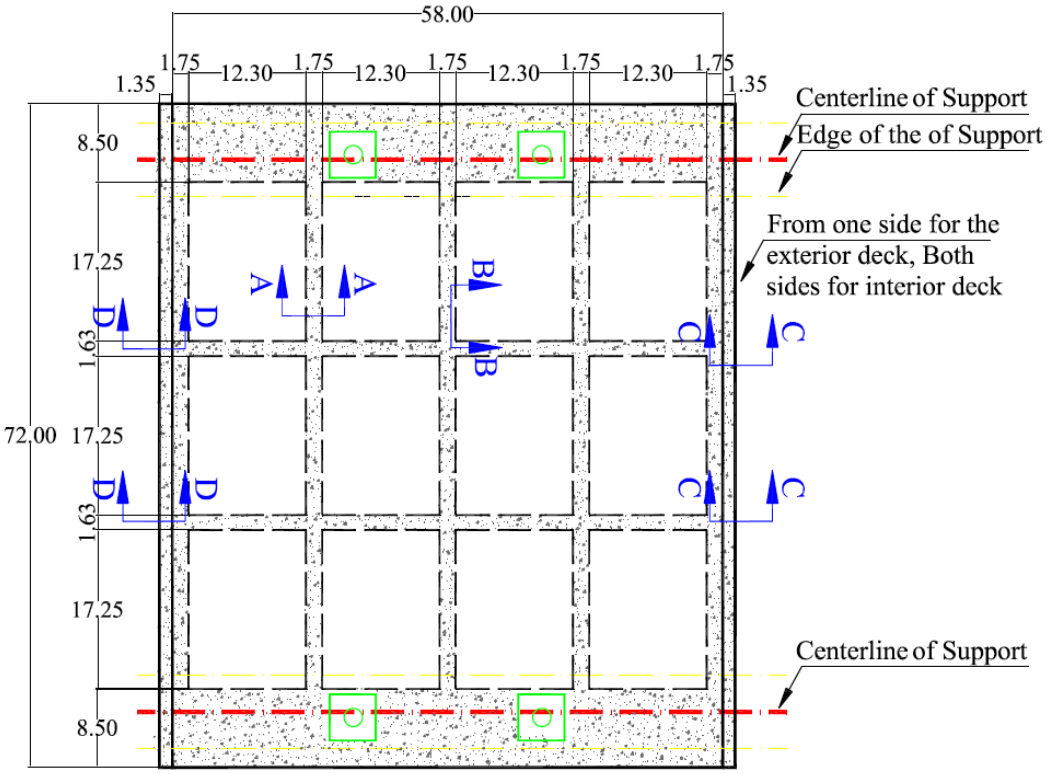

Figure 4.23 Panel 2 (UHPC-HSS)

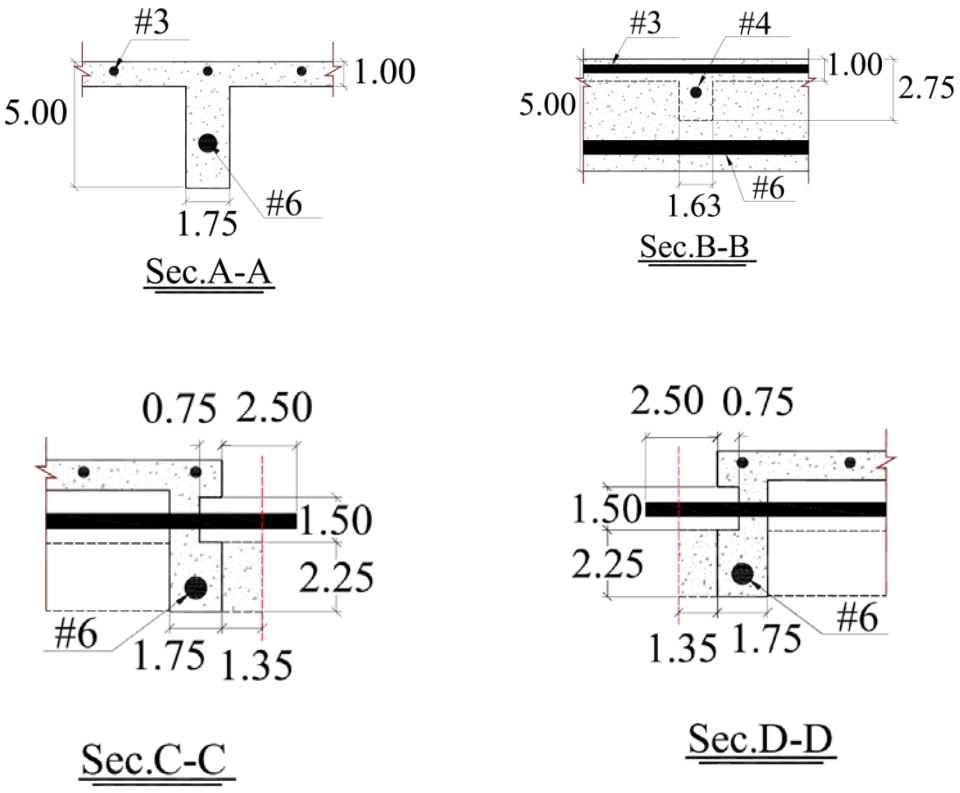

Figure 4.24 Detail of Panel 2 (UHPC-HSS)

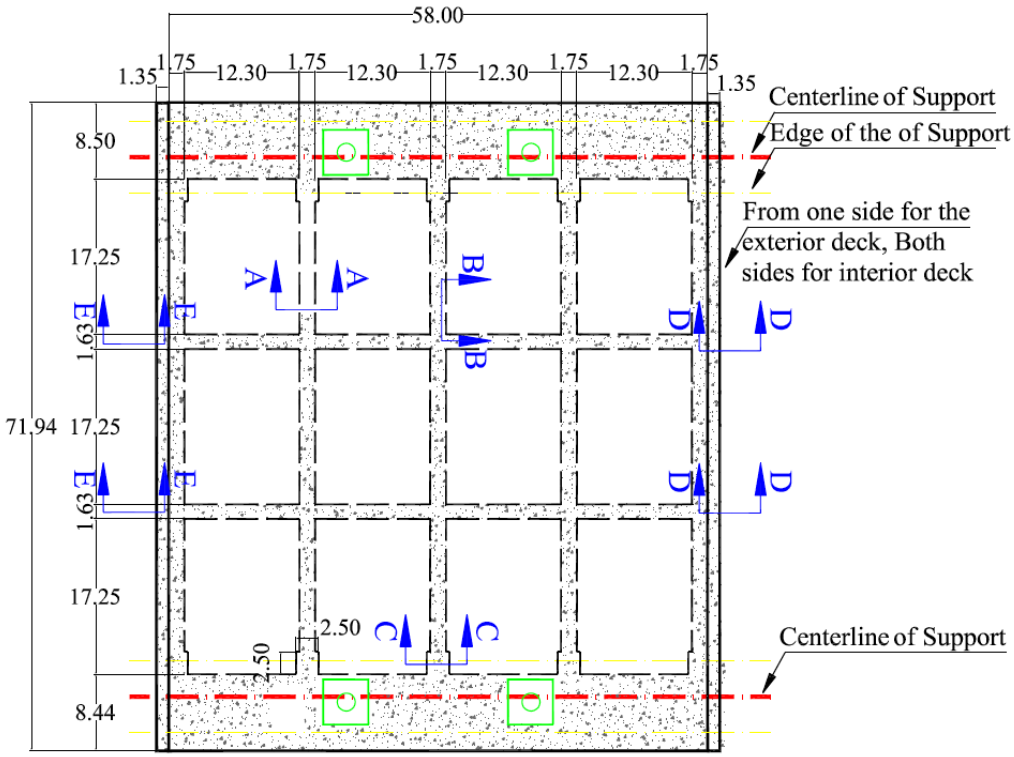

Figure 4.25 Panel 3 (UHPC-CFRP)

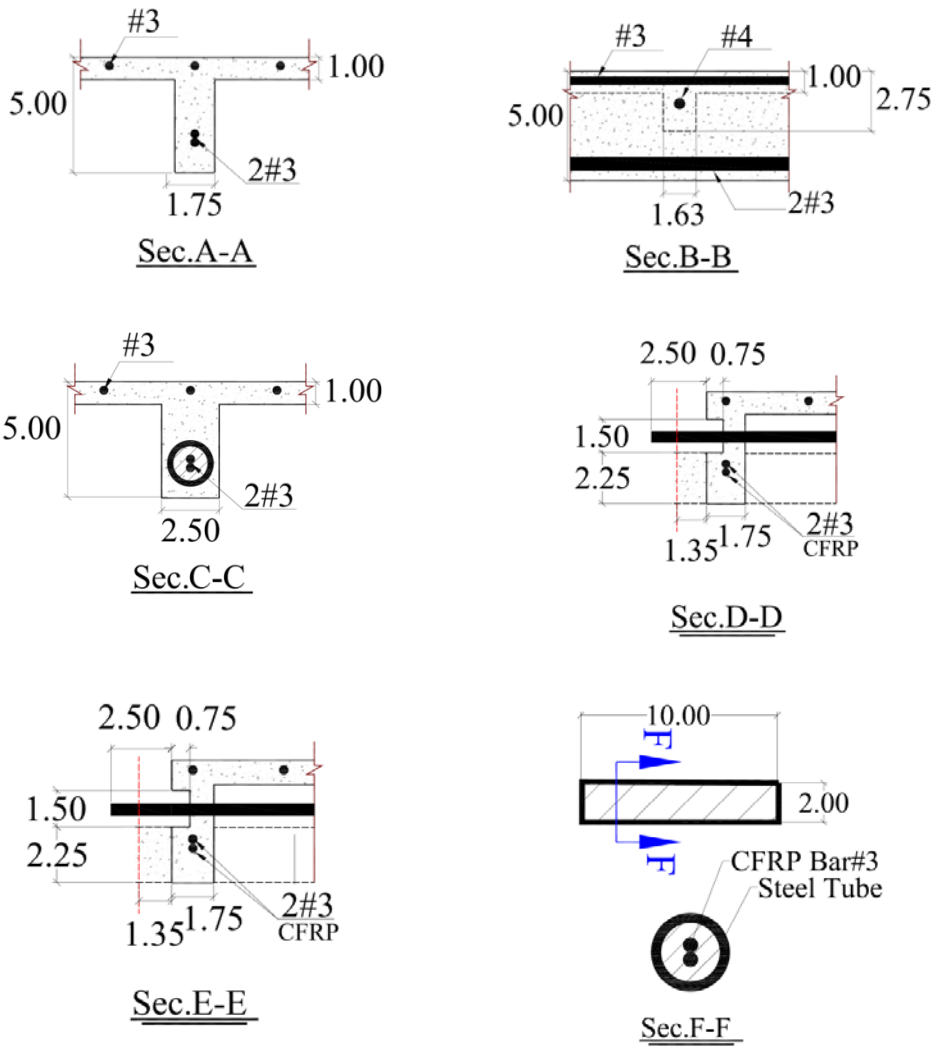

Figure 4.26 Detail of Panel 3 (UHPC-CFRP)

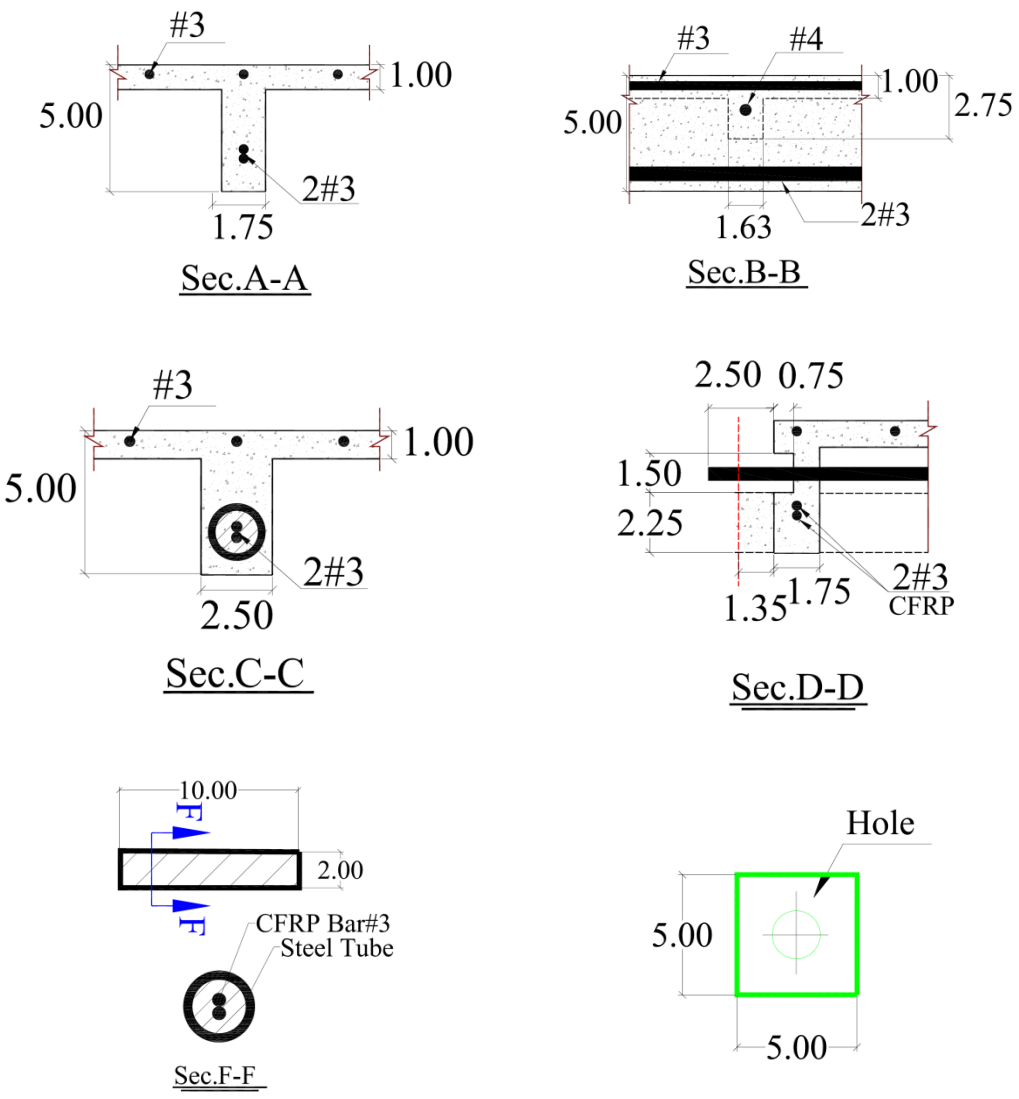

Figure 4.27 Detail of Panel 4 (UHPC-CFRP)

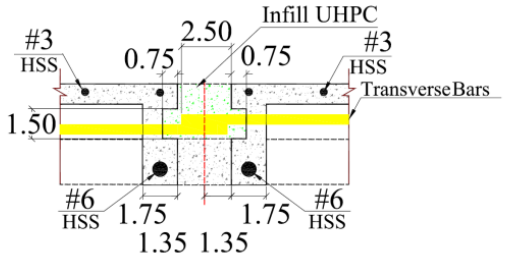

Detail A

UHPC-HSS to UHPC-HSS Connection

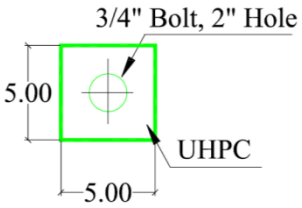

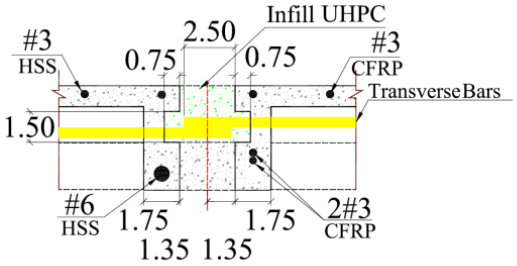

Detail B

UHPC-HSS to UHPC-CFRP Connection

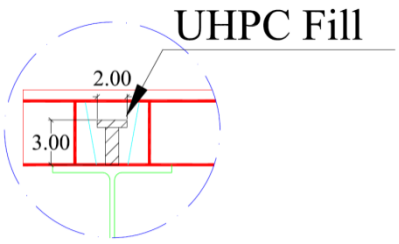

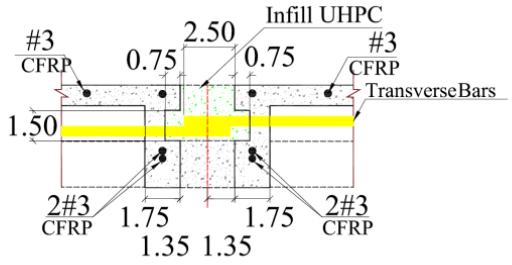

Detail C

UHPC-CFRP to UHPC-CFRP Connection

Figure 4.28 Detail of Connections

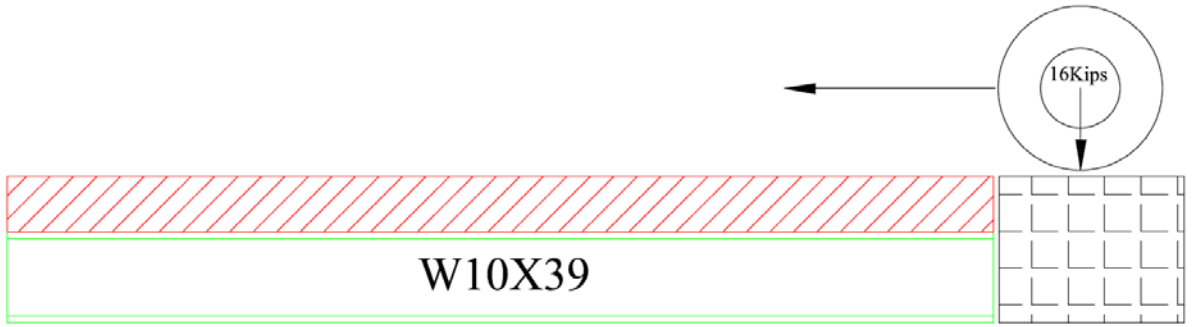

Figure 4.29 Loading Plan

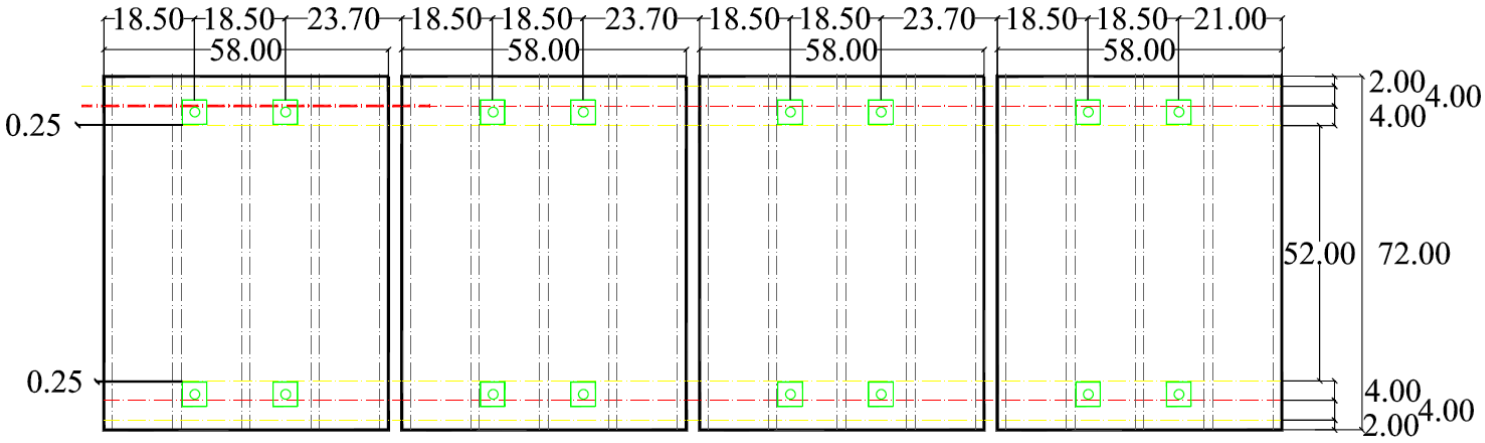

Figure 4.30 Location of Blockouts

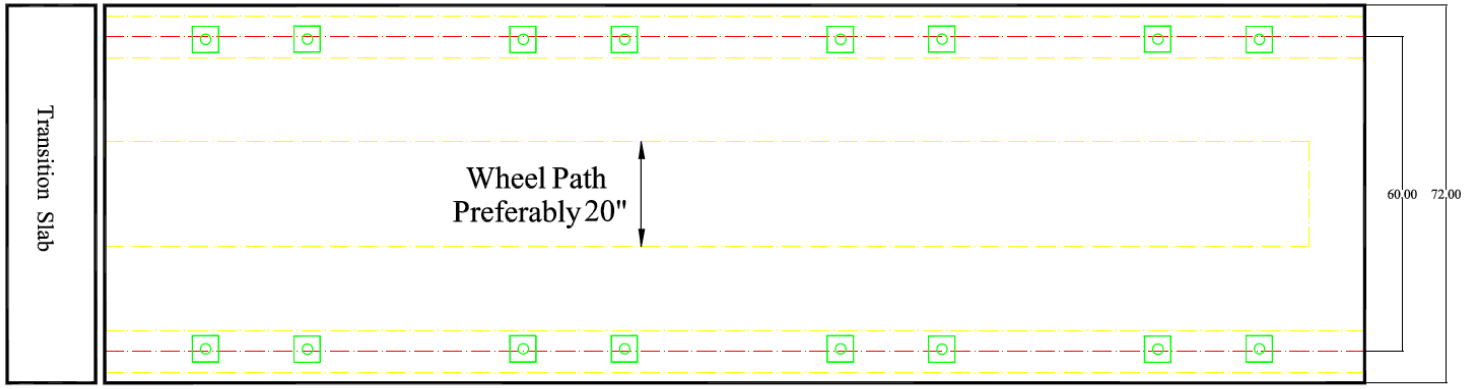

Figure 4.31 Wheel Path Dimensions

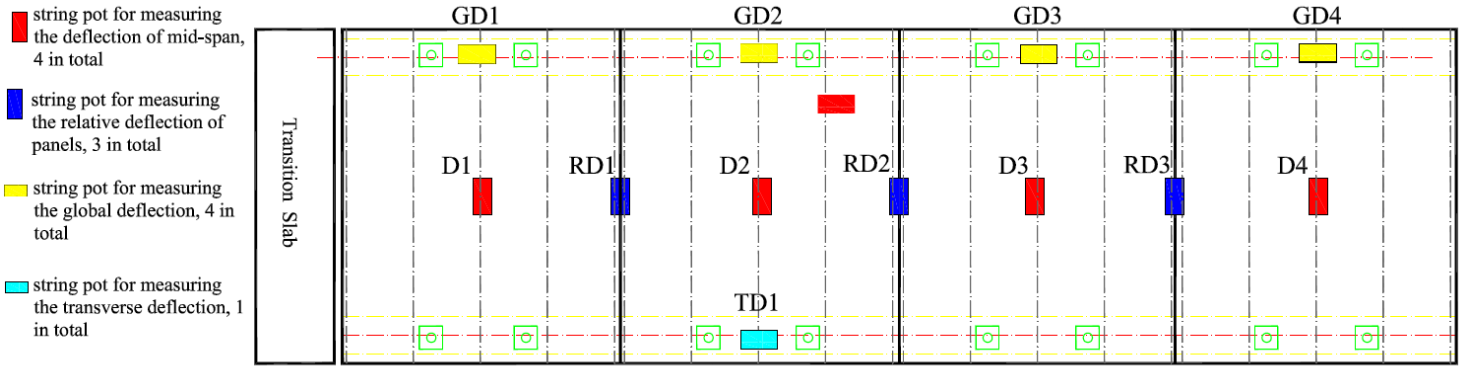

Figure 4.32 Instrumentation Plan (String Pots)

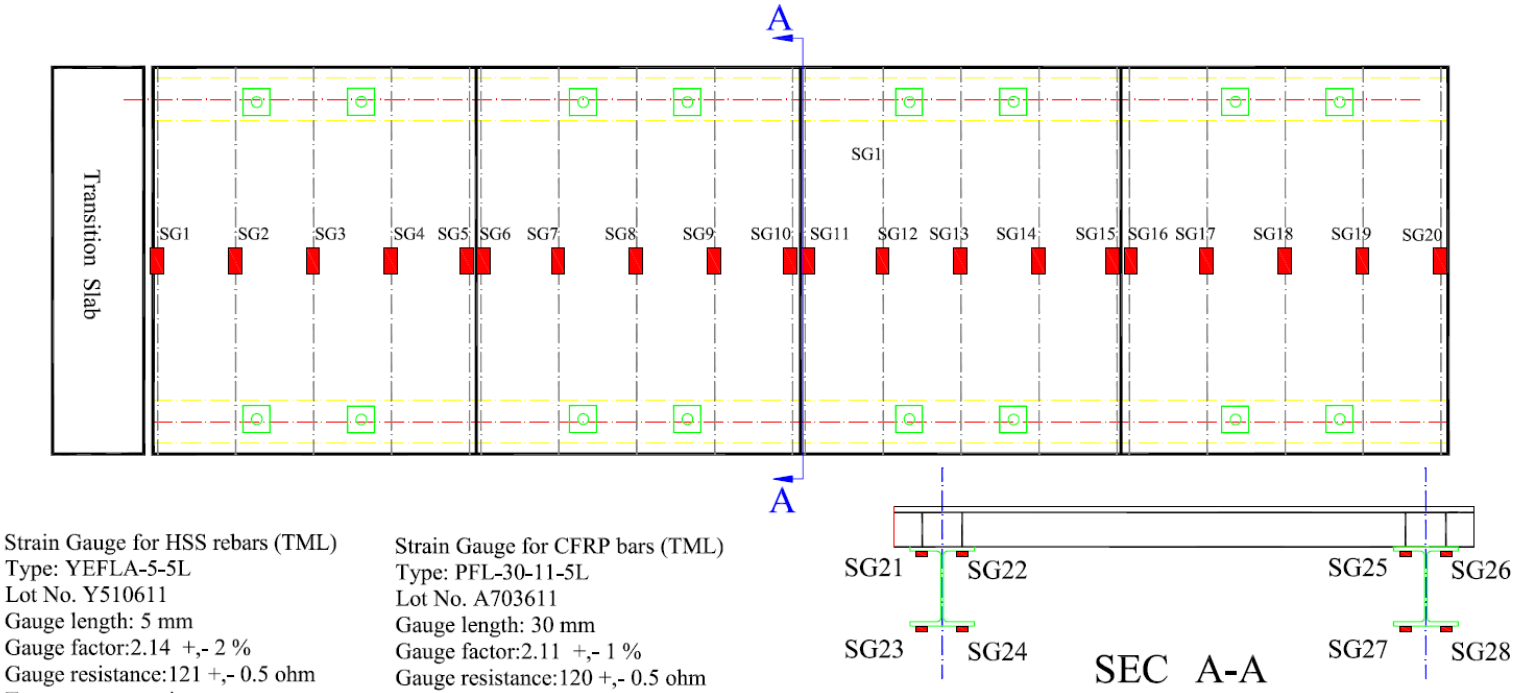

Strain Gauge for HSS rebars (TML)
Type: YEFLA-5-5L
Lot No. Y510611
Gauge length: 5 mm
Gauge factor:2.14 +,- 2 %
Gauge resistance:121 +,- 0.5 ohm
Temp. compensation:-
Transverse sensitivity:-0.1 %
Lead wire: 10/0.12 5m

Strain Gauge for CFRP bars (TML)
Type: PFL-30-11-5L
Lot No. A703611
Gauge length: 30 mm
Gauge factor:2.11 +,- 1 %
Gauge resistance:120 +,- 0.5 ohm
Temp. compensation:11e-6 degree C
Transverse sensitivity:-0.6 %
Lead wire: 10/0.12 5m

*Thermocouples may be installed as previous tests.

Strain gauge on longitudinal bar (20 in total)

In case of limitation for having 16 strain gauges in total, please eliminate SG1, SG2, SG4, SG5, SG16, SG17,SG19,SG20, SG21, SG23, SG26, and SG28.

Figure 4.33 Instrumentation Plan (Strain Gauge)

4.2.9. APT Results and Discussion

Figure 4.34 shows the strain responses of HSS bars vs. number of truck passages. According to the test results, the maximum strain recorded was 0.0012 which was significantly smaller than the yield strain of HSS bar, as 0.004. The strain responses of CFRP bars vs. number of truck passages are illustrated in Figure 3.35.

Figure 4.36 represents the Defection of Panels vs. the Number of Truck Passages. The maximum deflection recorded for UHPC-HSS panels was 0.018 in. and for UHPC-CFRP panels was 0.021. Comparing to the prior APT test (3^{rd} phase of testing) results the deflections of the panels under APT was fairly lower. This phenomenon could be considered as a result of three reasons. First of all, there is an increase in the thickness of the slab from ¾ in. to 1 in. Secondly, the connections between the panels enhanced the overall performance of the bridge deck by benefiting the better load distribution as compared to a single panel deck. At last, the blockouts which used to connect the bridge deck to the stringers made the supports slightly fixed comparing to the pinned-pinned supports in the previous phases.

Relative deflections between the panels were recorded to assess the performance of the connections. The results are presented in Figure 4.37. The maximum relative deflection was recorded as 0.0011 in. which is 1/220000 of the total length of the deck. Therefore, it could be considered as negligible.

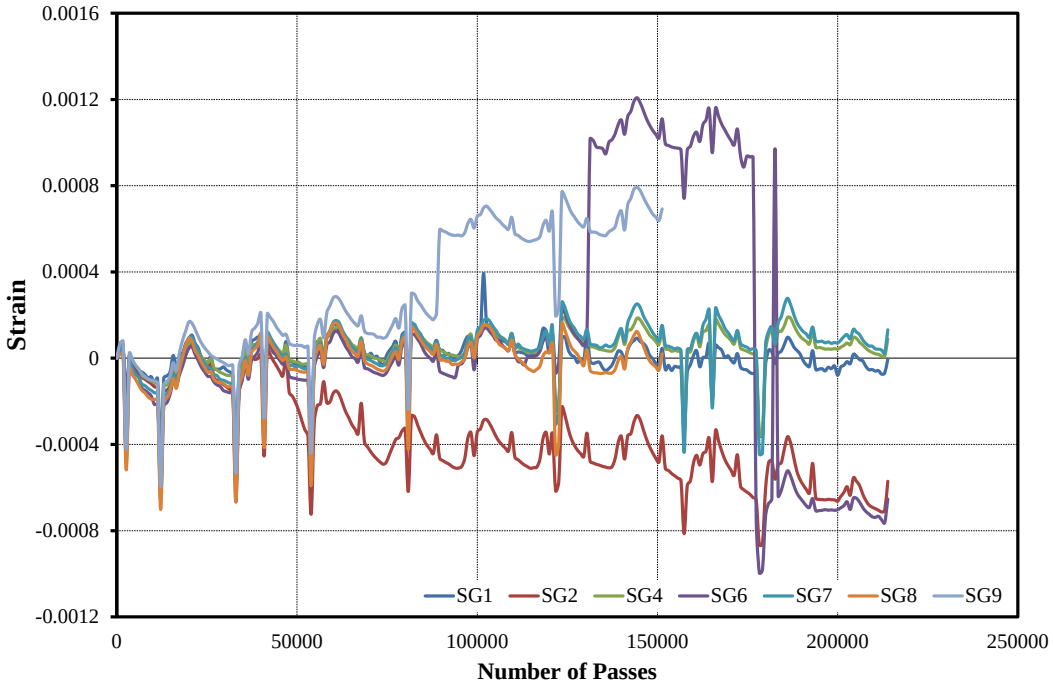

Figure 4.34 Strain Responses of HSS Bars vs. the Number of Truck Passages

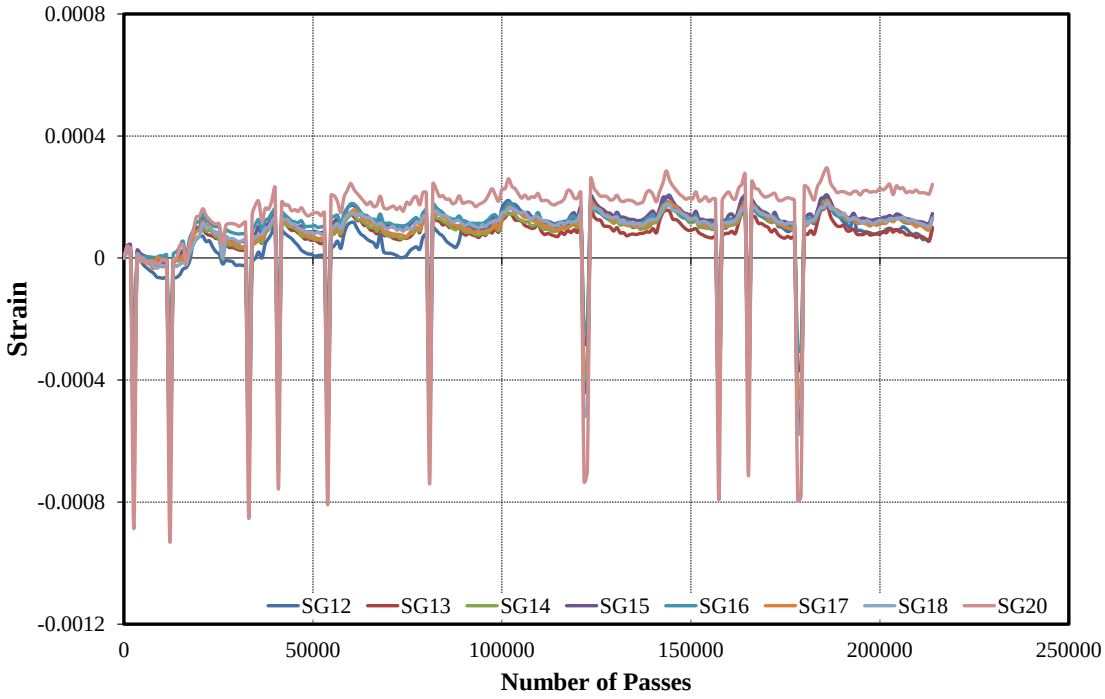

Figure 4.35 Strain Responses of CFRP Bars vs. the Number of Truck Passages

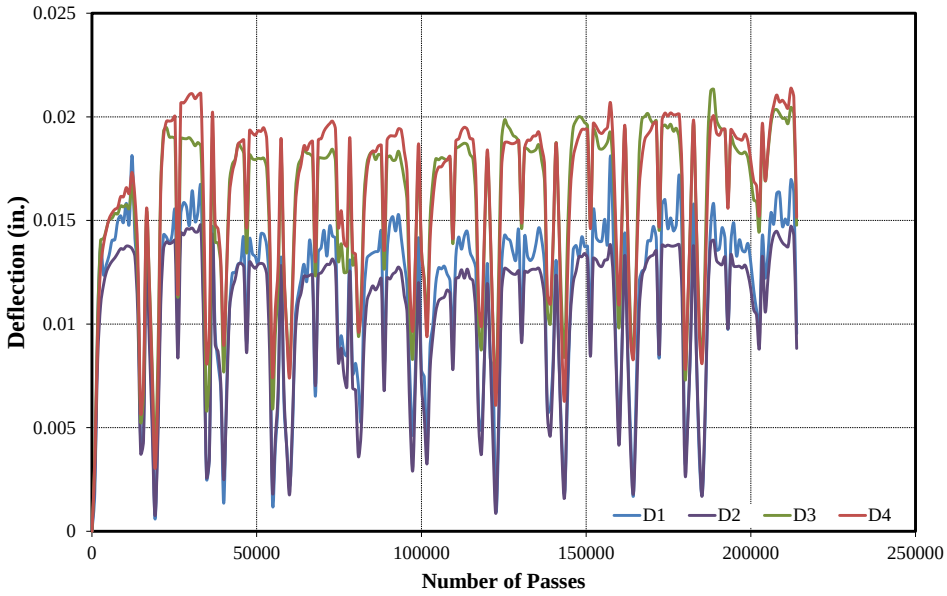

Figure 4.36 Deflections of Panels vs. the Number of Truck Passages

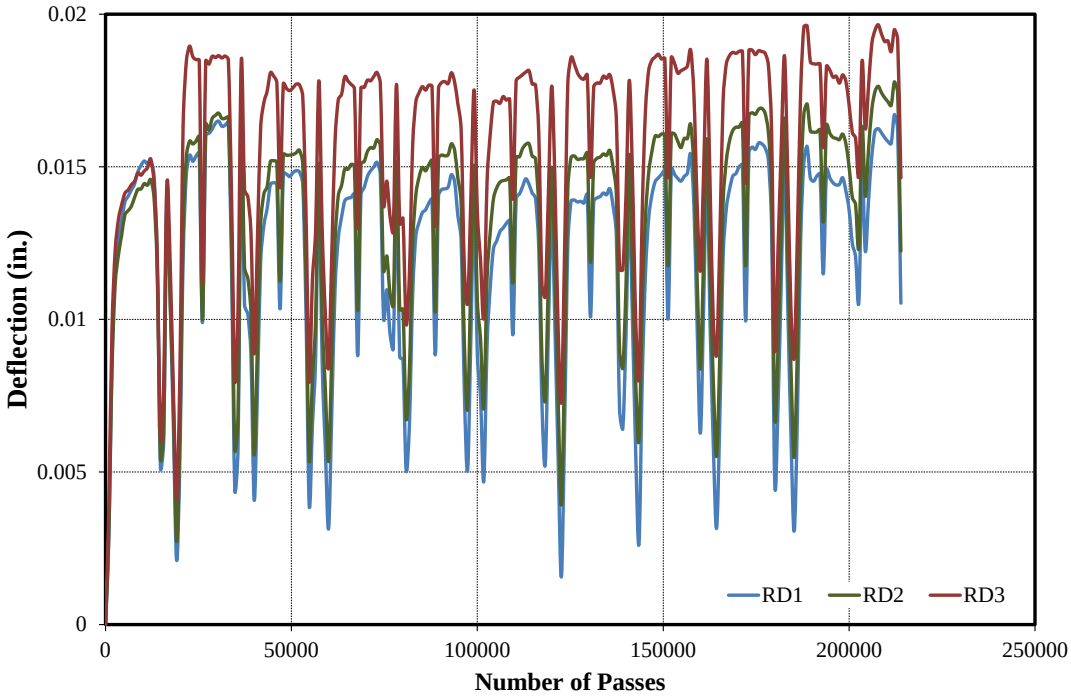

Figure 4.37 Relative Deflections of Panels vs. the Number of Truck Passages

Figure 4.38 shows the deck after the test. As seen in the Figure 4.38 (b), some minor cracks were observed on the connection parts. Also, Figure 4.38 (c) presents the cracks formed on the top of the panel 2 (UHPC-HSS Panel) followed by a close up view of the cracks in Figure 4.38 (d). The average crack width measured was 0.015-0.02 inch.

(a)

(b)

(c)

(d)

Figure 4.38 Deck Status after the APT, (a) Deck Overview, (b) Cracks on the Connection Parts, (c) Cracks on the top of Panel 2 (d) Close up view of the Cracks on Panel 2

5. ACCELERATED PAVEMENT TESTING ON FRP BRIDGE SYSTEM

5.1. Introduction

Performance of FRP bridge decks under static and fatigue loading tests have been evaluated in the previous phase of this research studies (Mirmiran et al. 2012). The deck is a composite section made of foams, GFRP layers, and polymer concrete. GFRP layers are used as shear reinforcement as well as flexural reinforcement and they are laid up in both longitudinal and transverse directions (See Figure 5.1)

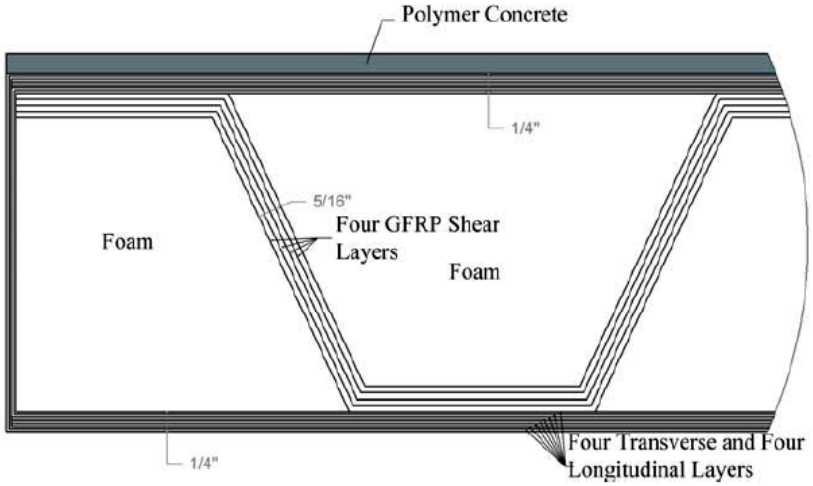

Figure 5.1 Components of the FRP Bridge Deck
(made by Structural Composite Inc.)

According to the results from previous phases (Mirmiran et al., 2012) , the FRP bridge deck met the AASHTO LRFD loading requirements under static and fatigue test and was able to withstand two million cycle of AASHTO-specified fatigue loading without any sign of damage or failure. The deflections exceeded the AASHTO criteria for deflection (i.e, L/800). In order to better understand the behavior of the deck under real

traffic, the FRP composite deck was tested at the Accelerated Pavement Testing (APT) facility in Gainesville under Heavy Vehicle Simulator (HVS) under dynamic loading. The experimental work along with the results and discussion is presented in the following.

5.2. Experimental Work

Figure 5.2 shows the 3D view of the test setup. As seen in the figure four slabs are connected together to form a 20 ft. continuous bridge decks sitting on support beams (W10×39). Center to center of the support beams are 5 ft. and the total width of the slabs are 6 ft.

The heavy vehicle simulator applied 15 kips load to the specimens (See Figure 5.3 and 5.4a). Detail B presents the connections between the decks and the support beams (Figures 5.4b and 5.4c). The loading path is shown in Figure 5.5a along with the details of deck connections to the support beam in Figure 5.5b. Two types of connections including “butted epoxy joints” and “chevron epoxy joints” were used to connect the decks to each other. More details about the connections are illustrated in Figures 5.5c and 5.5d.

Figure 5.6 presents the instrumentation plan on the slab including strain gauges and string pots. Moreover, eight strain gauges were used to measure the strain on the support beams. They were placed under the top and bottom flanges of the support beams at mid-span.

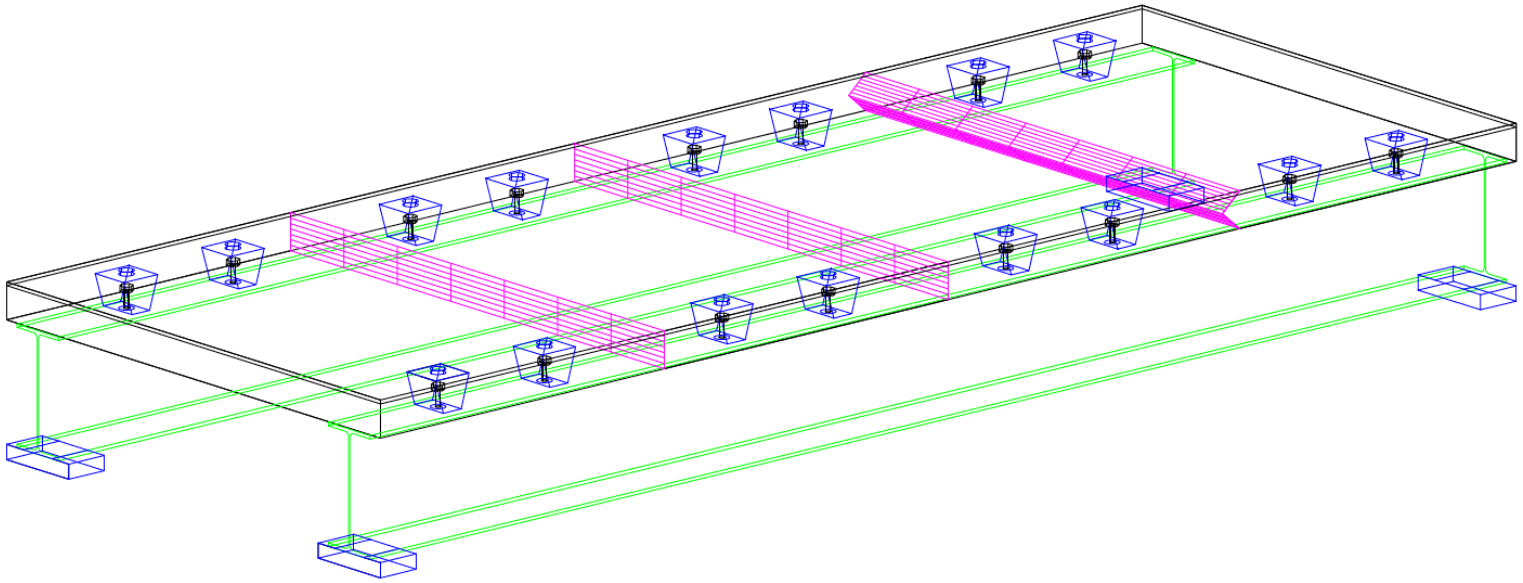

Figure 5.2 3D View of the Test Setup

Figure 5.3 HVS Machine

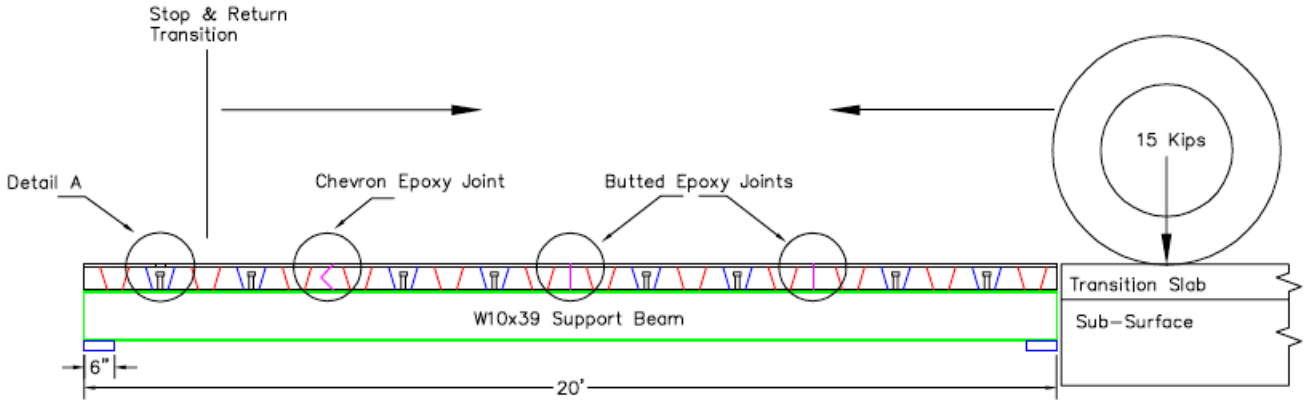

(a)

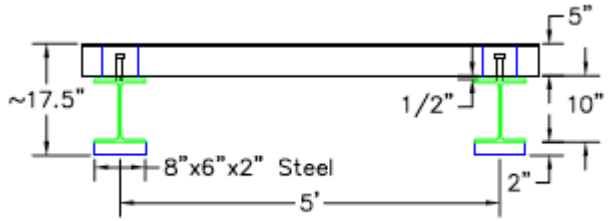

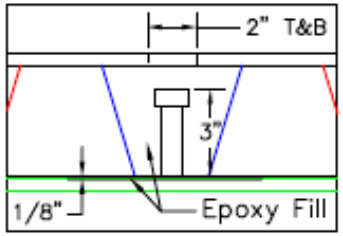

(b) (c)

Figure 5.4 Test Setup, (a) Elevation View Including Loading Plan, (b) Cross-Section View of the Test Setup, and (c) Detail A

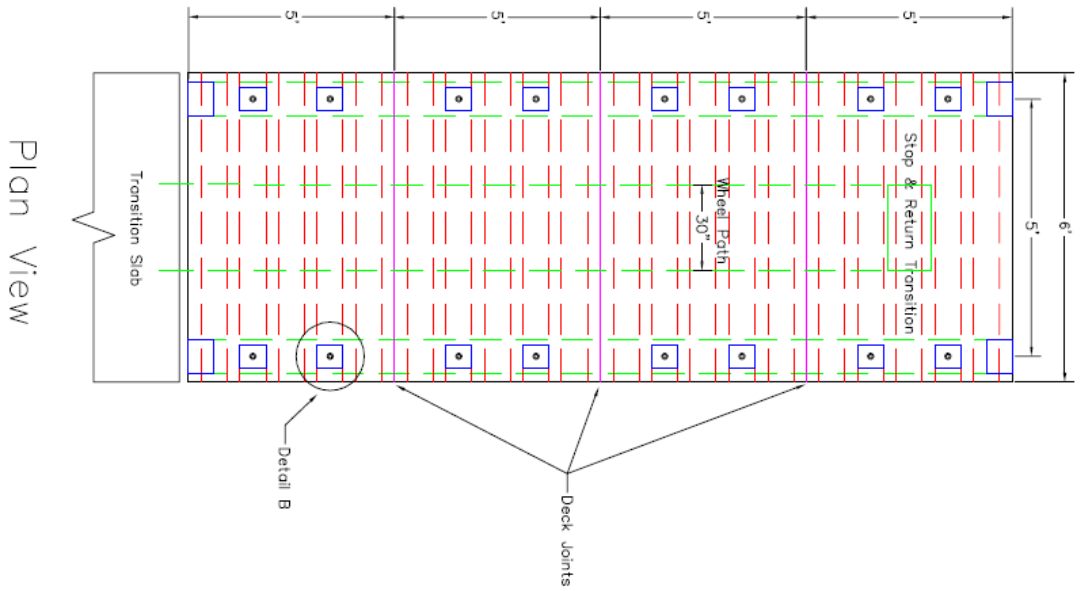

(a)

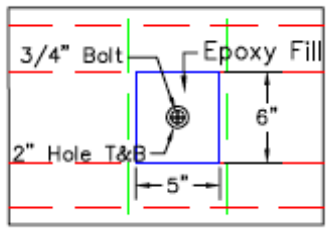

(b)

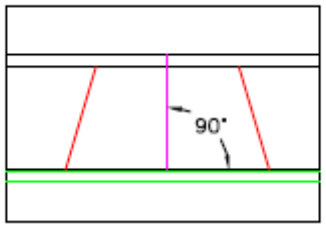

(c)

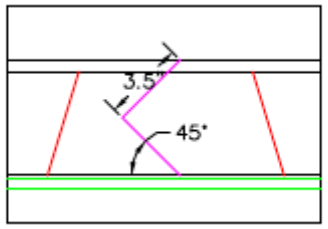

(d)

Figure 5.5 (a) Loading Path Plan, (b) Detail B, (c) Butted Epoxy, and (d) Chevron Epoxy

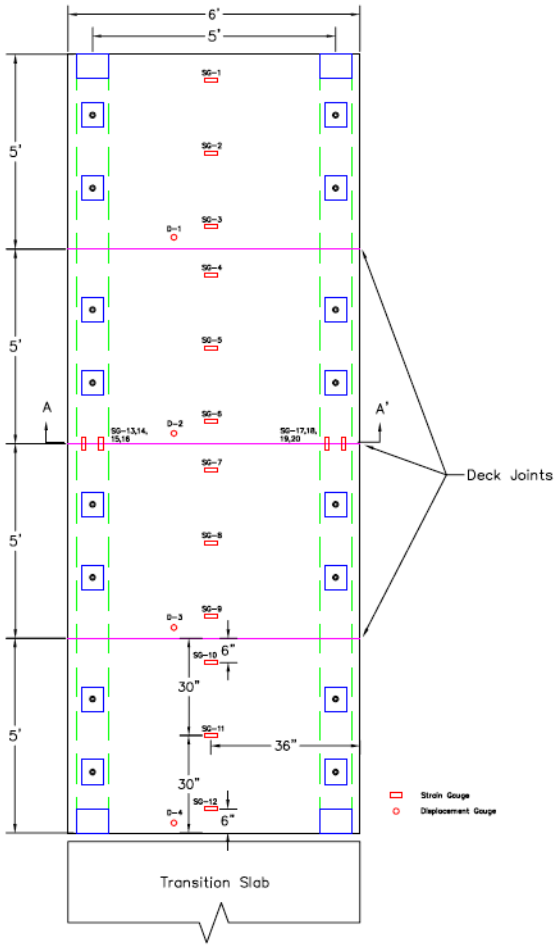

(a)

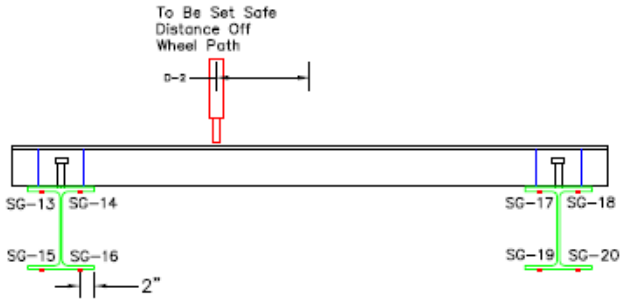

(b)

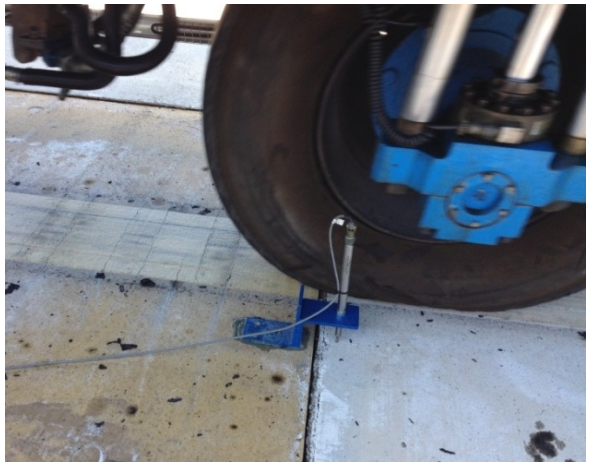

(c)

Figure 5.6 Instrumentation Plan on Decks and Support Beam

5.3. Test Results and Discussions

Figure 5.7a shows the cracks appeared on the deck top surface. The deflected shape of the decks at the connection of the panels is shown in Figure 5.7b.

(a) (b)

Figure 5.7 Cracks on (a) at Mid-Span, and (b) at the connection

Defection curves versus the number of truck passage are compared in Figure 5.8 for four panels. As seen in the figure, the deflection was constant during the test except for the beginning which may be attributed to the seating of the panels and support beams. String pot 2 shows a significant change at 150,000 passes. No specific reason was stated in the test log. The measured deflections for Panels 1 to 4 at the constant points are 0.51 in., 0.35 in., 0.21 in., and 0.48 in., respectively. The maximum service deflection according to AASHTO is 0.3 (i.e., l/800). Except for Panel 2, all panels would not meet those deflection criteria.

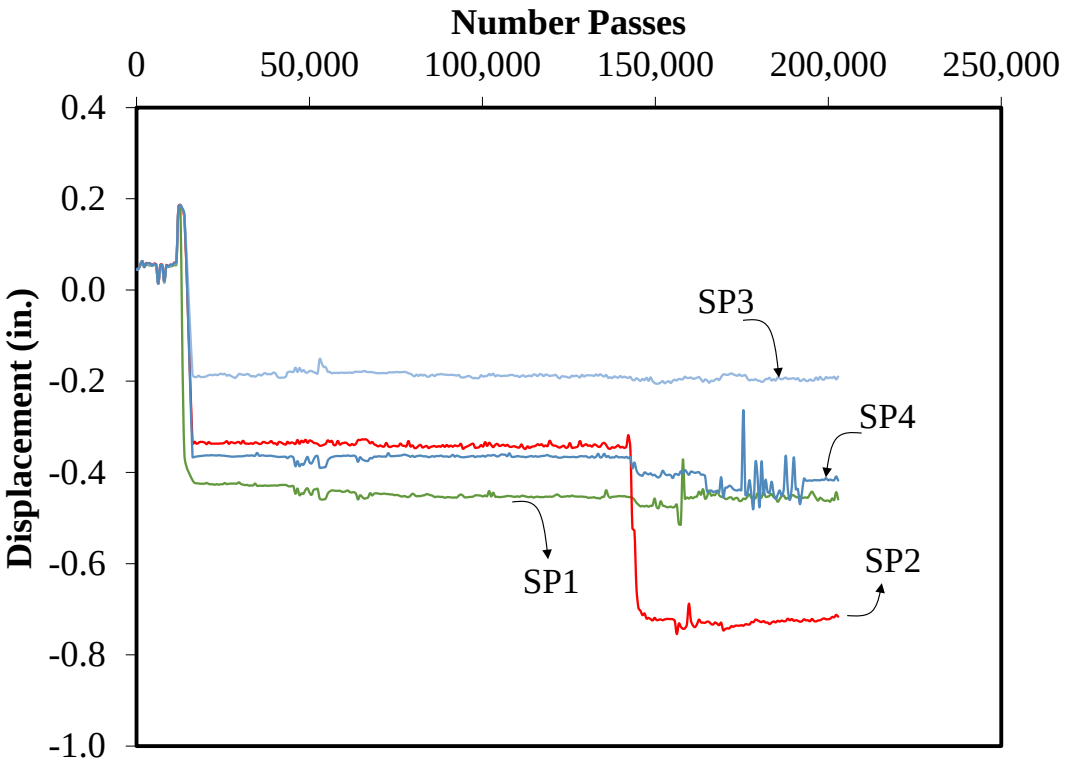

Figure 5.8 Deflections of Panels vs. the Number of Truck Passages

Surface-mounted strain gauges were installed at critical points to capture the strains. Figure 5.9 shows the strain response of the deck panels at mid-span of each panel (corresponding to SG2, SG5, SG8, and SG11 in Figure 5.6a). The maximum strain recorded for SG2, SG5, SG8, and SG11 are 0.008, 0.008, 0.008, and 0.007, respectively.

Figure 5.10 shows the strain response for the instruments attached to next to the connections which recorded the same results as the strain gauges at mid-span (corresponding to SG3, SG4, SG6, SG7, SG 9 and SG11 in Figure 5.6a). SG1 and SG12 and the strain gauges on the top and bottom flanges did not show any reasonable results. The responses curves are shown in **Appendix C**.

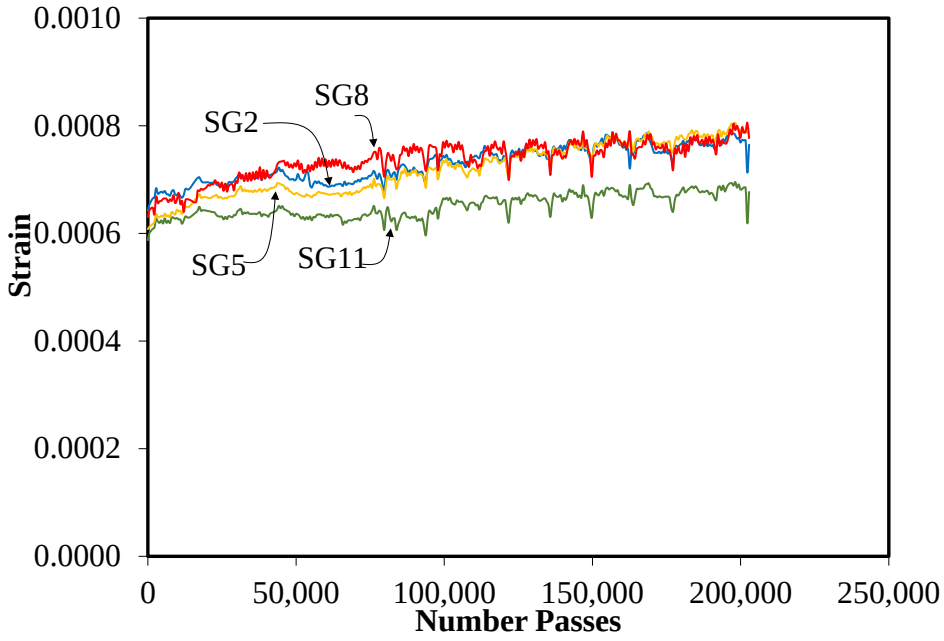

Figure 5.9 Strain Responses at Mid-Span of Each Panel

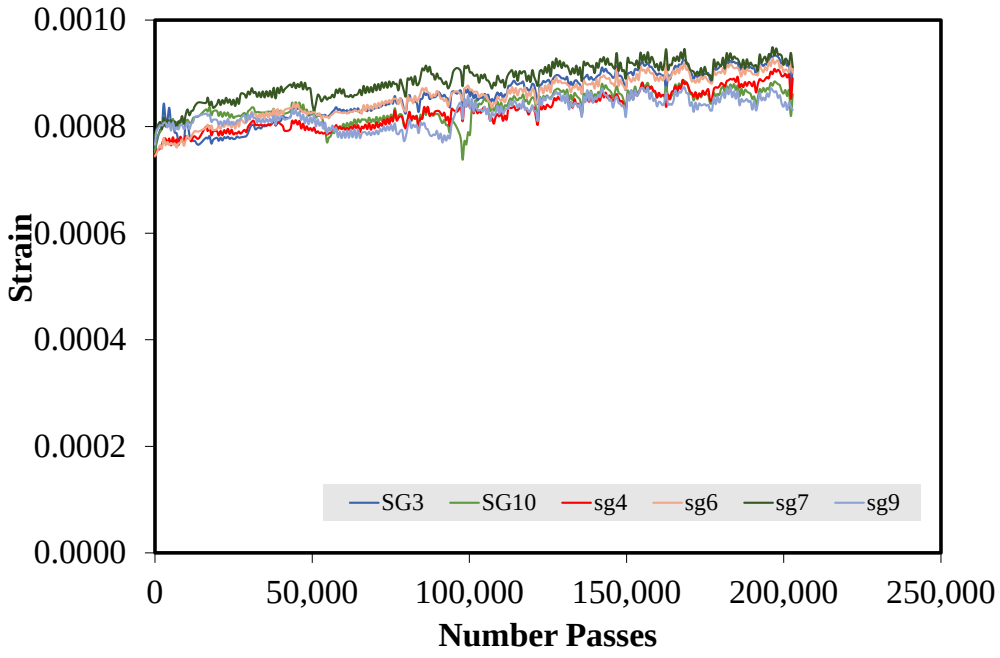

Figure 5.10 Strain Responses next to the Connection Sections

Figure 7.11 shows the maximum and minimum temperature of the top and bottom of the bridge decks. As seen in the Figures the mean temperatures at all locations were steady during the testing period, except for the minimum temperature at the bottom of the deck on Day 10.

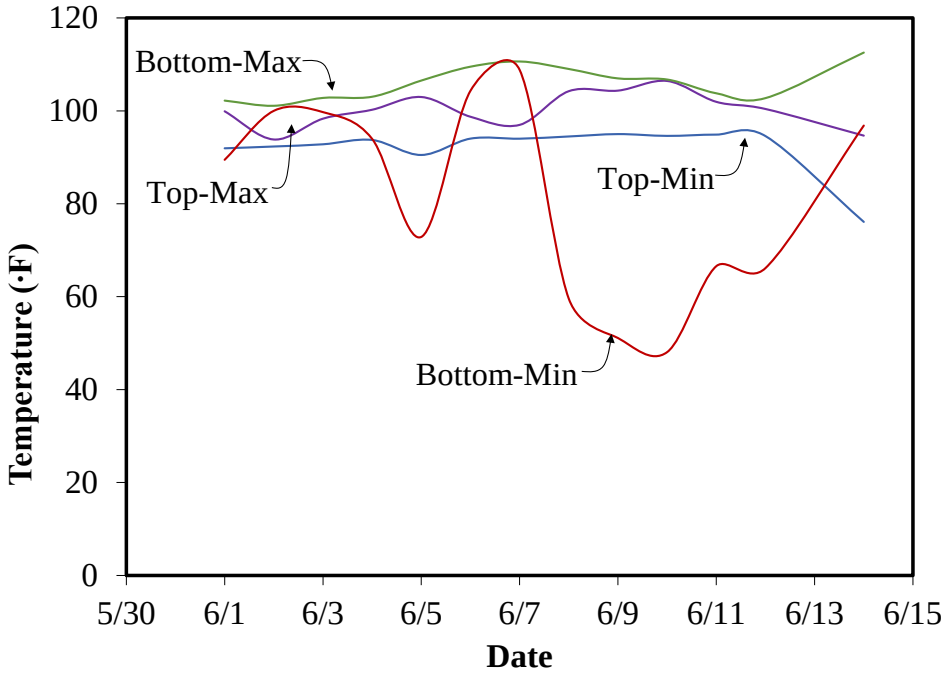

Figure 5.11 Maximum and Minimum Temperature of the FRP Deck

5.4. Conclusions

A detailed study on dynamic loading under HVS was conducted on FRP composite bridge deck. According to the test results, the FRP bridge decks met the AASHTO LRFD strength and loading requirement. However, the deflection of the bridge deck turned out to be greater than the allowable deflection by standard which suggests an

improvement may be necessary for the deck system. One suggestion is to enhance the stiffness of the system by using UHPC as the top layer.

6. SUMMARY AND CONCLUSION

The main objective of this research was to develop lightweight solid deck alternatives for movable bridges. The alternatives should meet the AASHTO LRFD loading and serviceability requirements while satisfying 21 psf self-weight requirements. Three different bridge deck systems were considered for this purpose, including UHPC waffle deck with HSS reinforcement, UHPC waffle deck with CFRP reinforcement, and FRP composite deck. Detailed experimental and analytical evaluation of these systems let to the following conclusions and recommendations.

6.1. UHPC-HSS Bridge Deck System

Detailed component and ancillary tests were carried out to evaluated UHPC waffle deck with HSS reinforcement in three phases. The results let to the following conclusions:

1. The system showed viability to serve as an alternative for light-weight bridge decks. It was shown by the experimental and analytical evaluations that the system meets the load and displacement requirements.
2. The dominant mode of failure was beam shear cracks. The cracks initiated on the web near the supports and propagated toward the slab which eventually resulted in load drop and final failure.

3. The main bar in longitudinal ribs yielded in single-rib simple-span specimens, but not in two-span or multi-rib specimens.
4. No sign of punching shear failure was observed in any of the optimized deck panels for the 4-ft. spacing of the stringers. The punching observed in the panels with 5-ft. span was addressed by increasing the thickness of the flange.
5. In regards to load distribution among primary ribs, the middle rib takes 33% of the load, while each of the adjacent ribs take 22% and 11% of the load.
6. The finite element analysis showed a good agreement with the test results.

6.2. UHPC-CFRP Bridge Deck System

Similar studies were carried out on UHPC-CFRF bridge deck system in three phases. The results can be summarized as follows:

1. The system showed its capability to work as an alternative for light-weight bridge decks by satisfying load and displacement requirements.
2. The dominant mode of failure for all but the first four specimens was beam shear cracks. The cracks started on the web next to the supports and widened and propagated toward the slab; resulting the eventual failure and significant load drops. In the first four specimens, the anchorage system was with GFRP wrap impregnated in epoxy resin, and did not provide adequate anchorage against bar slippage. As such, shear cracks in those specimens began at the mid-point between supports and edge of loading pad and propagated toward the loading pad.

3. Performance for punching shear was quite similar to the decks with HSS reinforcement.
4. Load distribution among primary ribs was similar to the decks with HSS reinforcement.
5. The finite element analysis showed a good agreement with the test results.

6.3. FRP Composite Bridge Deck System

Similar to the results obtained from static and fatigue tests on FRP composite deck system in the previous phases of this research study, the deck system satisfied the AASHTO LRFD loading requirements while its deflection exceeded the deflection limit by AASHTO.

6.4. Suggestion for Future Work

The residual strength test as well as real field application of the UHPC panels with continuous monitoring is suggested for future work.

It is necessary to improve the FRP composite deck system. One such improvement is through hybridizing the system with UHPC, as described earlier.

REFERENCES

Aaleti, S., & Sritharan, S. (2014). Design of ultrahigh-performance concrete waffle deck for accelerated bridge construction. *Transportation Research Record: Journal of the Transportation Research Board*, *2406*(1), 12-22.

Aaleti, S., Sritharan, S., Bierwagen, D., & Wipf, T. (2011). Structural Behavior of Waffle Bridge Deck Panels and Connections of Precast Ultra-High-Performance Concrete: Experimental Evaluation. *Transportation Research Record: Journal of the Transportation Research Board*, (2251), 82-92.

AASHTO, LRFD. (2013). Bridge design specifications. *American association of state highway and transportation officials.* Washington, D.C.

ABAQUS/Standard User's Manual, Version 6.13-4.

ACI Committee, American Concrete Institute, & International Organization for Standardization (2011). *Building code requirements for structural concrete (ACI 318-11) and commentary*. *American Concrete Institute*.

Ahlborn, T. M., Peuse, E. J., & Misson, D. L. (2008). Ultra-high-performance-concrete for michigan bridges material performance–phase I.

ASCE. (2013). Report card for America's infrastructure. *American society of civil engineers*. Reston, VA.

ASTM Standard D7205/D7205M. (2011). Standard test method for tensile properties of fiber reinforced polymer matrix composite bars. *ASTM international*. West Conshohocken, PA.

Blais, P. Y., & Couture, M. (1999). Precast, prestressed pedestrian bridge-world's first reactive powder concrete structure. *Pci journal*, *44*, 60-71.

Chen, D., & El-Hacha, R. (2011). Behaviour of hybrid FRP–UHPC beams in flexure under fatigue loading. *Composite Structures*, *94*(1), 253-266.

Culmo, M. P. (2011). Accelerated Bridge Construction-Experience in Design, Fabrication and Erection of Prefabricated Bridge Elements and Systems.

El-Hacha R., El-Agroudy H., Rizkalla SH. (2006). Bond Characteristics of High-Strength Steel Reinforcement. *ACI Structural Journal, 103* (6), 771-782.

Frostlechner, F.X. (2012). Composite Structures Made of Ultra-High Performance Concrete and Fiber-Reinforced Polymers. *Proceedings of the 9th fib International PhD Symposium in Civil Engineering*, Karlsruhe Institute of Technology (KIT), Karlsruhe, Germany

Ghasemi, S., Mirmiran, A., Xiao, Y., & Mackie, K. (2015). Novel UHPC-CFRP Waffle Deck Panel System for Accelerated Bridge Construction. *Journal of Composites for Construction*, 04015042.

Graybeal, B. (2011). Ultra-high performance concrete. *Technote*.

Graybeal, B. A. (2007). Compressive behavior of ultra-high-performance fiber-reinforced concrete. *ACI Materials Journal*, *104*(2).

Graybeal, B. A. (2006). Structural behavior of ultra-high performance concrete prestressed I-girders.

Graybeal, B. A. (2006). Material property characterization of Ultra-high performance concrete. *Publication No. FHWA-HRT-06-103*

Graybeal, B. A., & Hartmann, J. L. (2003). Strength and durability of ultra-high performance concrete. *Concrete Bridge Conference*, *Portland Cement Association*.

Habel, K., Viviani, M., Denarié, E., & Brühwiler, E. (2006). Development of the mechanical properties of an ultra-high performance fiber reinforced concrete (UHPFRC). *Cement and Concrete Research*, *36*(7), 1362-1370.

Hajar, Z., Simon, A., Lecointre, D., & Petitjean, J. (2003). Construction of the first road bridges made of ultra-high-performance concrete. *Proceedings, 2003 International Symposium on High Performance Concrete*.

Harris, D. K., & Roberts-Wollmann, C. L. (2005). Characterization of the punching shear capacity of thin ultra-high performance concrete slabs.

Heimann, J. (2013). The implementation of full depth UHPC waffle bridge deck panels. *Publication No. FHWA-HIF-13-031*.

Hughes Brothers. “Carbon fiber reinforced polymers (CFRP) bar - Aslan™ 200 Series.” Seward, NE (2011) Hughes Brothers

Kahl, S. (2007). Corrosion Resistant Alloy Steel (MMFX) Reinforcing Bar in Bridge Decks.

Keierleber, B., Phares, B., Bierwagen, D., Couture, I., & Fanous, F. (2007). Design of Buchanan County, Iowa, Bridge Using Ultra High Performance Concrete and PI Girders. *Proceedings of the 2007 Mid-Continent Transportation Research Symposium, Ames, IA*.

Mirmiran, A., Mackie, K., Saleem, M. A., Xia, J., Zohrevand, P., & Xiao, Y. (2012). Alternatives to Steel Grid Decks-Phase II.

Mirmiran, A., Saleem, M. A., Mackie, K., & Xia, J. (2009). Alternatives to steel grid decks.

Schesser, D., Yang, Q., Nanni, A., & Giancaspro, J. (2013). Expansive Grout-Based Gripping Systems for Tensile Testing of Large-Diameter Composite Bars. *Journal of Materials in Civil Engineering*, *26*(2), 250-258.

Saleem, M. A., Mirmiran, A., Xia, J., & Mackie, K. (2012). Development length of high-strength steel rebar in ultrahigh performance concrete. *Journal of Materials in Civil Engineering*, *25*(8), 991-998.

Saleem, M. A. (2011). *Alternatives to steel grid bridge decks*. Florida International University.

Saleem, M. A., Mirmiran, A., Xia, J., & Mackie, K. (2011). Ultra-high-performance concrete bridge deck reinforced with high-strength steel. *ACI Structural Journal*, *108*(5).

Shann, S. V. (2012). Application of ultra high performance concrete (UHPC) as a thin-bonded overlay for concrete bridge decks.

APPENDICES

Appendix 1 Load-Strain Response for UHPC-HSS Waffle Bridge Deck

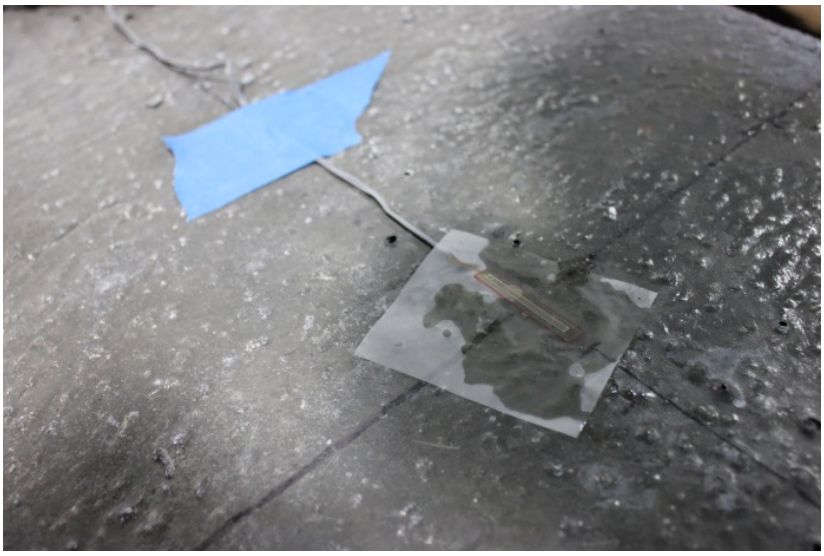

Figure A.1 Strain Gauge Attached to the Top Surface of the UHPC (Specimen 1T1S)

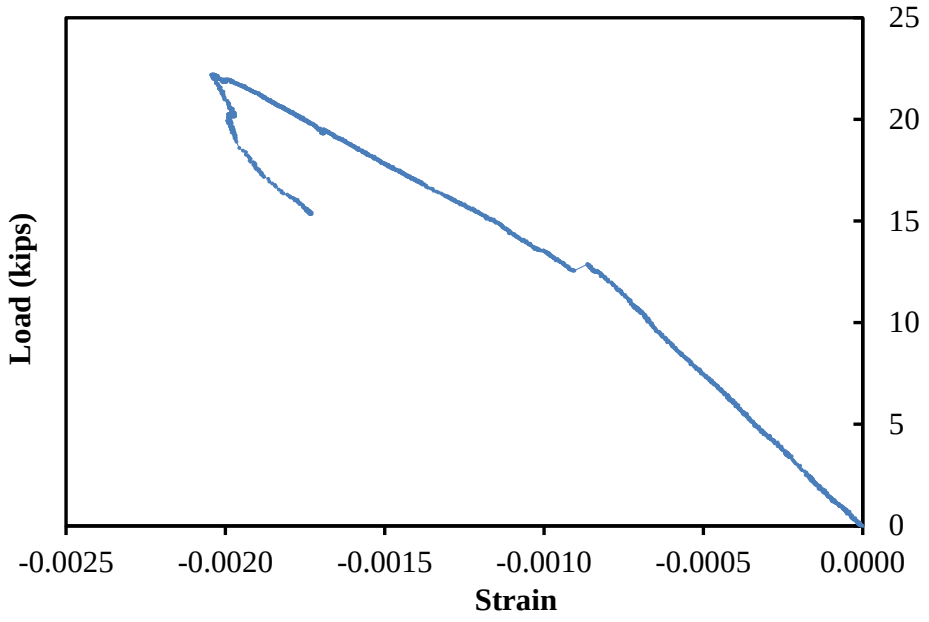

Figure A.2 Load-Strain Responses of Strain Attached to the Top Surface (Specimen 1T1S)

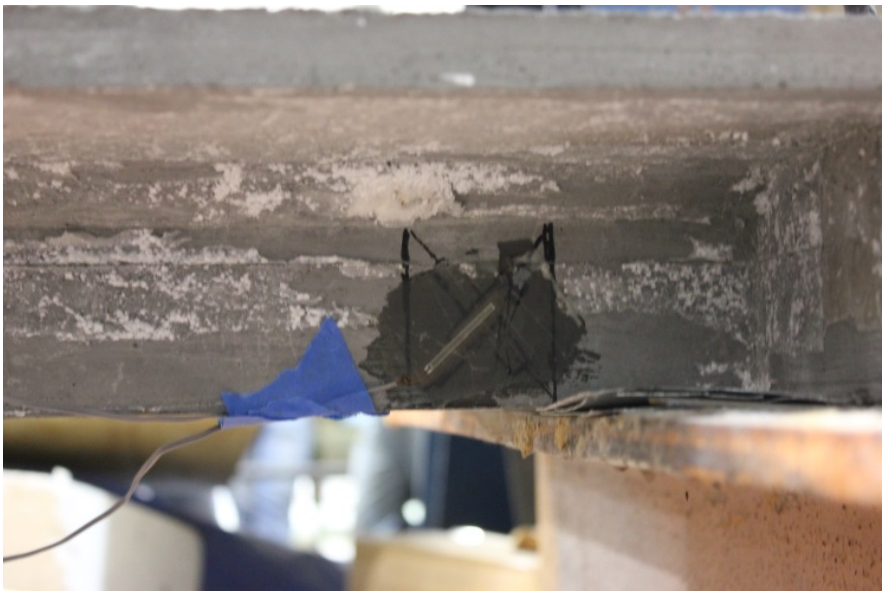

Figure A.3 Strain Gauge Attached to the Web (Specimen 1T1S)

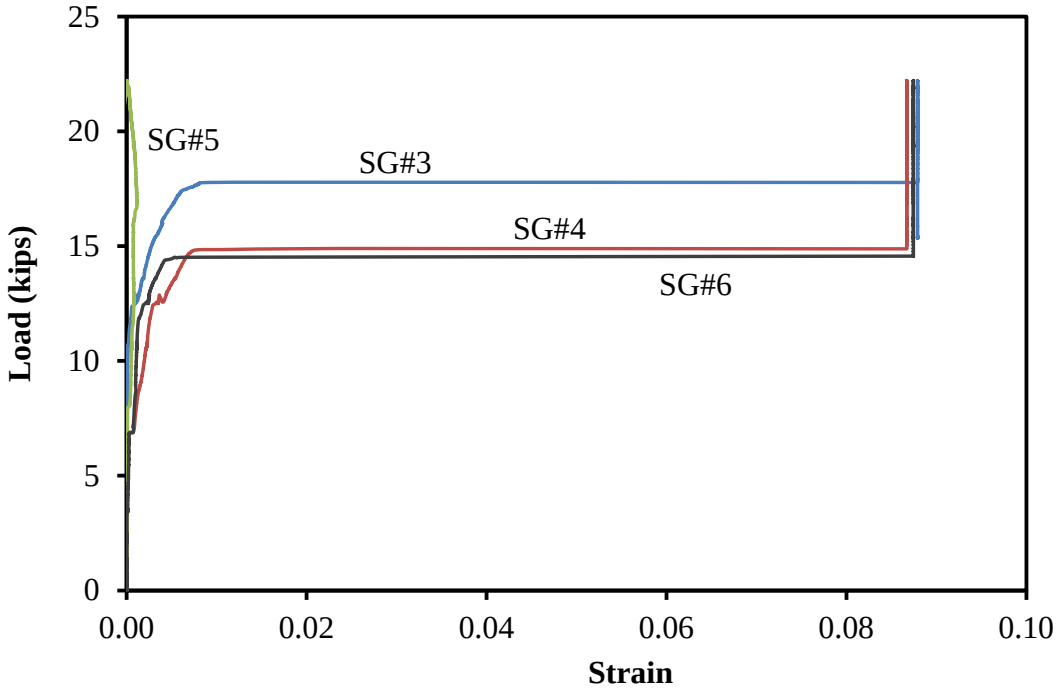

Figure A.4 Load-Strain Responses of Strain Attached to the Web (Specimen 1T1S)

Appendix B Load-Strain Response for UHPC-CFRP Waffle Bridge Deck

Figure B.1 Strain Gauge Attached to the Web (Specimen 1T1S)

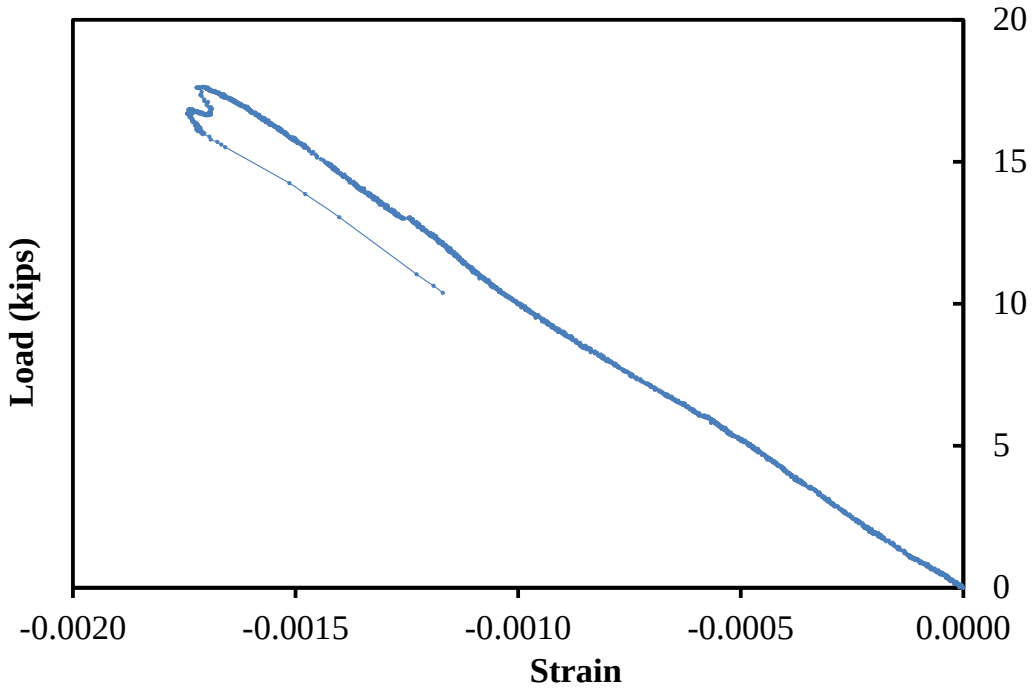

Figure B.2 Load-Strain Responses of Strain Attached to the Web (Specimen 1T1S)

Appendix C Strain Response for FRP Composite Deck and Support Beams

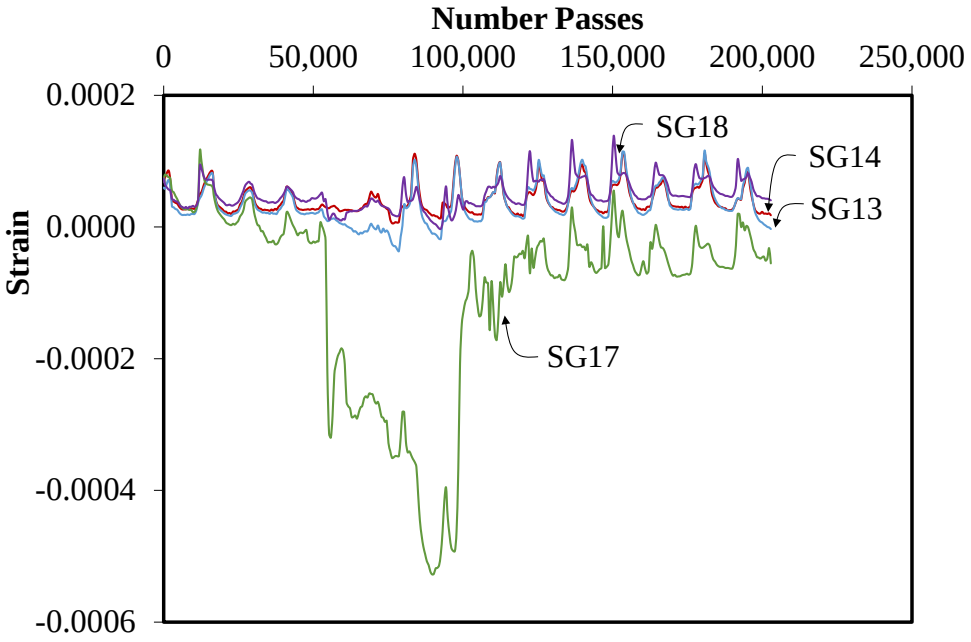

Figure C.1 Strain Responses of the Strain Gauges attached to Top Flange

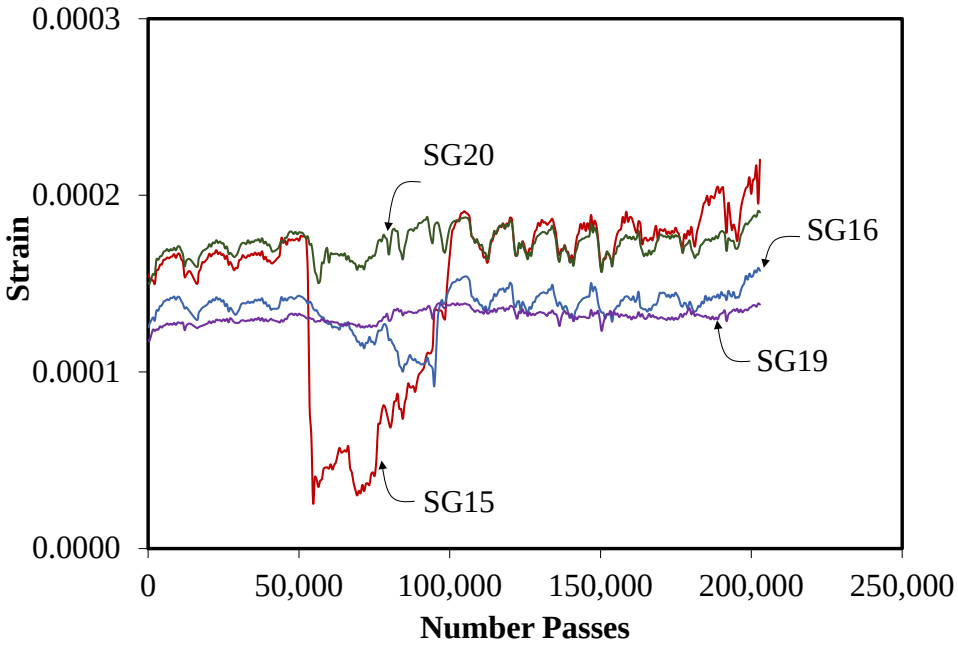

Figure C.2 Strain Responses of the Strain Gauges attached to Bottom Flange

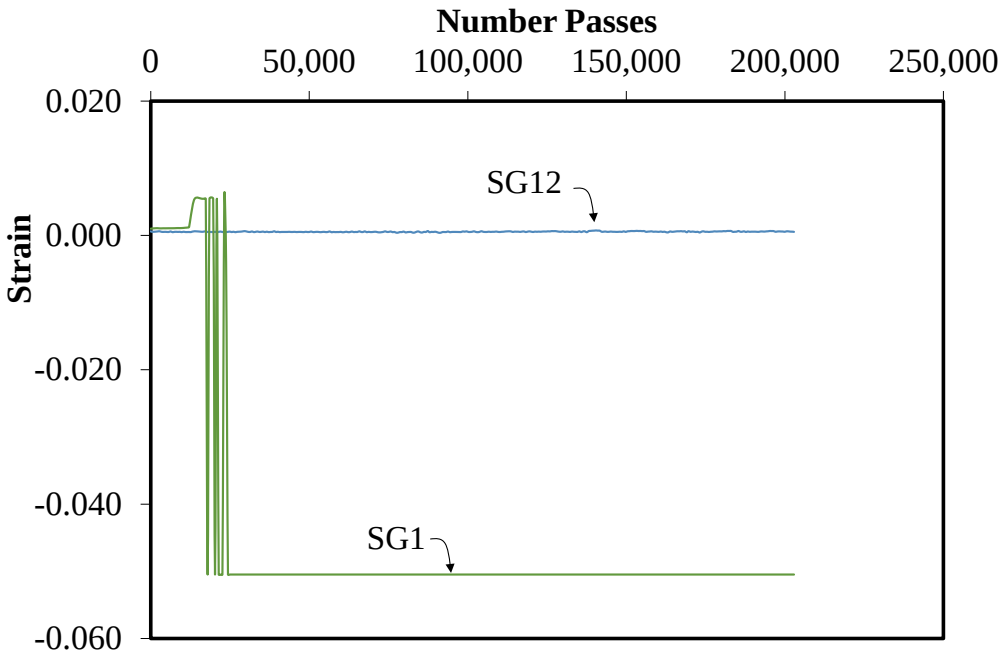

Figure C.3 Strain Responses for SG1 and SG12

VITA

SAHAR GHASEMI

Born, Sari, Iran

2000-2004	B.Sc., Civil Engineering University of Mazandaran Mazandaran, Iran
2004-2007	M.Sc., Civil Engineering- Earthquake Engineering University of Tehran Tehran, Iran
2013 -2015	Doctoral Candidate Florida International University Miami, Florida, US
2007 -2012	Structural Engineer/ Project Manager Consultant Engineers Sari, Iran
2013 -2015	Research/Teaching Assistant Florida International University Miami, Florida, US

PUBLICATIONS AND PRESENTATIONS

Ghasemi, S., Mirmiran, A., Xiao, Y., and Mackie, K., (2015). A Novel UHPC-CFRP Deck panel System for Accelerated Bridge Construction. *ASCE's Journal of Composites for Construction, 10.1061/(ASCE)CC.1943-5614.0000607.* 04015042.

Ghasemi, S., Zohrevand, P., Mirmiran, A., Xiao, Y., and Mackie, K. (2015) A Super Lighweight UHPC-HSS Deck Panel for Movable Bridges. *Journal of Engineering Structures*.

Ghasemi, S., Mirmiran, A., M., Mackie, K., Fouad, F. (2014). Innovative Modular High Performance Lightweight Decks for Accelerated Bridge Construction. *University Transportation Center (UTC) Conference for the Southeastern Region.* Atlanta, GA.

Al-Ramaheea, M., Mackie, K., Mirmiran, A., Ghasemi, S., Fouad, F., and Waldrone, C. (2015). *University Transportation Center (UTC) Conference for the Southeastern Region.* Birmingham, AL.